SAFE SATELLITE NAVIGATION WITH MULTIPLE CONSTELLATIONS: GLOBAL MONITORING OF GPS AND GLONASS SIGNAL-IN-SPACE ANOMALIES

A DISSERTATION
SUBMITTED TO THE DEPARTMENT OF ELECTRICAL ENGINEERING
AND THE COMMITTEE ON GRADUATE STUDIES
OF STANFORD UNIVERSITY
IN PARTIAL FULFILLMENT OF THE REQUIREMENTS
FOR THE DEGREE OF
DOCTOR OF PHILOSOPHY

Liang Heng
December 2012

I certify that I have read this dissertation and that, in my opinion, it is fully adequate in scope and quality as a dissertation for the degree of Doctor of Philosophy.

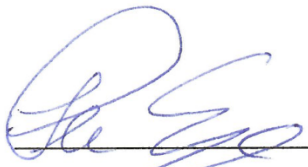

(Per Enge) Principal Adviser

I certify that I have read this dissertation and that, in my opinion, it is fully adequate in scope and quality as a dissertation for the degree of Doctor of Philosophy.

(Balaji Prabhakar)

I certify that I have read this dissertation and that, in my opinion, it is fully adequate in scope and quality as a dissertation for the degree of Doctor of Philosophy.

(Todd Walter)

Approved for the University Committee on Graduate Studies

Abstract

With the modernization of the United States Global Positioning System (GPS), the revitalization of the Russian Global'naya Navigatsionnaya Sputnikovaya Sistema (GLONASS), and the advent of the Chinese Compass and European Galileo, airborne navigators are eager to use multiple constellations to enhance navigation performance and safety. As these global navigation satellite systems (GNSS) are all based on the principle of multilateration, the quality of satellite ephemeris and clock parameters carried by the signal in space (SIS) plays a vital role in ensuring positioning accuracy and integrity. In practice, GPS and GLONASS SIS anomalies occasionally occur, resulting in user range errors (UREs) of tens of meters or even more, with the potential to expose users to hazardously misleading information. The primary goal of this dissertation is to enable comprehensive, systematic, efficient global monitoring of GPS and GLONASS SIS anomalies using low-cost but imperfect data from a global receiver network.

The first part of this dissertation presents methods used to monitor GPS SIS anomalies with emphasis on my innovative data-cleansing algorithm and automated anomaly verification process. The GPS SIS anomalies are identified by a comparison of broadcast ephemerides and clocks with post-processed precise ephemerides and clocks. Then, the identified anomalies are verified using ground observation data. Unfortunately, the broadcast navigation data obtained from a global tracking network, such as the International GNSS Service (IGS), are sometimes corrupted by data-logging errors, which lead to far more false anomalies than true ones. I developed a voting-based algorithm to cleanse the messy navigation data of various errors and inconsistencies. Finally, I identified 1256 GPS SIS anomalies since June 2000, and verified 28 true anomalies since January 2004. The results show that the GPS SIS integrity performance has met the performance standard, and never have two anomalies or more occurred simultaneously over the past eight years.

The second part of this dissertation extends SIS anomaly monitoring to GLONASS.

Unlike the situation of GPS, there are still no generally accepted precise GLONASS clocks. I addressed this long-standing issue by aligning multiple inconsistent precise clock solutions that have been independently produced by several IGS Analysis Centers. In addition, facing the fact that the GLONASS SIS integrity performance standard has not yet been established, I defined my own anomaly criteria on the basis of the statistics of actual GLONASS SIS UREs. Finally, 192 GLONASS SIS anomalies have been identified since January 2009. Four events of simultaneous multiple anomalies were discovered, including a constellation-wide clock change on 28 October 2009 which impacted all satellites. An analysis of geographic dependency shows that anomalies occur twice as frequently when satellites are not monitored by the GLONASS ground control.

The last part of this dissertation thoroughly characterizes nominal GPS and GLONASS SIS errors using three years of data. I developed robust statistical techniques to analyze the bias, distribution, and correlation of ephemeris errors, clock errors, and UREs. The statistics of actual errors show a certain degree of deviation from traditional idealized assumptions. Some of the statistics help define correct criteria for anomaly monitoring. The results also reveal two issues specific to GLONASS SIS: ephemeris error growth with propagation distance and geographic dependency.

The methods developed for monitoring GPS and GLONASS SIS anomalies are applicable to other GNSS. The results provided in this dissertation are of great importance for enabling safety-of-life applications based on multiple constellations.

Acknowledgements

This dissertation would have been impossible without the immeasurable help and support from many kind people physically or spiritually around me, to only a subset of whom it is possible to give particular mention here.

In the first place, I owe my sincerest gratitude to my principal research adviser, Prof. Per Enge, for the continuous guidance, encouragement, and support he has provided throughout the course of my PhD candidacy. I am extremely lucky to have such an adviser who has helped me present myself and build self-confidence, who always brings laughter to me and everyone, and who has created an ideal research environment that is made up of not only the brightest minds but also the warmest hearts. One simply could not wish for a better or friendlier adviser.

Besides my adviser, I would like to express my deep appreciation to my research mentors, Dr. Todd Walter and Dr. Grace Xingxin Gao, for orienting and directing me with promptness and proficiency, for being patient and encouraging in times of new ideas and difficulties, for their splendid work that has inspired me and set an example for me, and for their 100% availability and approachability.

In addition, I wish to extend my gratitude to Prof. Balaji Prabhakar, Prof. Paul Segall, Prof. Dan Boneh, and Prof. Marco Pavone for being gracious enough to serve on my reading and oral committee. Their thoughtful questions, perceptive insights, valuable suggestions, and keen comments have helped me improve this dissertation.

The work reported in this dissertation was sponsored by the Federal Aviation Administration (FAA) Satellite Navigation Office under CRDA 08-G-007. On behalf of the whole Stanford GPS group, I would like to acknowledge FAA for their generous financial support.

Furthermore, I have greatly enjoyed working with and learning from the GPS group members and alumni: Prof. Dennis Akos, Dr. Juan Blanch, Dr. Alan Chen, Dr. Yu-Hsuan Chen, Myungjun Choi, Dr. Juyong Do, Prof. Jiyun Lee, Dr. Sherman Lo, Dr. David De Lorenzo,

Dr. Alexander Mitelman, Prof. Bradford Parkinson, Dr. R. Eric Phelts, Dr. Sam Pullen, Dr. Di Qiu, Tyler Reid, Prof. James Spilker Jr., Kazushi Suzuki, Haochen Tang, Prof. Frank Van Diggelen, and Gabriel Wong. Thanks to them all for their legacy, collaboration, help, feedback, and friendship.

My special thanks belong to Douglas Archdeacon, Amy Duncan, Sherann Ellsworth, Dana Parga, Fiona Walter, and Godwin Zhang for their quick, professional administrative, editorial, and technical assistance.

I wish to add my thanks to the collaborators out of Stanford: Tom McHugh (FAA); Stuart Riley (Trimble); Steffen Thöelert, Stefan Erker, Johann Furthner, and Michael Meurer (DLR). The collaborations with them have not only enriched my research but also expanded my horizons.

It is very fortunate for me to have many great friends at Stanford, in the Bay Area, in the States, in China, and all over the world. Considering the difficulty to name all of them here, I just wish to thank them for putting up with me through the whole PhD process and making this process unexpectedly colorful and memorable.

Last but not least, to my father Wenzhi Heng and mother Yumei Li, I am grateful beyond words for their unconditional, unlimited, endless love, faith, support, and sacrifice, which has enabled me to make it to this point today. It is to my parents that I humbly dedicate this dissertation.

Contents

List of Tables

List of Figures

Chapter 1

Introduction

1.1 Golden Age of Satellite Navigation

> *It was the best of times, . . . we had everything before us, . . .*
>
> — Charles Dickens, *A Tale of Two Cities* (1859).

The United States Global Positioning System (GPS) has revolutionized the field of navigation during the past two decades. The modernization of GPS, the revitalization of the Russian Global'naya Navigatsionnaya Sputnikovaya Sistema (GLONASS), and the advent of new constellations will change the landscape of satellite navigation in the next decade. Several key milestones from the last three years are listed below.

On 27 May 2010, the first GPS Block IIF satellite, designated Space Vehicle Number (SVN) 62, was launched from the Cape Canaveral Air Force Station [1]. It began transmitting the first usable L5 navigation signal [2]. This launch was the advent of dual frequency diversity for safety-of-life users.

On 2 October 2011, a GLONASS-M satellite, identified as No. 742, was launched from the Plesetsk Cosmodrome [3]. This replenishment made the GLONASS constellation fully restored to 24 satellites, for the first time since 1996.

On 21 October 2011, Europe launched the first two operational Galileo satellites from the Guiana Space Centre [4]. This launch marked the beginning of the second phase of the Galileo program—In-Orbit Validation.

On 2 December 2011, China launched the 10th Compass satellite from the Xichang Satellite Launch Center [5]. Three weeks later, the Compass (BeiDou-2) Navigation Satellite

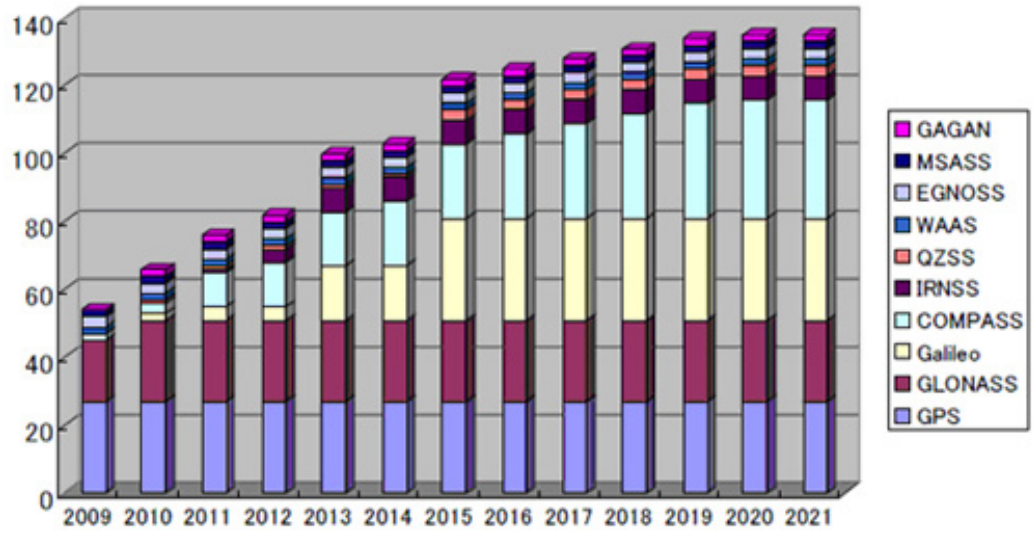

Figure 1.1: Number of satellites in GNSS, RNSS, and SBAS (adapted from `http://www.furuno.com/en/business_product/gps/technical/tec_multi.html`).

System was declared to have the initial operational capability in China and its neighboring areas [6].

In addition to the progress of the four global navigation satellite systems (GNSS), several regional navigation satellite systems (RNSS) and satellite-based augmentation systems (SBAS) have been or are being built. As shown in Figure 1.1, although GPS and GLONASS are the only two fully operational GNSS at present, in 2020 Galileo and Compass are expected to achieve full operational capability, with the total number of navigation satellites rising to 130.

Besides the multiplicity of satellites, frequency diversity will become available to civil users over the next decade. As shown in Figure 1.2, each satellite will broadcast civil signals on at least two frequencies: L1 (1575.42 MHz) and L5 (1176.45 MHz). Both L1 and L5 signals locate in the Aeronautical Radio Navigation Services (ARNS) radio band, a frequency band reserved exclusively for worldwide aircraft.

The increased number of satellites from diverse constellations as well as the increased frequency diversity will be of great benefit to billions of GNSS users, especially aviation users who are keen on navigation safety.

One benefit to users is improved integrity. A promising example here is advanced receiver

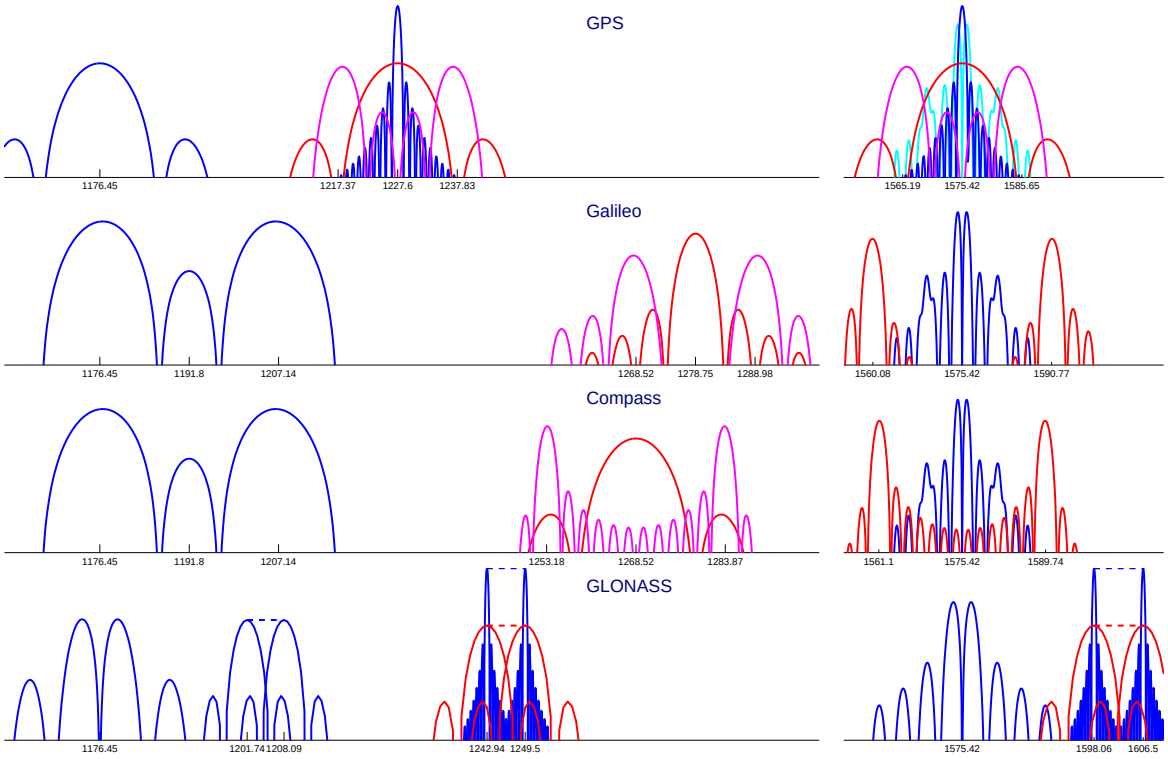

Figure 1.2: Current and future GNSS spectrum. Civil signals are in cool colors, whereas military signals are in warm colors. Signal structures are based on [7–10].

autonomous integrity monitoring (advanced RAIM or ARAIM) for vertical guidance. The increased number of satellites and constellations, together with dual-frequency signals, are expected to enable ARAIM to achieve worldwide coverage of vertical guidance down to 200 feet above the runway with minimal ground infrastructure [11–13].

Another benefit is strengthened robustness and continuity. For instance, with an increased number of satellites in view, a user receiver can raise the antenna mask angle to overcome low-elevation radio frequency interference (RFI) but still comply with accuracy and integrity requirements [14, 15].

A third benefit is enhanced accuracy and availability in some unfavorable environments. Examples include aircraft vertical guidance in polar regions [16] and pedestrian and vehicular navigation in urban canyons [17].

Although the use of multiple constellations offers a golden opportunity to enhance

navigation safety, this opportunity comes with great challenges. One of the challenges is that the signal-in-space (SIS) performance, especially anomalous performance, of each constellation has not yet been thoroughly studied. In the next section, ARAIM is used as an example to explain why a thorough understanding of SIS performance is necessary.

1.2 Motivation

There are four essential requirements for virtually any navigation system: accuracy, availability, continuity, and integrity. In terms of navigation safety, the greatest among these is integrity [18].

Integrity is a measure of the trust that can be placed in the correctness of the information supplied by the total system [19]. In other words, integrity refers to a navigation satellite system's ability to provide timely warning when it fails to meet the stated accuracy. An integrity failure may expose users to hazardously misleading information. Although GPS has been carefully designed and operated to ensure a fairly high level of integrity [18, 20–22], the ability of stand-alone GPS is insufficient to meet the stringent requirements for any phase of flight [23–25].

In the era of "GPS only," a few augmentation systems, such as the Wide Area Augmentation System (WAAS) [26] and the Local Area Augmentation System (LAAS) [27], have been developed to help GPS meet the aviation integrity requirements [23]. Based on the principle of differential GPS (DGPS) [28, 29], these augmentation systems rely on not only a network of fixed, ground-based reference stations to measure the GPS satellites' signals, but also a reliable spaceborne or terrestrial data link to convey corrections and integrity flags to users in a timely manner. Therefore, it is very difficult, for technical, financial, and political reasons, to expand such augmentation systems worldwide.

Unlike the augmentation systems which need continuous, real-time support from the ground, RAIM is a technology to enhance integrity by self-contained fault detection. With a single GPS constellation and a single frequency, RAIM has been successfully used to support lateral guidance during the approach phase of flight [12, 30]. With multiple constellations, highly redundant pseudorange measurements from unprecedentedly many GNSS satellites can enable a user receiver to achieve sufficiently high integrity for vertical guidance everywhere on Earth. ARAIM is one such technique being investigated for this purpose.

Figure 1.3 illustrates a solution separation algorithm used in ARAIM [31]. This algorithm

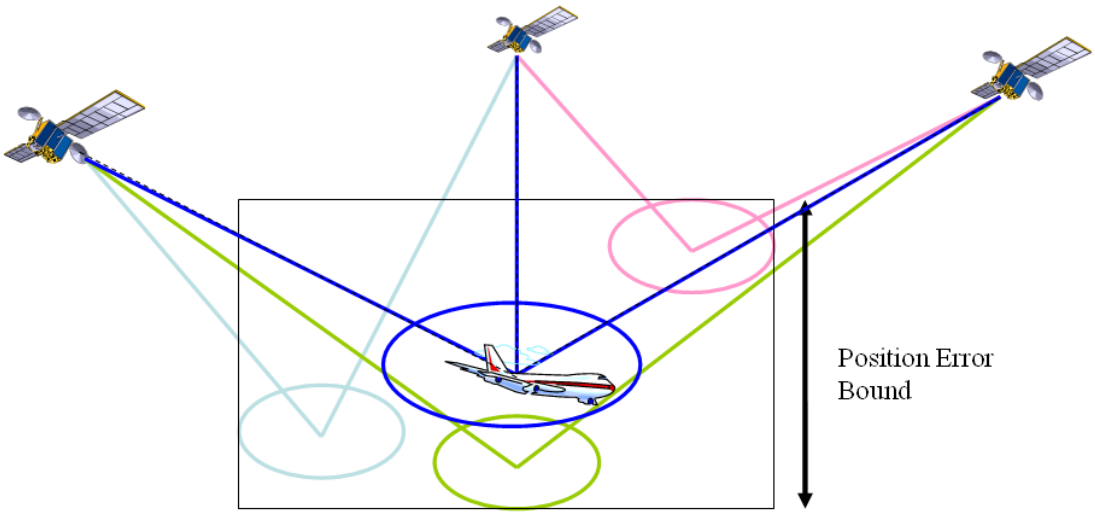

Figure 1.3: A solution separation algorithm used in ARAIM (Courtesy of J. Blanch).

calculates a three-dimensional position error bound based on all position solutions obtained with various subsets of the visible satellites. A warning will be issued if the calculated error bound exceeds pre-determined "hazardous" thresholds.

The solution separation algorithm has computational complexity that strongly depends on the maximum number of simultaneous satellite faults. As shown in Table 1.1, for 20 visible satellites in two GNSS constellations, the number of subsets that need to be evaluated increases nearly 70 times if we assume up to 3 faults at a time instead of up to 1 fault at a time. Additionally, assuming more simultaneous satellite faults can deteriorate ARAIM

Assumptions	Number of subsets that need to be evaluated		
	Formula	One constellation (typically $n = 10$)	Two constellations (typically $n = 20$)
≤ 1 fault	$\binom{n}{1}$	10	20
≤ 2 faults	$\binom{n}{1} + \binom{n}{2}$	55	210
≤ 3 faults	$\binom{n}{1} + \binom{n}{2} + \binom{n}{3}$	175	1350

Note: n is the number of visible satellites.

Table 1.1: ARAIM computational complexity depends on the assumption of the maximum number of simultaneous satellite faults.

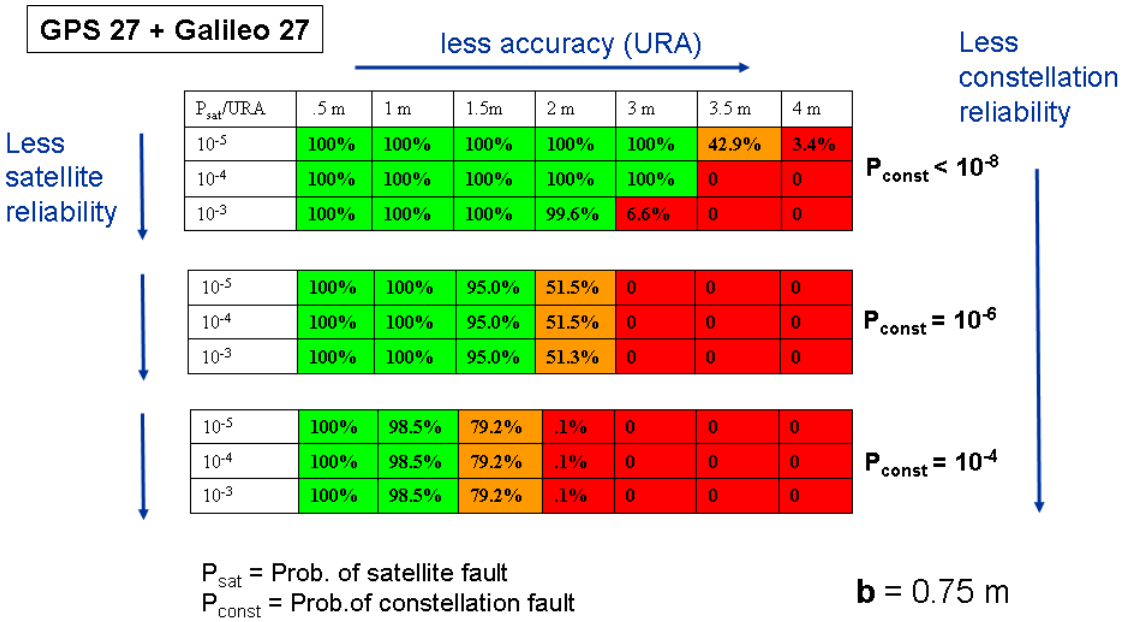

P_{sat}/URA	.5 m	1 m	1.5m	2 m	3 m	3.5 m	4 m
10^{-5}	100%	100%	100%	100%	100%	42.9%	3.4%
10^{-4}	100%	100%	100%	100%	100%	0	0
10^{-3}	100%	100%	100%	99.6%	6.6%	0	0
10^{-5}	100%	100%	95.0%	51.5%	0	0	0
10^{-4}	100%	100%	95.0%	51.5%	0	0	0
10^{-3}	100%	100%	95.0%	51.3%	0	0	0
10^{-5}	100%	98.5%	79.2%	.1%	0	0	0
10^{-4}	100%	98.5%	79.2%	.1%	0	0	0
10^{-3}	100%	98.5%	79.2%	.1%	0	0	0

Table 1.2: Global availability of ARAIM based on 27 GPS satellites and 27 Galileo satellites (Courtesy of J. Blanch).

performance [31].

Furthermore, the prior information about probability of satellite fault, probability of constellation fault, and user range accuracy (URA)[1] directly affects the availability performance of ARAIM, as shown in Table 1.2.

All in all, accurate answers to the following five fundamental questions for each GNSS will help not only ARAIM but also other integrity monitoring systems [33] and multi-constellation GNSS applications [15–17].

- How often does a satellite fault occur?
- How often do n ($n \geq 2$) satellite faults occur simultaneously?
- How often does a constellation fault occur?
- How are UREs actually distributed for a certain URA?
- Are UREs for different satellites correlated?

Among the above questions, the first three are mainly related to SIS anomaly performance,

[1] URA is a parameter broadcast by the satellites. It is intended to describe the accuracy of user range errors (URE) and indicate an upper limit on their likely magnitude [32]. More discussion of URE and URA can be found in Sections 2.3 and 2.4.

and the last two are associated with nominal SIS error performance. Unfortunately, neither anomalous nor nominal SIS performance has been thoroughly studied, even for the two fully operational constellations, GPS and GLONASS. The main focus of this dissertation is to develop systematic methods for monitoring GPS and GLONASS SIS anomalies using imperfect data from a global tracking network. A thorough documentation and characterization of anomalies and nominal errors provided by this dissertation will be adequate for quantitatively answering the five questions.

1.3 Previous Work

1.3.1 GPS SIS anomalies

As early as the 1980s, people became aware of GPS satellite faults and started to design RAIM to cope with them [34]. Since then, quite a few anomalies, not only SIS integrity anomalies, but also continuity interruptions and signal deformations, have been discovered and investigated [22, 35–41]. Unfortunately, few of these studies attempted to provide a complete compilation of anomalies that occurred globally, partially because most of these studies relied on the observation data from a receiver or a small receiver network with limited geographic distribution. Moreover, they were directed at specific signal faults or rare normal events, such as ionospheric storms [42, 43].

In the late 1980s, the worldwide scientific community started to build global networks of GNSS receivers. One of the best known networks is the International GNSS Service (IGS) [44], which unites more than 400 volunteer receivers all over the world. IGS routinely collects broadcast navigation message data, and generates precise GPS ephemerides[2] and clocks from the observation data. With these data, GPS SIS errors can be readily computed by comparing broadcast ephemerides and clocks with precise ephemerides and clocks. Some researchers have thus succeeded in characterizing GPS SIS accuracy performance [45, 47–50]. However, when some of them attempted to identify GPS SIS anomalies using this approach, they found themselves in an awkward predicament in which there are far more "anomalies" than expected [45, 50, 51]. In fact, the broadcast navigation data from the IGS tracking network contains various data-logging errors [49], which result in many false anomalies. This dissertation systematically treats and removes these false anomalies.

[2] In this dissertation, "ephemeris" is defined as an accurate model of satellite orbits. In some literature [45, 46], "ephemeris" refers to an accurate model of satellite orbits *and* clocks.

1.3.2 GLONASS SIS anomalies

In the early 1990s, P. Misra initiated a series of studies on GLONASS, from positioning accuracy to the performance of dual-constellation-based RAIM [52, 53]. These studies were based on the data collected by their own GPS and GLONASS receivers.

In the mid-1990s, GLONASS generated wide interest in the GNSS community because it reached full operational capability and had no selective availability (SA)[3]. In 1998, the IGS launched a worldwide GLONASS observation campaign, named IGEX-98. During IGEX-98, B. Burke encountered a GLONASS SIS anomaly event, in which an off-schedule change in the navigation message took place replacing the clock bias and clock rate parameters with incorrect values, and producing clock biases in error by approximately 24 kilometers [56]. Afterward, N. Jonkman reported eight GLONASS SIS anomalies during the period September 1998 to December 1999; he also noticed that some GLONASS navigation messages were corrupted by data-logging errors [57].

After the one-time campaign IGEX-98, the IGS initiated a long-term project for routine collection and processing of GLONASS data [58]. Using the IGS broadcast and precise GLONASS ephemerides, researchers successfully characterized nominal GLONASS SIS accuracy performance [59–62]. Again, due to data-logging errors, few attempts have been made to monitor GLONASS SIS anomalies. We treat this issue herein.

1.4 Goals and Challenges

The primary goal of this dissertation is to enable comprehensive, systematic, efficient global monitoring of GPS and GLONASS SIS anomalies using low-cost but imperfect data from a global receiver network. In order to facilitate the anomaly monitoring as well as to answer the last two questions in Section 1.2, the second goal is a thorough statistical characterization of nominal GPS and GLONASS SIS errors.

To achieve these goals, the following challenging issues must be addressed.

- Massive data
  - 38,000,000 GPS navigation messages logged per year
  - 31,000,000 GLONASS navigation messages logged per year

[3]Selective availability was an intentional degradation of civil GPS signals implemented from the early 1990s until May 2000 [54, 55].

- Messy data
  - 135,000 navigation messages corrupted by data-logging errors every year
  - 11 false anomalies for every true anomaly
- Missing information
  - No indication of satellite trackability in navigation message data
  - No URA information in GLONASS data
  - No official GLONASS integrity performance standard
  - No generally accepted precise GLONASS clocks

1.5 Contributions

The specific contributions of this dissertation are as follows.

- Systematic identification of GPS SIS anomalies [63–67]
  1. Developed deep cleansing algorithms for messy navigation data
  2. Automated anomaly verification using unreliable ground observation data
- The first revelation of GLONASS SIS anomalies [68]
  3. Invented an algorithm to align multiple inconsistent precise clock estimates
  4. Proposed anomaly criteria from the statistics of actual SIS errors
- In-depth characterization of nominal GPS and GLONASS SIS errors [69–71]
  5. Developed robust statistical techniques to analyze the biases, distributions, and correlations of nominal GPS and GLONASS SIS errors

As one contribution may be useful for multiple purposes, the matrix below shows how a contribution is related to a certain purpose. The numbers 1–5 in the matrix correspond to the five contributions in the above list.

	Anomalies	Nominal errors
GPS SIS	1, 2	1, 5
GLONASS SIS	1, 3, 4	1, 3, 5

Finally, although the methods and results presented in this dissertation were primarily developed in the context of GPS and GLONASS, they are generally applicable to other

GNSS becoming operational in the next decade.

1.6 Outline

This dissertation is organized in order of the above-listed contributions.

Chapter 2 introduces GPS and GLONASS fundamentals that can help the reader understand this dissertation, including system architectures, contents of navigation message, sources and metrics of range errors, and integrity performance standards.

Chapter 3 presents Phase I of GPS anomaly monitoring—identifying potential anomalies by comparing broadcast ephemerides and clocks with precise values. The data cleansing algorithm is described in detail, and the anomalies identified in the past 12 years are presented.

Chapter 4 discusses Phase II of GPS anomaly monitoring—verifying the potential anomalies by checking them against ground observation data. The major steps of our automated anomaly verification are described, and the verification results for the anomalies in the past eight years are presented and compared with the Phase I results.

Chapter 5 extends SIS anomaly monitoring to GLONASS, with emphasis on our clock alignment algorithm and anomaly criteria. The anomalies identified in the past three years are presented, with in-depth analyses of anomaly probability, simultaneous multiple anomalies, and geographic dependency.

Chapter 6 is devoted to statistical characterization of nominal GPS and GLONASS SIS errors. Robust statistical techniques are introduced, and the statistics of bias, distribution, and correlation are presented. In addition, two particular issues with GLONASS, ephemeris error growth with propagation distance and geographic dependency, are discussed at the end of this chapter.

Chapter 7 summarizes the methods and major findings, and offers several possible directions for future work.

In addition, Appendix A lists the abbreviations and acronyms used throughout this dissertation, as well as some key definitions and notation conventions. Appendix B derives the global average URE for GPS, GLONASS, and other constellations.

Chapter 2

GPS and GLONASS Fundamentals

For GPS and GLONASS, as well as the other GNSS, the user receiver uses multilateration[1] to determine its position. As illustrated in Figure 2.1, the pseudorange measurements from

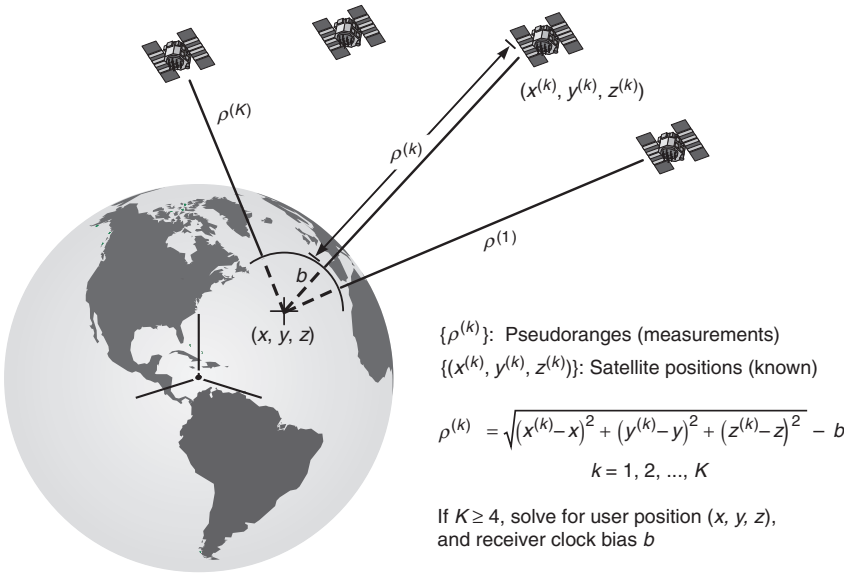

Figure 2.1: The principle of satellite navigation. The user-satellite TOA range measurements are biased by the difference between the satellite and receiver clocks, and thus called pseudoranges [72].

[1]Traditionally, "multilateration" referred to the positioning method using measurements of time difference of arrival (TDOA) at (or from) three or more sites, while "trilateration" referred to the positioning method using measurements of time of arrival (TOA) from three sites. Nowadays, the satellite navigation and wireless localization communities tend to use "multilateration" to represent the TOA-based positioning method with any number of sites, and "hyperbolic positioning" to represent any TDOA-based positioning methods.

a receiver to at least four visible satellites and the positions and clocks of these satellites are prerequisite for the receiver to perform a position fix [72]. To this end, a navigation satellite system must commit itself to providing users with accurate and trustworthy information about satellite orbits and clocks. In this chapter, Sections 2.1 and 2.2 describe the essential elements in GPS and GLONASS that make this possible. Furthermore, Section 2.3 introduces the cause of range errors, and several commonly used metrics. Section 2.4 describes integrity performance standards and the definition of SIS anomaly. Familiarity with these fundamentals helps understand this dissertation.

2.1 System Architecture

GPS architecture

As shown in Figure 2.2, GPS is made up of three segments: the space segment, the control

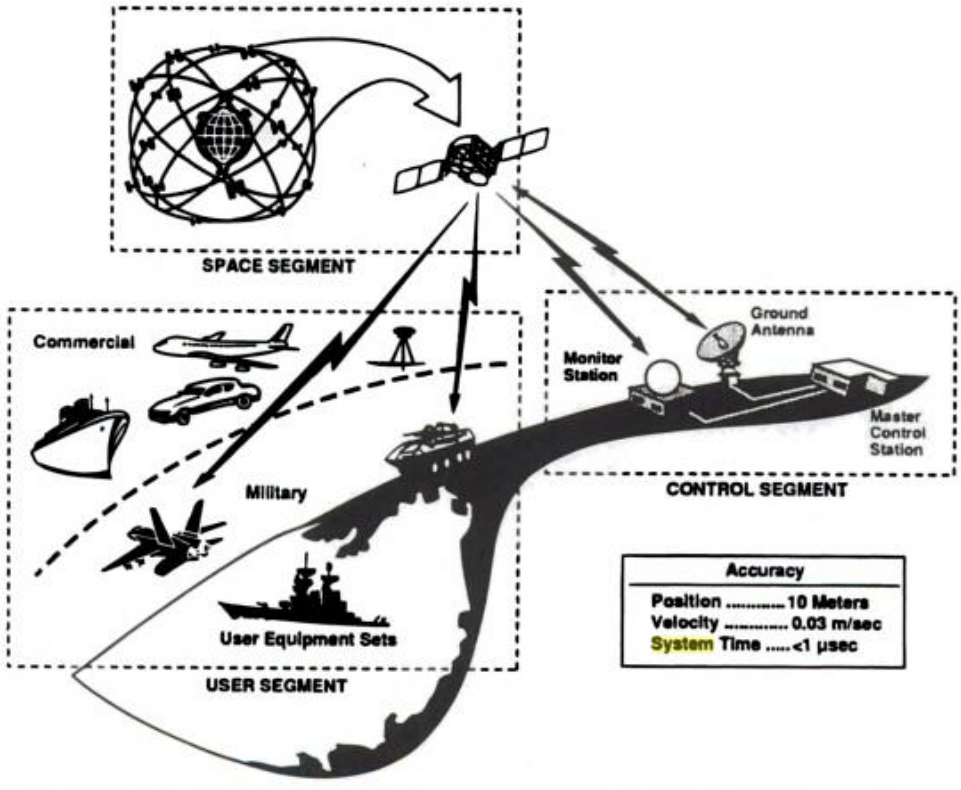

Figure 2.2: GPS consists of three segments: space, control, and user [73].

segment, and the user segment [73].

The space segment consists of at least 24 medium Earth orbit (MEO) satellites in six orbital planes inclined at 55°. The orbital period is one-half a sidereal day, i.e., 11 hours 58 minutes. The orbits are arranged so that at least six satellites are almost always within line of sight from everywhere on Earth's surface. Each satellite continuously transmits code division multiple access (CDMA) ranging signals on L1, L2, and L5 frequencies[2], as shown in Figure 1.2. These ranging signals carry the navigation messages describing current satellite orbits and clock drifts. Multiple rubidium and cesium atomic clocks on board the satellites keep time within 30 nanoseconds of Coordinated Universal Time (UTC) [72].

The control segment, also referred to as the Operational Control System (OCS), includes a master control station (MCS), six dedicated monitor stations, and five dedicated ground antennas. The monitor stations track satellites, the MCS predicts future satellite orbits and clock corrections, and the ground antennas periodically upload these predicted navigation data to each satellite.

Figure 2.3: OCS and NGA monitor station networks [74].

[2]The civil L2 signal (L2C) and L5 signal are not available on all satellites at present. L2C is transmitted by Block IIR-M and later design satellites, and L5 is transmitted by Block IIF and later design satellites.

Figure 2.3 shows the location of the six OCS monitor stations and 11 National Geospatial-Intelligence Agency (NGA) monitor stations[3]. The observation data from the NGA stations have been incorporated into the MCS processing since August 2005 in order to improve the SIS accuracy [74]. These globally-distributed monitor stations achieve 100% tracking coverage for all satellites at all times[4].

The user segment contains both civil and military users. Civil users only have access to the GPS Standard Positioning Service (SPS), primarily provided by means of the GPS L1 coarse/acquisition (C/A) code ranging signal. Military users have access to the GPS Precise Positioning Service (PPS), provided by means of the precision (P(Y)) code ranging signals on both L1 and L2 frequencies[5].

GLONASS architecture

In the same fashion, GLONASS also consists of three segments: space, control, and user [78]. The function of each segment is the same as that in GPS. Key differences between GPS and GLONASS are now discussed.

The GLONASS space segment is nominally comprised of at most 24 MEO satellites in three orbital planes[6] inclined at 65°. The higher inclination ensures better satellite visibility in high latitudes. Each satellite continuously transmits frequency division multiple access (FDMA) ranging signals on L1 and L2 frequencies, as shown in Figure 1.2. Although the FDMA signal may have a better cross-correlation performance than the CDMA signal used in GPS [80], it results in inter-frequency carrier phase biases up to 5 centimeters [81].

The GLONASS control segment has a similar structure to that of GPS. Nevertheless, all the GLONASS monitor stations are within the Russian territory [82], as can be seen in Figure 2.4. Consequently, the GLONASS monitor stations can only achieve a 49.8% tracking coverage, as illustrated by the shaded areas in Figure 2.5. Due to the relatively low tracking coverage, the GLONASS ephemeris accuracy and the occurrence of SIS anomalies show significant geographic dependency (Sections 6.4.5 and 5.4.3).

[3] NGA was previously known as the National Imagery and Mapping Agency (NIMA) and is part of the Department of Defense. NGA is dedicated to providing geospatial intelligence in support of national security. The NGA monitor stations were originally fielded to help define the GPS reference frame [75, 76].

[4] In fact, each satellite can be tracked by at least 3 stations at all times (assuming 5-degree antenna mask angle) [74].

[5] Although the civil users have no knowledge of the encrypted Y codes, they can use so-called codeless or semicodeless techniques to gain access to the P(Y) signals [77].

[6] There is a plan to expand the GLONASS constellation to 30 satellites using six orbital planes [79].

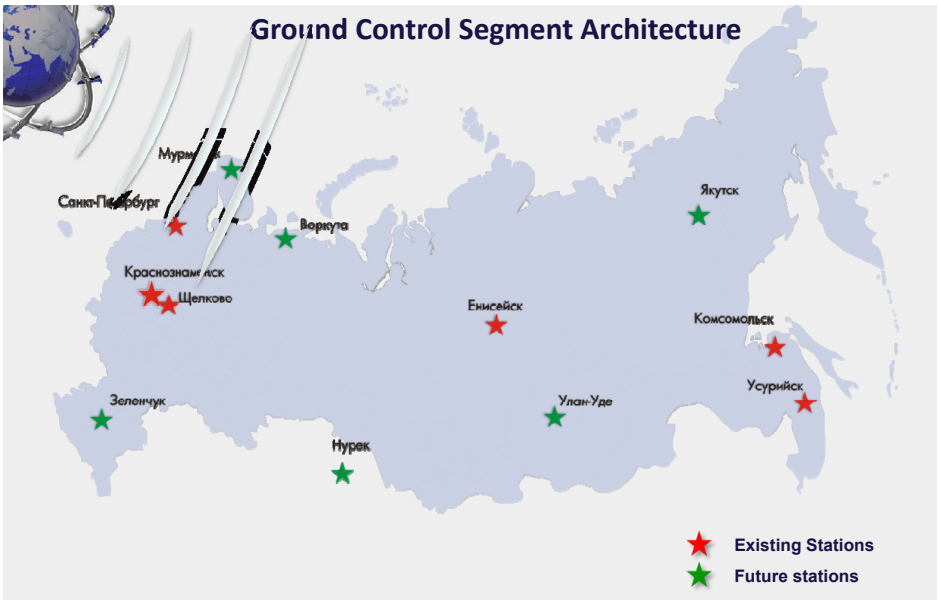

Figure 2.4: Limited geographic distribution of GLONASS monitor stations [82].

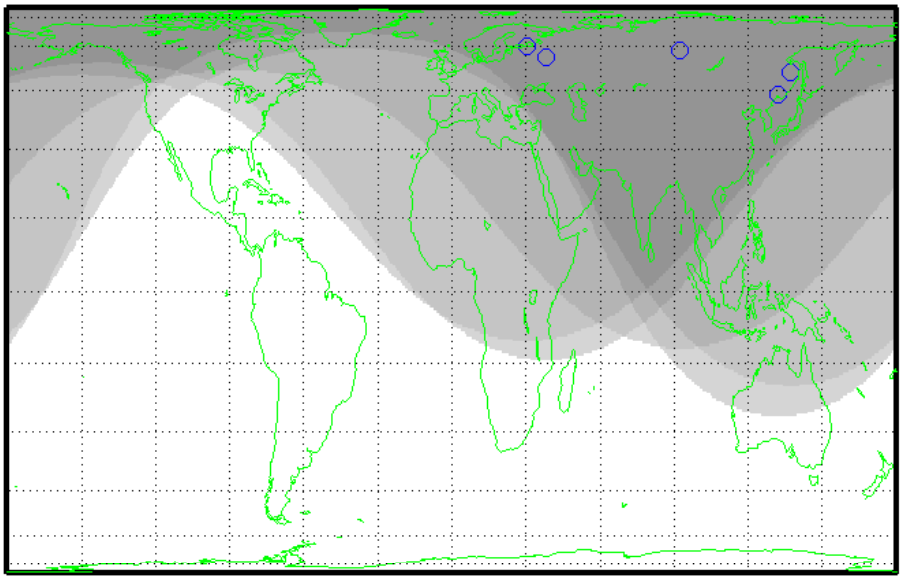

Figure 2.5: GLONASS monitor station tracking coverage (indicated by the shaded areas) is 49.8%. The percentage is calculated based on a 5-degree antenna mask angle and the actual GLONASS constellation from January 2010 to August 2012.

The GLONASS user segment contains both civil and military users as well. The Russia Space Agency has made the accurate, formerly military-only signal freely available to civil users since May 2007 [83].

2.2 Navigation Message

As discussed in Section 2.1, each GPS or GLONASS satellite can be seen as a "bent pipe" of navigation data. A satellite receives predicted navigation data from the ground antennas, and sends them back to the user through the navigation message. Modulated on top of ranging signals, the navigation message usually has a format shown in Figure 2.6. The navigation message generally contains the following items that the user receiver needs to calculate its position.

- Ephemeris parameters: a model of satellite orbits for calculating real-time satellite coordinates with meter-level accuracy;
- Clock corrections: a quadratic or linear model of satellite clock drift for calculating real-time satellite clock biases with meter-level accuracy;

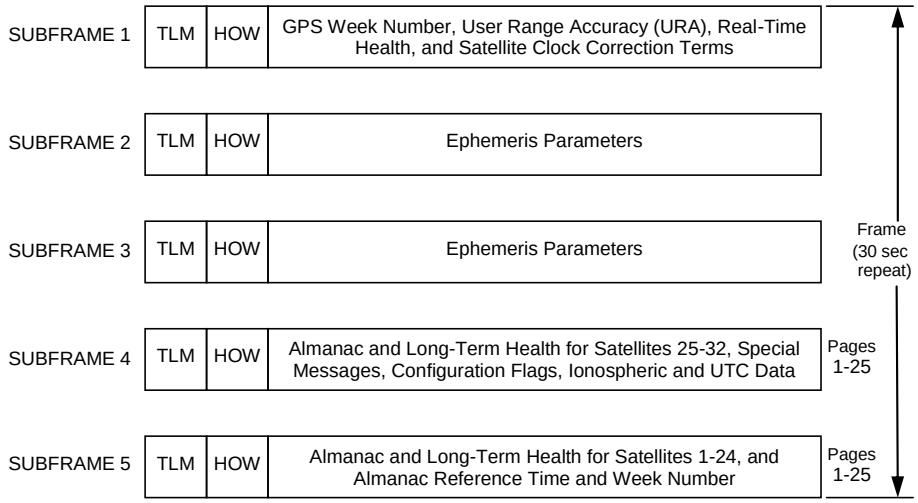

Figure 2.6: GPS navigation message content and format [19]. Each subframe is divided into 10 words. The first word is a telemetry word (TLM), which includes a fixed preamble to assist the receiver in detecting the beginning of a subframe. The next word is the handover word (HOW), which provides the GPS time of week and the subframe number 1–5 [84].

- Integrity and accuracy indicator: a satellite health flag and user range accuracy (URA);
- Ionospheric parameters: a global ionospheric model to allow a single-frequency receiver to correct for ionospheric errors;
- Almanacs: a reduced-accuracy model of satellite orbits for calculating the position of all satellites in the constellation to facilitate signal acquisition.

The rest of this section introduces the format of the GPS and GLONASS navigation message with emphasis on their similarities and differences.

GPS navigation message

The GPS navigation message is formatted into frames of 1500 bits and transmitted at 50 bits per second. One frame is divided into 5 subframes of 300 bits each. The content is illustrated in Figure 2.6. As each frame contains only 1/25 of the total almanac, 12.5 minutes are required to receive the entire almanac from a single satellite.

The GPS ephemeris includes a set of quasi-Keplerian parameters [85] to describe the satellite orbit, as shown in Table 2.1. The GPS Interface Specification [86] provides an

M_0	Mean Anomaly at Reference Time
Δn	Mean Motion Difference From Computed Value
e	Eccentricity
$\sqrt{A}$	Square Root of the Semi-Major Axis
Ω_0	Longitude of Ascending Node of Orbit Plane at Weekly Epoch
i_0	Inclination Angle at Reference Time
ω	Argument of Perigee
$\dot{\Omega}$	Rate of Right Ascension
IDOT	Rate of Inclination Angle
C_{uc}	Amplitude of the Cosine Harmonic Correction Term to the Argument of Latitude
C_{us}	Amplitude of the Sine Harmonic Correction Term to the Argument of Latitude
C_{rc}	Amplitude of the Cosine Harmonic Correction Term to the Orbit Radius
C_{rs}	Amplitude of the Sine Harmonic Correction Term to the Orbit Radius
C_{ic}	Amplitude of the Cosine Harmonic Correction Term to the Angle of Inclination
C_{is}	Amplitude of the Sine Harmonic Correction Term to the Angle of Inclination
t_{oe}	Reference Time Ephemeris (reference paragraph 20.3.4.5)
IODE	Issue of Data (Ephemeris)

Table 2.1: Ephemeris parameters in the GPS navigation message [86].

analytical algorithm to calculate real-time satellite positions. The ephemeris includes the issue of data, ephemeris (IODE) term, an 8-bit integer, which provides the user with a convenient means to detect any change in the ephemeris parameters. The clock corrections also include the issue of data, clock (IODC) term, a 10-bit integer, whose 8 least significant bits (LSBs) should match the IODE.

The GPS control segment typically uploads predicted navigation data to the satellite every 24 hours. A new navigation message is broadcast by the satellite every 2 hours. In nominal conditions, a navigation message is valid for 4 hours after the earliest transmission time of message (TTOM). Figure 2.7 shows the scenario of an ephemeris update. A user receiver is expected to use the latest received ephemeris and not to use any ephemeris that is no longer valid.

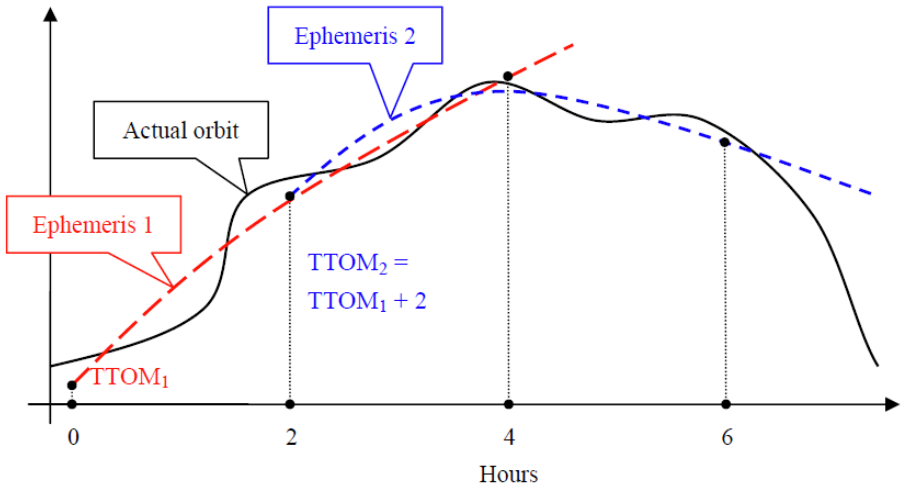

Figure 2.7: Illustration of an ephemeris update. Ephemeris 1 is first transmitted at 0 o'clock, and remains valid until 4 o'clock. Ephemeris 2 is first transmitted at 2 o'clock, and remains valid until 6 o'clock. A broadcast ephemeris matches the actual orbit very well when it is within the 4-hour fit interval.

GPS Time is the reference time used in the GPS navigation message. It is a continuous time scale (without leap seconds) defined by the control segment on the basis of the atomic clocks at the monitor stations and onboard the satellites [72]. The GPS broadcast ephemeris is based on the World Geodetic System 1984 (WGS-84), developed by the US Department of Defense (DoD). The refined frame WGS-84 (G1150) introduced in 2002 agrees with the International Terrestrial Reference Frame 2000 (ITRF2000) at the centimeter level [87, 88].

GLONASS navigation message

As in GPS, the navigation message in GLONASS is also formatted into frames of 1500 bits and transmitted at 50 bits per second. Nevertheless, one frame of a GLONASS navigation message is divided into 15 strings of 100 bits each. Strings 1–4 include immediate data of the transmitting satellite, such as a reference epoch t_e (also referred to as t_b in Section 5 and [78]), healthy flag, ephemeris parameters, and clock corrections. Instead of Keplerian orbital elements, the GLONASS ephemeris consists of the instantaneous satellite position, satellite velocity, and lunisolar acceleration in Earth Centred Earth Fixed (ECEF) Cartesian coordinates, as shown in Table 2.2. Therefore, a numerical integration has to be used to calculate real-time satellite positions within the interval $t_e \pm 15$ minutes [78]. Strings 5–15 include non-immediate data of the other satellites, such as almanac parameters and the GLONASS Time offset with respect to GPS. As each frame contains 1/5 of the total almanac, only 2.5 minutes are required to receive the entire almanac from a single satellite [78]. This is five times faster than receiving the entire almanac from a single GPS satellite.

Parameter	Explanation
t_e	Ephemerides reference epoch
$x(t_e)$	Coordinate at t_e in PZ-90
$y(t_e)$	Coordinate at t_e in PZ-90
$z(t_e)$	Coordinate at t_e in PZ-90
$v_x(t_e)$	Velocity component at t_e in PZ-90
$v_y(t_e)$	Velocity component at t_e in PZ-90
$v_z(t_e)$	Velocity component at t_e in PZ-90
$X''(t_e)$	Moon and sun acceleration at t_e
$Y''(t_e)$	Moon and sun acceleration at t_e
$Z''(t_e)$	Moon and sun acceleration at t_e
$\tau_n(t_e)$	SV clock offset
$\gamma_n(t_e)$	SV relative frequency offset

Table 2.2: Ephemeris and clock parameters in the GLONASS navigation message (adapted from `http://www.navipedia.net/index.php/GLONASS_Satellite_Coordinates_Computation`).

The GLONASS control segment typically uploads predicted navigation data to the satellite twice a day [89]. A new set of immediate data is nominally transmitted every 30 minutes with a valid period from $t_e - 15$ minutes to $t_e + 15$ minutes [78].

GLONASS Time is the reference time used in the GLONASS navigation message. In contrast to GPS, Galileo, and Compass, it implements leap seconds, like UTC [78]. The

GLONASS broadcast ephemeris is based on the Parametry Zemli 1990 (Parameters of the Earth 1990, abbreviated as PZ-90) coordinate frame, which was not very consistent with ITRF [90]. Since September 2007, GLONASS has adopted an improved frame, PZ-90.02, which is much more consistent with ITRF. GNSS users are recommended to use zero transformation parameters between PZ-90.02 and ITRF because the difference is at the sub-meter level and the accurate transformation parameters have not yet been established [89, 91].

2.3 Range Errors

Error sources

In multilateration, the positioning error is dependent on the geometry of receiver-satellite vectors and the errors in the pseudorange measurement. The latter, total pseudorange measurement inaccuracy, is often referred to as user equivalent range error (UERE) in the field of satellite navigation [92]. The three major sources of UERE are listed below [19, 72].

- Control and space segment errors: the pseudorange inaccuracy due to the SIS, also referred to as SIS URE or just URE[7], including satellite ephemeris errors (an example is shown in Figure 2.7), satellite clock errors, satellite antenna variations [93], signal imperfections [94, 95];
- Propagation errors: the pseudorange inaccuracy due to atmospheric propagation modeling, including ionosphere delay compensation errors and troposphere delay compensation errors;
- Measurement errors: the pseudorange inaccuracy due to the receiver and the environment, also referred to as user equipment error (UEE), including multipath and receiver noise.

For a single-frequency receiver, the ionospheric error is usually the largest component in UERE. However, when a dual-frequency receiver is used, the SIS URE becomes the most important factor for positioning accuracy and integrity, especially for airborne navigation where the multipath is less problematic.

[7] In some literature [72], URE is defined to be the total pseudorange inaccuracy. This dissertation follows the definitions in [19], and uses URE and SIS URE interchangeably.

SIS URE and various representations

The SIS URE is dominated by ephemeris and clock errors because antenna variations and signal imperfections are usually at centimeter or millimeter level [93–95]. For an arbitrary ephemeris error and an arbitrary clock error, SIS URE is different for users at different locations on Earth. Neglecting antenna variations and signal imperfections, the instantaneous SIS URE (I URE) for a user at the location $\boldsymbol{u}$ is given by

$$\text{I URE} = (\boldsymbol{r}' - \boldsymbol{r}) \cdot \frac{\boldsymbol{r} - \boldsymbol{u}}{\|\boldsymbol{r} - \boldsymbol{u}\|} - c(b' - b), \tag{2.1}$$

where $\cdot$ is the vector dot product, $\|\boldsymbol{x}\| = \sqrt{\boldsymbol{x} \cdot \boldsymbol{x}}$ is the vector norm, c is the speed of light in vacuum, $\boldsymbol{r}$ is the actual satellite position, b is the actual satellite clock bias, $\boldsymbol{r}'$ is the satellite position calculated from the broadcast ephemeris, and b' is the satellite clock bias calculated from the broadcast clock. Since I URE is spatially dependent, two spatially-independent measures are defined as follows.

- Global average SIS URE (GA URE): the root mean square (rms) URE across the portion of the globe in view of the satellite (see Appendix B and [19] for the derivation), generally a performance metric of SIS accuracy,

$$\text{GA URE} \approx \begin{cases} \sqrt{(0.98R - T)^2 + (A^2 + C^2)/49} & \text{for GPS,} \\ \sqrt{(0.98R - T)^2 + (A^2 + C^2)/45} & \text{for GLONASS,} \end{cases} \tag{2.2}$$

  where R is the radial ephemeris error, A is the alongtrack ephemeris error, C is the crosstrack ephemeris error, and T is the clock error;

- Worst case SIS URE (WC URE): the largest URE across the portion of the globe in view of the satellite, generally a performance metric of SIS integrity,

$$\text{WC URE} = \widetilde{\max}_{|\theta| \le \vartheta}(R\cos\theta - T + \sqrt{A^2 + C^2}\sin\theta), \tag{2.3}$$

  where the function $\widetilde{\max}(x)$ maximizes $|x|$ and returns the corresponding x, θ is the off-nadir angle[8], and the maximum off-nadir angle $\vartheta = 13.85°$ and $14.48°$ for GPS and GLONASS, respectively.

WC URE can be computed either numerically from I UREs or analytically from (R, A, C, T) using the algorithms described in Section 3.5.

[8] An off-nadir angle is the angle between the ray from the satellite to the Earth center and the ray from the satellite to the receiver.

The above equations indicate that the clock error and the radial ephemeris error dominate the URE. In practice, the radial ephemeris error is usually much better modeled and predicted than the clock error, and thus the clock error becomes the decisive factor in the URE.

2.4 Integrity Performance Standard

As introduced in Section 2.2, the GPS navigation message contains a parameter URA, which is intended to be a conservative representation of each satellite's expected GA URE, and is also meant to indicate an upper limit on the likely magnitude of the I UREs [32]. URA is quantized to the levels represented by a 4-bit unsigned index[9] [19, 86, 96], as shown in Table 2.3.

SPS URA Index "N"	Typical Expected URE, 1-sigma	Numerical URA Value, Representing the Bounds on the Expected URE, 1-sigma		
0	2.0 m	0.00 m	< URA ≤	2.40 m
1	2.8 m	2.40 m	< URA ≤	3.40 m
2	4.0 m	3.40 m	< URA ≤	4.85 m
3	5.7 m	4.85 m	< URA ≤	6.85 m
4	8.0 m	6.85 m	< URA ≤	9.65 m
5	11.3 m	9.65 m	< URA ≤	13.65 m
6	16.0 m	13.65 m	< URA ≤	24.00 m
7	32.0 m	24.00 m	< URA ≤	48.00 m
8	64.0 m	48.00 m	< URA ≤	96.00 m
9	128.0 m	96.00 m	< URA ≤	192.00 m
10	256.0 m	192.00 m	< URA ≤	384.00 m
11	512.0 m	384.00 m	< URA ≤	768.00 m
12	1024.0 m	768.00 m	< URA ≤	1536.00 m
13	2048.0 m	1536.00 m	< URA ≤	3072.00 m
14	4096.0 m	3072.00 m	< URA ≤	6144.00 m
15	No Expectation Provided	6144.00 m	< URA	Use at own risk

Table 2.3: URA index to expected URE relationship [19].

In the GPS SPS Performance Standard (PS) [19] as well as the latest version of the Interface Specification [86], the GPS SPS SIS URE integrity standard assures that for any healthy SIS, there is an up-to-10^{-5} probability over any hour of any I URE exceeding the not-to-exceed (NTE) threshold without a timely alert during normal operation. The NTE threshold is currently defined to be 4.42 times the upper bound (UB) on the URA value broadcast by the satellite [19]. Before September 2008, the NTE threshold was defined

[9] There is a plan to extend the URA index to a 5-bit signed integer in order to represent sub-meter accuracy [86].

differently, as the maximum of 30 meters and 4.42 times URA UB [96]. The reason for the "magic" number 4.42 here is the Gaussian assumption of the URE[10], although this assumption is questionable (Section 6.3.2).

In this dissertation, a GPS SIS anomaly is defined as a threat to the SIS integrity, i.e., a condition during which a healthy, trackable SIS results in WC URE exceeding the NTE threshold. Therefore, the SIS anomaly is also referred to as "misleading SIS information" or simply "satellite fault." Since the definition of the NTE threshold is different before and after September 2008, both of the two NTE thresholds are considered in this dissertation for the sake of completeness and consistency.

Unfortunately, the performance standard of GLONASS SIS has not yet been issued. This dissertation employs a statistic-based NTE threshold for GLONASS SIS, as defined in Section 5.2.4.

[10]For a zero-mean Gaussian distribution, ± 4.42 sigma corresponds to a probability level of $1 - 10^{-5}$.

Chapter 3

GPS Anomaly Monitoring

3.1 Two Approaches to Finding Anomalies

According to the definition of SIS anomaly in Section 2.4, finding GPS anomalies consists of the following two steps:

1. Compute the UREs of each satellite at each epoch;
2. Check the WC URE against the NTE threshold.

Section 2.3 indicates that there are two ways to calculate the URE:

$$\text{URE} = \text{projected ephemeris error} + \text{clock error}, \tag{3.1}$$

$$= \text{UERE} - \text{propagation errors} - \text{UEE}. \tag{3.2}$$

The approach (3.1) is based on the fact that the URE is dominated by the ephemeris and clock errors. To calculate the ephemeris and clock errors, we need to compare broadcast ephemeris and clock with the ground truth—the actual satellite position and clock. A good candidate of ground truth is the precise ephemeris and clock generated by some organizations, such as IGS and NGA, which routinely post-process observation data. Although this approach (3.1) has been referred to as a "bottom-up approach" in [97], this dissertation prefers the more intuitive name "space approach" because it seems to need only the information related to the satellite.

The other approach (3.2) is based on the fact that UERE is a sum of URE, the propagation error, and UEE. In this approach, the pseudorange measurements from ground receivers are the ground truth. Therefore, this dissertation refers to it as "ground approach" instead of

	Space approach (3.1)	Ground approach (3.2)
Ground truth	precise ephemerides/clocks	ground observation data
Accuracy	sub-meter level	meter level
Reliability	excellent	so-so (for a single receiver)
Calculation of WC URE	always accurate	depends on receiver's location
Computational cost	low	high
Sampling period	15 minutes	30 seconds
Satellite trackability	no indication	indicated
Suitable for	Anomaly identification	Anomaly verification

Table 3.1: Comparison between two approaches to computing SIS UREs. Pros are in green, while cons are in red.

the abstruse name "top-down approach" used in [97].

Table 3.1 summarizes the pros and cons of both approaches. It can be seen that the space approach is more suitable for detecting anomalies, especially because of the low computational cost. However, the space approach may result in false anomalies for the following two reasons:

- Rare errors may exist in precise ephemerides and clocks;
- A satellite can indicate an unhealthy state through the use of untrackable SIS [19, 21], but neither broadcast nor precise ephemeris/clock data include the information of satellite trackablity.

In addition, precise ephemerides and clocks are usually provided for 15-minute intervals. This sampling rate is too low to enable a detailed depiction of SIS anomalies.

Fortunately, the ground approach can patch the holes in the space approach because ground receiver data indicate satellite trackablity and have a high sampling rate. The disadvantage of low reliability can be mostly alleviated by using the data from multiple receivers. The high computational cost is no longer a problem because only the I UREs of certain satellites during certain periods need to be computed.

Therefore, the whole process of anomaly monitoring consists of two phases:

- Phase I: Anomaly identification using the space approach,
- Phase II: Anomaly verification using the ground approach.

This chapter focuses on the anomaly identification, and Chapter 4 is devoted to the anomaly verification. The remainder of this chapter is organized as follows. Section 3.2 outlines the whole process of anomaly identification. Sections 3.3 to 3.5 describe data sources, our data cleansing algorithm, and our anomaly detection method, respectively. Section 3.6 presents all the anomalies identified in the past 12 years. Finally, a summary appears in Section 3.7.

3.2 Overview of Anomaly Identification

In the space approach, GPS SIS anomalies are identified by comparing broadcast ephemerides and clocks with precise values determined by post-processing. As shown in Figure 3.1, the whole process consists of three steps: data collection, data cleansing, and anomaly detection.

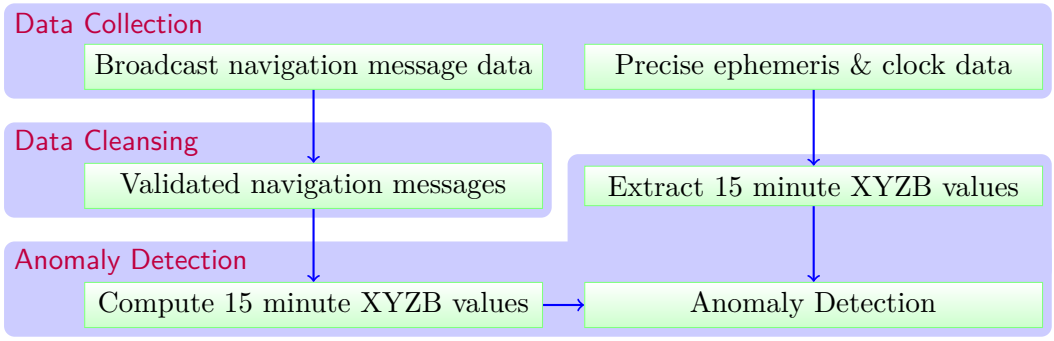

Figure 3.1: Whole process of GPS SIS anomaly identification. XYZB values refer to satellite coordinates and clock bias.

In the first step, the navigation message data files are downloaded from IGS. Two different products of precise ephemerides and clocks are downloaded from IGS and NGA, respectively. The details about these data sources are discussed in Section 3.3.

As each GPS satellite can be observed by many IGS stations at any instant, each navigation message is logged redundantly. In the second step, a data cleansing algorithm exploits the redundancy to correct the errors made on the ground. This step distinguishes our work from most previous work [45, 47, 48, 50, 97] because the false anomalies due to data-logging errors would otherwise be very troublesome.

The last step is computing WC UREs and detecting SIS anomalies. The validated navigation messages prepared in the second step are used to propagate broadcast orbits/clocks

at 15-minute intervals coinciding with the precise values. WC UREs are computed from a comparison between the broadcast and precise satellite orbits/clocks. A potential SIS anomaly is then detected by checking WC UREs against the SIS URE NTE threshold.

The details of the algorithms introduced above are thoroughly discussed in Sections 3.4 and 3.5.

3.3 Data Sources

3.3.1 Broadcast navigation message data

Broadcast GPS navigation message data files are publicly available at the IGS website [98]. All the data are archived in the receiver independent exchange (RINEX) n-type format [99], which includes not only the ephemeris/clock parameters broadcast by satellites but also some necessary information produced by ground receivers, such as the pseudorandom noise (PRN) signal number and the transmission time of message (TTOM).

The IGS tracking network is made up of more than 300 volunteer stations all over the world (a map is shown in Table 3.2) to ensure seamless, redundant data logging. Each station generates one data file per day, which is expected to include all the navigation messages it receives on that day. As broadcast navigation messages are usually updated every 2 hours (Figure 2.7), no single station can record the navigation messages broadcast by all the GPS satellites. For the ease of users, two of the IGS archive sites, Crustal Dynamics Data Information System (CDDIS)[1] and Scripps Orbit and Permanent Array Center (SOPAC)[2], provide two kinds of ready-to-use daily global combined broadcast navigation message data files, `brdc`*`ddd`*`0.`*`yy`*`n` [102] and `auto`*`ddd`*`0.`*`yy`*`n` [103], respectively. Unfortunately, these files sometimes contain data-logging errors. The data-logging errors result in false anomalies, which can be 11 times more than true anomalies, as shown in Section 3.6.2.

Therefore, we devise and implement a data cleansing algorithm to generate the daily global combined navigation messages as close as possible to the navigation messages that the satellites actually broadcast. This algorithm makes use of all available raw navigation message data files from all IGS stations to vote each value in a navigation message. As every

[1] CDDIS is a dedicated data bank to archive and distribute space geodesy related data acquired by the National Aeronautics and Space Administration (NASA), IGS, and other national and international programs [100]. CDDIS is located at NASA Goddard Space Flight Center in Greenbelt, MD.

[2] SOPAC archives high precision geodetic and geophysical measurements for the study of geophysics and meteorology [101]. SOPAC is located at University of California, San Diego in La Jolla, CA.

value in our navigation messages is validated by a majority of the raw data, we refer to our navigation messages as "validated navigation messages," as shown in Figure 3.1. The data cleansing algorithm is detailed in Section 3.4.

3.3.2 Precise ephemeris and clock data

Precise GPS ephemerides and clocks are regarded as ground truth in this dissertation because they are accurate to a few centimeters [104–107]. These data are usually provided in the Extended Standard Product 3 Orbit Format (SP3) [108].

The precise data are generated by some organizations such as IGS and NGA, which each own a global receiver network and routinely post-process observation data. The IGS precise GPS data are a weighted-mean combination of the independent precise ephemeris and clock estimates generated by a number of IGS Analysis Centers (ACs). Each AC uses its own processing strategy to post-process the observation data collected by the IGS stations it trusts. The NGA precise GPS data are generated by post-processing the observation data from its owns tracking network, the OCS monitor stations (Figure 2.3), and three selected IGS stations. The NGA precise ephemerides and clocks are considered the DoD standard

IGS tracking network	NGA tracking network
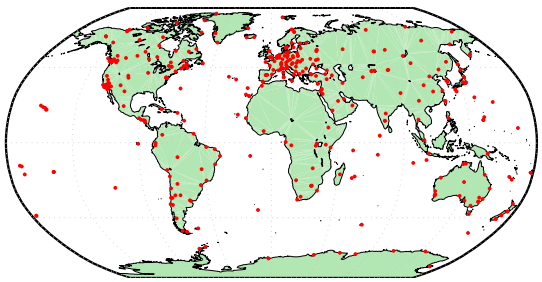	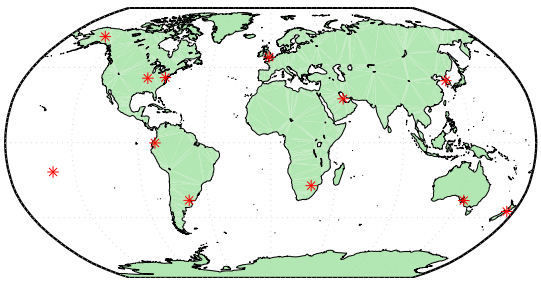
Publicly available data since 1994 or earlier	Publicly available data since 2004-01-04
Bad/absent data†: 1.5%	Bad/absent data†: 0.009%
Every 15 minutes synchronized to either GPS Time (before 2004-02-21) or IGS Time (after 2004-02-22)	Every 15 minutes (before 2012-02-27) or 5 minutes (after 2012-02-28) synchronized to GPS Time
Center of Mass only, no Antenna Phase Center	Both Center of Mass and Antenna Phase Center

† Statistics of the data from 2006-11-05 to 2008-10-04

Table 3.2: Comparison of IGS and NGA precise ephemeris/clock data.

and used in the quality control for GPS operations [76].

Table 3.2 shows a side-by-side comparison between the IGS and NGA precise ephemeris/clock data, in which the green- and red-colored text indicates pros and cons, respectively. For NGA data, the only issue is that the data have been publicly available since 2004-01-04 [75]. Accordingly, for the broadcast ephemerides/clocks before 2004-01-03, the IGS precise ephemeris/clock is the only reference. As for the IGS precise ephemerides/clocks, care must be taken when using them due to the following three issues.

The first issue with the IGS precise ephemerides/clocks is the relatively high rate of bad/absent data, as shown in the third row of Table 3.2. For a GPS constellation of 30 healthy satellites, 1.5% bad/absent data is tantamount to unavailable precise ephemerides or clocks for approximately 11 satellite-hours per day! This issue can result in undetected anomalies (false negatives).

The second issue is that, as shown in the fourth row of Table 3.2, IGS has switched to IGS Time [109] for their precise ephemeris/clock data since 2004-02-22. The IGS clock is not synchronized to GPS Time and the differences between the two time references can reach as large as 3 meters [50]. Fortunately, the time offsets can be extracted from the IGS clock data files [106]. Besides, a similar problem is that the IGS precise ephemeris is based on ITRF, whereas the broadcast GPS ephemeris is based on WGS-84. Nevertheless, a transformation is not considered necessary in this dissertation because the differences between ITRF and WGS-84 are on the order of a few centimeters, as discussed in Section 2.2.

The last, but not the least important issue with the IGS precise ephemerides is that the data are provided only for the satellite center of mass (CoM). Because the broadcast ephemerides are based on the antenna phase center (APC), the CoM data must be converted into the APC before being used. Both IGS and NGA provide antenna corrections for every GPS satellite [110, 111]. In spite of the fact that the IGS CoM values usually match the NGA CoM values to a few centimeters [107], the IGS satellite antenna corrections differ considerably from the NGA's—for some GPS satellites, the difference in radial axis can reach as large as 1.6 meters [112]. The disagreement on the antenna corrections is mainly due to the different methods used to produce them: the IGS antenna corrections are based on the statistics from more than 10 years of IGS data, while the NGA's are probably from the calibration measurements on the ground [112]. In order to know whose satellite antenna corrections can better match the broadcast ephemerides, the broadcast orbits for all GPS satellites in 2009 are computed and compared with three different precise ephemerides: IGS

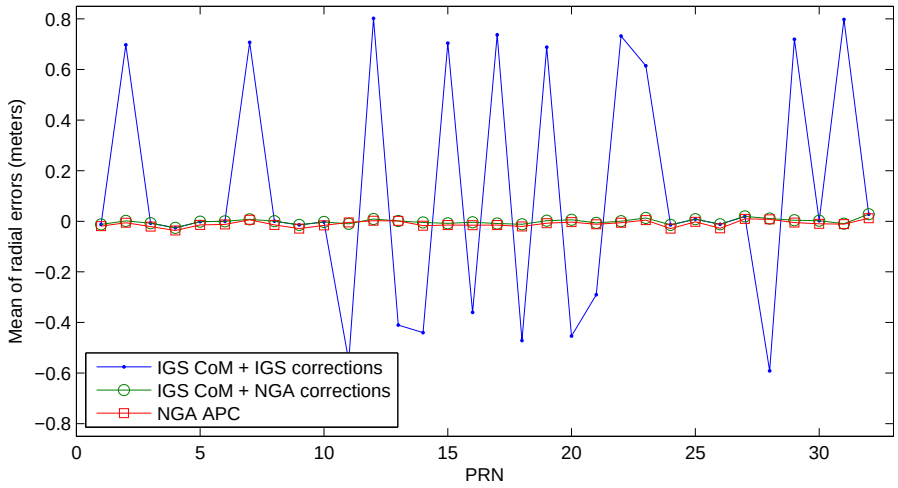

Figure 3.2: Comparison between the NGA and IGS antenna corrections. The NGA antenna corrections match the broadcast ephemeris better than the IGS antenna corrections.

CoM + IGS antenna corrections, IGS CoM + NGA antenna corrections, and NGA APC. The 20% trimmed mean[3] of radial ephemeris errors for each satellite is plotted in Figure 3.2. Generally, radial ephemeris errors are expected to have a zero mean, just as the green curve "IGS CoM + NGA antenna corrections" and red curve "NGA APC" in Figure 3.2. However, the combination "IGS CoM + IGS antenna corrections" results in radial ephemeris errors with an obvious non-zero mean for more than half of the GPS satellites. Therefore, the NGA antenna corrections are chosen to convert the IGS CoM data into the APC.

3.4 Data Cleansing

Figure 3.3 illustrates a scenario of data cleansing. A small proportion of the navigation data files from the IGS stations have defects such as losses, duplications, inconsistencies, discrepancies, and errors, as shown in Table 3.3. These data-logging errors are mainly due to accidental bad receiver data and various hardware/software bugs. Therefore, more than just removing duplications, the generation of our validated daily global combined navigation messages is composed of two complicated steps: voter registration and voting.

[3]Also known as truncated mean. A $100\alpha\%$ trimmed mean function, $\text{mean}_\alpha(\cdot)$, calculates the mean after discarding the samples at the $50\alpha\%$ high end and $50\alpha\%$ low end. As a robust estimator of central tendency, the trimmed mean is actually a compromise between the mean and the median [113].

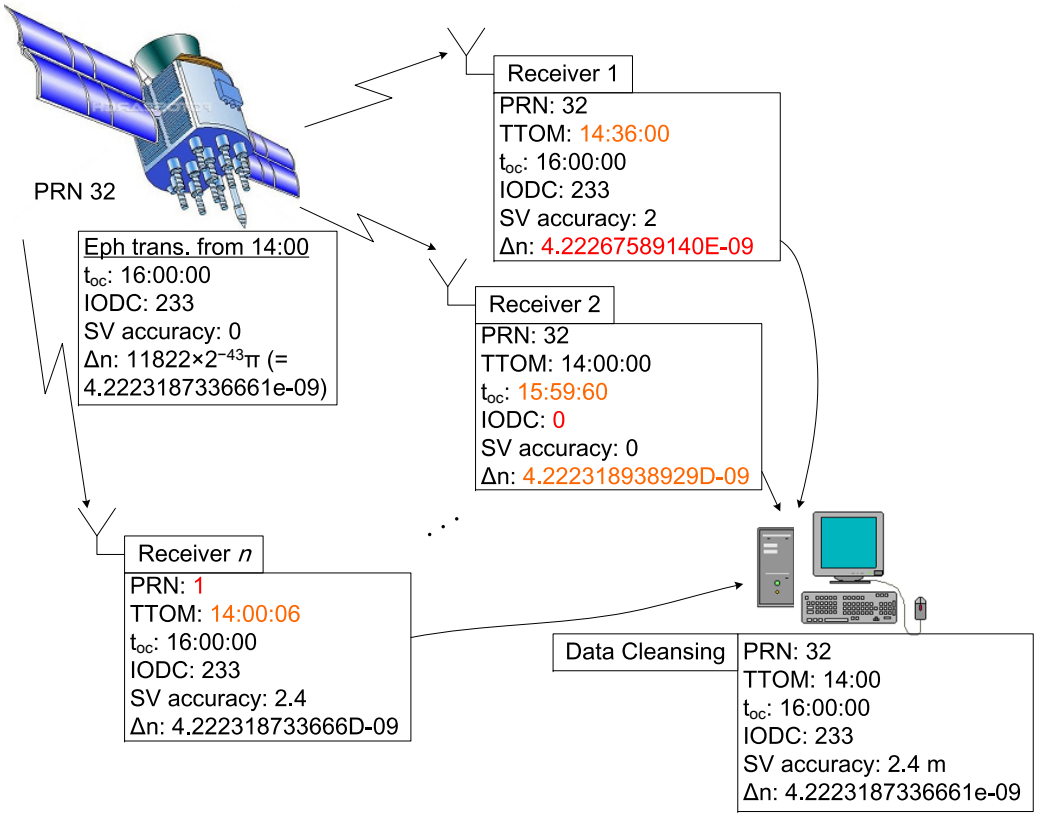

Figure 3.3: A scenario of data cleansing. The GPS satellite PRN 32 started to transmit a new navigation message at 14:00:00. Receiver 1 had not tracked the satellite until 14:36:00, and thus the TTOM in its record was 14:36. Additionally, Receiver 1 made a one-bit error in Δn ($4.22267589140 \times 10^{-9} \approx 11823 \times 2^{-43}\pi$). Receiver 2 perhaps had some bugs in its software: the IODC was unreported, and the reference time of clock (t_{oc}) and Δn were written in an unusual way. Receiver n used an incorrect ranging code, PRN 1, to despread and decode the signal of PRN 32; fortunately, all the parameters except TTOM were perfectly recorded. Moreover, the three receivers interpreted URA in different ways. A computer equipped with our data cleansing algorithms is used to process all the data from the receivers. The receiver-induced errors are corrected and the original navigation message is recovered.

Voter registration Suppose that we want to generate the validated navigation messages for all GPS satellites on Day n. In the first step, we apply the following operations sequentially to the navigation data files collected by each IGS station between Day $n-1$ and Day $n+1$:

1. Various floating-point representations of the same parameter value

```
ffmj0190.09n: 17  9  1 19  2  0  0.0 0.446424819529E-04 0.909494701773E-12 ...
ganp0190.09n: 17 09  1 19  2  0  0.0 4.464248195291D-05 9.094947017729D-13 ...
glsv0190.09n: 17 09  1 19  2  0  0.0 4.464250000000D-05 9.094950000000D-13 ...
```

2. Incorrect PRN number

```
adis2000.08n (Line 186-188):
32  8  7 18  3 59 44.0 0.307788141072E-03 0.284217094304E-11 0.000000000000E+00
    0.420000000000E+02 0.883750000000E+02 0.394552148966E-08 0.291634527708E+01
    0.458024442196E-05 0.139177759411E-01 0.104866921902E-04 0.515382606506E+04
ffmj2000.08n (Line 202-204):
 1  8  7 18  3 59 44.0 0.307788141072E-03 0.284217094304E-11 0.000000000000E+00
    0.420000000000E+02 0.883750000000E+02 0.394552148966E-08 0.291634527708E+01
    0.458024442196E-05 0.139177759411E-01 0.104866921902E-04 0.515382606506E+04
```

3. Incorrect/inconsistent t_{oc}

```
davr0140.08n: 15 08  1 14  9 59 44.0 -.714603811502D-04 -.102318153949D-11 ...
glsv0140.08n: 15  8  1 14  9 59  4.0-0.714604000000E-04-0.102318000000E-11 ...
bucu0020.08n: 18  8  1  2 10  0  0.0-2.151140943170D-04 2.728484105319D-12 ...
trev0020.08n: 18  8  1  2  9 59 60.0-2.151140943170D-04 2.728484105319D-12 ...
```

4. Unreported values such as issue of data, clock (IODC) and URA

```
zouf3410.07n (Line 1407-1414):
 1 07 12  7 22  0  0.0 1.711458899081D-04 2.387423592154D-12 0.000000000000D+00
    9.000000000000D+00-1.070312500000D+02 3.856232056115D-09-1.532781392555D+00
                    ... ... (4 lines omitted) ... ...
    2.000000000000D+00 0.000000000000D+00-3.725290298462D-09 9.000000000000D+00
    5.040000000000D+05 4.000000000000D+00
bucu3410.07n (Line 1420-1427):
 1  7 12  7 22  0  0.0 1.711458899081D-04 2.387423592154D-12 0.000000000000D+00
    9.000000000000D+00-1.070312500000D+02 3.856232056115D-09-1.532781392555D+00
                    ... ... (4 lines omitted) ... ...
    0.000000000000D+00 0.000000000000D+00 0.000000000000D+00 0.000000000000D+00
    5.112000000000D+05 0.000000000000D+00 0.000000000000D+00 0.000000000000D+00
```

Table 3.3: Examples of inconsistencies/errors/losses in navigation message data files.

1. Parse the RINEX n-type file;
2. Recover the least significant bit (LSB);
3. Classify URA values;
4. Remove the navigation messages not on Day n;
5. Remove duplications;
6. Add all remaining navigation messages into a set O.

The reason why the data files on Day $n \pm 1$ are considered is that some navigation messages around midnight may be mistakenly included in a data file one day before or after. The duplication removal is applied here because some stations write many copies of one navigation message in one data file, which violates the principle of voting: one station one vote for each navigation message. The details about LSB recovery, URA classification, and duplication removal are explained in Sections 3.4.1, 3.4.2, and 3.4.3, respectively.

Voting At the end of the first step, we have the set O that includes all the navigation messages broadcast by all the GPS satellites on Day n. The set O still has duplications because a broadcast navigation message can be reported by many IGS stations. A duplication removal algorithm similar to the one used in the first step is applied to remove all the duplications and vote correct parameters (Section 3.4.3). Then the correct TTOM is found for each navigation message (Section 3.4.4). Finally, the navigation messages confirmed by a large number of stations are kept, whereas those confirmed by only a few stations are discarded (Section 3.4.5).

3.4.1 LSB recovery

The ephemeris and clock parameters in broadcast navigation messages are fixed-point numbers $\alpha \times 2^{\beta}$, where α is a signed or unsigned γ-bit integer, and 2^{β} is the scale factor, i.e., LSB [86]. The LSB exponent β and the number of bits γ may vary from parameter to parameter. The maximum value of γ is 32. In RINEX n-type format, however, all the parameters are described by 12-decimal-digit floating-point numbers. In spite of the fact that the 12 digits are precise enough to represent the parameter with even 32-bit precision, various software implementations lead to different representations of the same parameter value, as shown by the first row in Table 3.3. Figure 3.3 illustrates another example of an apparent mismatch of the ephemeris parameter Δn, `4.222318938929D-09` in the file `str13640.08n` versus `4.222318733666D-09` in the file `syog3640.08n`. They look different but are actually the same because Δn in the navigation message has only 16-bit precision.

To solve this problem, we employ an LSB recovery algorithm. It converts every floating-point number into its closest original format, a fixed-point number $\alpha \times 2^{\beta}$, and then converts the fixed-point number back to a double-precision floating-point number. After this step, any essentially equivalent values are converted into identical floating-point numbers in computer's memory.

3.4.2 URA classification

As introduced in Section 2.4, URA is represented by a 4-bit unsigned index in the navigation message. In RINEX n-type format, URA values in meters have been adopted since 1993 [99]. However, some IGS stations still use URA indices in their data files. An even more complicated issue is that one URA index corresponds to three possible values in meters: the typical, the lower bound of, and the upper bounds of expected URE, as shown in Table 2.3. A telling example of this chaos is from the CDDIS `brdc`*`ddd`*`0.`*`yy`*`n` files. In `brdc1290.07n`, all the URA values are in the set {2, 2.8, 4, 5.7, 8}, which are the typical expected UREs in meters. Just one day later, in `brdc1300.07n`, all the URA values are in the set {0, 1, 2, 3, 4, 8}, which are most likely the URA indices.

Fortunately, the usage of URA in a single data file is usually consistent. Therefore, this problem can be solved by a simple pattern-recognition-based 6-step classifier: the URA values in a data file are

1. The typical expected URE if all the URA values that are not greater than 4096 are in the set {2, 2.8, 4, 5.7, ..., 4096};
2. The upper bounds of expected URE if all the URA values that are not greater than 6144 are in the set {2.4, 3.4, 4.85, 6.85, ..., 6144};
3. The lower bounds of expected URE if all the URA that are not greater than 3072 are in the set {0, 2.4, 3.4, 4.85, ..., 3072};
4. The URA indices offset by +1 if all the URA values are in the set {1, 2, 3, ..., 16};
5. The URA indices if all the URA values are in the set {0, 1, 2, 3, ..., 15}; or
6. Unknown URA representations.

The unknown URA representations are still regarded as the URA in meters and quantized to the nearest typical expected UREs.

Admittedly, this simple sequential classifier is not a panacea. As an extreme example, a data file including the URA indices only in the set {2, 4, 8} will be incorrectly classified as the typical expected URE. However, this situation is rare in practice and the voting algorithm in Section 3.4.3 can correct these errors. Hence, although a more sophisticated classifier based on the historical statistics of each station could be considered, the resulting performance improvement is too marginal to be worthy of the increased computational complexity.

3.4.3 Duplication removal and majority voting

Duplication removal and majority voting is the most complicated operation in data cleansing. As mentioned at the beginning of this section, duplication removal and majority voting play a dual role. The first role is removing the duplicated navigation messages from one station because a few IGS stations write several copies of a single navigation message into one data file. The second role is removing the duplicated navigation messages from the set O (please refer to the beginning of this section for the definition of the set O). Because different stations may have different interpretations of a single broadcast navigation message, the second role is much more challenging, as described below.

After the LSB recovery and the URA classification, there are still some errors and inconsistencies in the set O. Several examples of typical problems are shown in Table 3.3 and also in [49]. Fortunately, most ephemeris and clock parameters (Table 2.1) in navigation message data files are usually reported correctly. Even when errors happen, the errors are so random that it is unlikely for many stations to agree on the same incorrect value. In this chapter, these parameters are referred to as robust parameters. On the contrary, some parameters, such as TTOM, PRN, URA and IODC, are more likely to be erroneous and when errors happen, several stations may make the same mistake. These parameters are referred to as fragile parameters. The causes of the fragile parameters include the physical nature (e.g., TTOM, PRN) and the carelessness in hardware/software implementations (e.g., URA, IODC).

The robust parameters are utilized to decide whether two logged navigation messages are variants from a single broadcast navigation message—two navigation messages are deemed identical if and only if they agree on all the robust parameters, although their fragile parameters can be different. Then, for a set of navigation messages whose robust parameters are identical, voting is applied to their fragile parameters except TTOM (the correct TTOM is found by a more sophisticated algorithm described in Section 3.4.4) under the principle that the majority is usually correct. Therefore, the goal of duplication removal and majority voting is a set P, in which any navigation message must have at least one robust parameter different from any other and has all fragile parameters confirmed by the largest number of stations that report this navigation message. P can be built by the algorithm below:

1. Initialize P to an empty set.
2. For each navigation message e in O, if there is already a navigation message f in P

having the same robust parameters as e then add the fragile parameters of e into f's database of fragile parameters; otherwise, add e into P.

3. For each navigation message f in P, vote each fragile parameter (except TTOM) according to f's database, and record the number of stations that report f.

3.4.4 TTOM estimation

TTOM is not a parameter in the broadcast navigation message but is recorded by each tracking station whenever it receives a new navigation message. As shown in Figure 2.7, it is important and necessary to know the correct TTOM because it determines which navigation message should be used in computing broadcast satellite orbits and clocks at a certain time.

Unfortunately, the correct TTOM cannot be simply determined by the earliest one because some IGS stations occasionally report an incorrect TTOM earlier than the actual. Nor can the correct TTOM be simply determined by the most frequent one. The reason is that, as the IGS stations are not evenly distributed on Earth, when a satellite starts to broadcast a new navigation message, it may be visible to only a few stations before it is

0. Original TTOMs								
	581412	597600	-7188	-7170	597630	-7170	-7170	0
1. Resolve the ambiguity due to GPS week cutover								
	-23388	-7200	-7188	-7170	-7170	-7170	-7170	0
2. Round to the latest 30 second epoch								
	-23400	-7200	-7200	-7170	-7170	-7170	-7170	0
3. Find the median value m								
	-23400	-7200	-7200	-7170	-7170	-7170	-7170	0
4. Discard all the values earlier than $m - 7200$ or later than $m + 7200$								
	~~-23400~~	-7200	-7200	-7170	-7170	-7170	-7170	0
5. Find the earliest value confirmed by 2 stations or more								
	~~-23400~~	-7200	-7200	-7170	-7170	-7170	-7170	0

Table 3.4: Procedure for finding the correct TTOM with examples.

seen by many stations.

Therefore, we develop a rather sophisticated procedure to solve this problem, as shown in Table 3.4. The first step is necessary because when there is a GPS week cutover [86], some receivers report the TTOM in GPS seconds of the previous GPS week, while the other receivers report the TTOM in GPS seconds of the current GPS week[4]. The reason for the second step is that each frame begins at the 30-second epoch (Section 2.2). In the third step, the median is used rather than the mean because the latter is very sensitive to outliers. The fourth step eliminates outliers by discarding the values earlier than $m - 7200$ or later than $m + 7200$ because the navigation message is usually updated every 2 hours. The last step requires the confirmation of at least 2 stations in order to eliminate any remaining outliers.

3.4.5 Minority discard

After the operations above, we have a set P in which there are no duplicated navigation messages in terms of robust parameters. In addition, all fragile parameters in P are as correct as possible. Nevertheless, a few navigation messages in P still have errors in their robust parameters. These unwanted navigation messages feature a small number of reporting stations. Hoever, it is not easy to set an appropriate threshold n_{th}, and delete all the navigation messages confirmed by n_{th} stations or less, because the IGS stations are not evenly distributed and sometimes a correct navigation message may be confirmed by a handful of stations. If n_{th} is too large, correct navigation messages may be discarded; if n_{th} is too small, incorrect navigation messages may be kept. Hence, a uniqueness criterion must be used to help determine the correct navigation messages.

IODC is a good candidate for the uniqueness criterion because for each GPS satellite, the transmitted IODC is expected to be different from any IODC transmitted during the preceding seven days [86]. Therefore, all navigation messages in P are screened; whenever several navigation messages have the same PRN and IODC, only the one confirmed by the largest number of stations is kept, whereas the others are discarded.

This IODC-based method is effective in most cases, but not always because the actual GPS system does not always meet the specification. As revealed in [63], an IODC may be occasionally reused by a satellite within a day. In such cases, the IODC-based method may discard some correct navigation messages. Thus, the reference time of clock (t_{oc}) is

[4]Our previous papers [63–66] neglected this step and resulted in a false anomaly—PRN 19 on 2007-05-20 [67].

chosen as a backup uniqueness criterion. Because of the the extremely low probability of two different navigation messages having the same IODC and t_{oc}, the correct navigation messages discarded by the IODC-based method can be retrieved by the t_{oc}-based method.

Since most incorrect navigation messages are excluded by the uniqueness criterion, a small threshold, e.g., $n_{\text{th}} = 9$, is used to remove all remaining incorrect navigation messages.

Finally, two versions of validated broadcast navigation messages, `sugl`*`ddd`*`0.`*`yy`*`n` and `sugl`*`ddd`*`1.`*`yy`*`n`[5], based on the IODC uniqueness criterion and the t_{oc} uniqueness criterion, respectively, are generated and stored in the RINEX n-type format. In the `sugl`*`ddd`*`m.`*`yy`*`n` files, we take advantage of the last two spare fields in the RINEX n-type format to store the following confidence information:

$$f_1 = t_0 + t_2/t_0, \quad f_2 = t_1 + t_3/t_0, \tag{3.3}$$

where t_0 is the total number of stations that report the navigation messages with the same PRN and IODC/t_{oc}, t_1 is the number of stations report the most frequent navigation message (the one kept in `sugl`*`ddd`*`m.`*`yy`*`n), t_2 is the number of stations that report the second most frequent navigation message (discarded) with the same PRN and IODC/t_{oc} but with at least one parameter different from the most frequent one, and t_3 is the number of stations that report the third most frequent (discarded, too). It is easy to see that $t_0 \geq t_1 + t_2 + t_3$ and $t_1 \geq t_2 \geq t_3$. Therefore, the four integers, $t_0, \ldots, t_3$, are able to be stored in two floating-point fields using (3.3). A large t_0 with $t_1 \approx t_0$, $t_2 \ll t_1$, and $t_3 \ll t_1$ indicates high confidence in this navigation message. Conversely, $t_2 \approx t_1$ may indicate something wrong, such as an IODC reuse problem [63].

3.5 Anomaly Detection

The validated broadcast navigation messages prepared in Section 3.4 are used to propagate broadcast satellite orbits and clocks using the algorithms in [86]. For each 15- or 5-miniute epoch t that coincides with precise ephemerides/clocks, the latest transmitted broadcast ephemeris/clock is chosen to calculate the WC URE.

The WC URE can be calculated either numerically or analytically. The brute-force numerical method is as follows:

[5]The filename follows the convention of RINEX format. The prefix `sugl` stands for Stanford University GPS Laboratory.

1. Generate a grid over Earth;
2. For each satellite at each epoch,
   (a) Compute I URE for the receiver at each node of the grid;
   (b) Find the I URE with the greatest absolute value.

This method is accurate as long as the grid is dense enough; a dense grid, however, leads to a heavy computational burden. Therefore, the geometric method is preferred. As shown in Figure 3.4, we assume Earth is a perfect sphere and calculate the WC URE using the following algorithm.

1. Find the plane that contains the center of Earth and the ephemeris error vector $\vec{v}$;
2. Find the angle α using the inner product, and β using the law of sines (please note that $\gamma = 90° + \text{mask angle}$);
3. Find the maximum and the minimum projection of $\vec{v}$ in the cone:

$$l_{\max} = \max_{|\theta| \le \beta} |v| \cos(\alpha + \theta),$$
$$l_{\min} = \min_{|\theta| \le \beta} |v| \cos(\alpha + \theta);$$

4. Find $l_{\max} - cB$ and $l_{\min} - cB$, where c is the speed of light and B is the satellite clock error. The one with the greatest absolute value is the WC URE.

The geometric method outperforms the brute-force method in terms of the computational

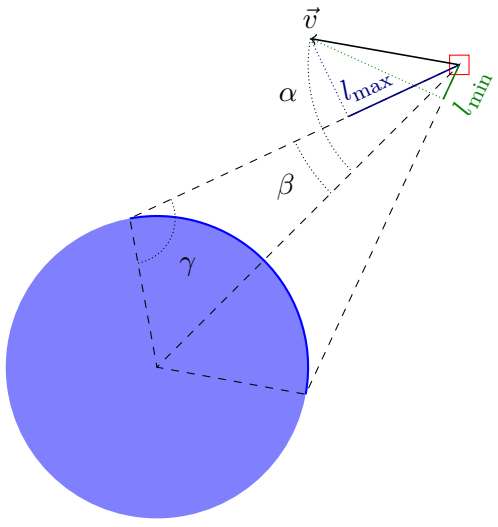

Figure 3.4: Geometric method for calculating the WC URE

complexity. A flaw of the geometric method is the assumption of a perfect sphere for Earth. Fortunately, the resulting approximation error is not more than 0.6%, perfectly acceptable for the purpose of this study.

Finally, a GPS SIS anomaly is claimed when all the following conditions are fulfilled.

- The WC URE exceeds the NTE threshold (see Section 2.4 for the definition);
  - GPS SPS PS 2001: $\max\{30 \text{ m}, 4.42 \cdot \text{URA UB}\}$,
  - GPS SPS PS 2008: $4.42 \cdot \text{URA UB}$;
- The broadcast navigation message is healthy, i.e.,
  - The RINEX field `SV health` [99] is 0, and
  - The URA UB $\leq$ 48 meters [19];
- The broadcast navigation message is in its fit interval, i.e., $\Delta t = t - \text{TTOM} \leq 4$ hours;
- The precise ephemeris/clock is available and healthy.

3.6 Identified GPS SIS Anomalies

A total of 454,335,307 GPS navigation messages collected by on average 400 IGS stations from 2000-06-01 (one month after the deactivation of SA) to 2012-07-16 have been processed. The NGA APC precise ephemerides/clocks and the IGS CoM precise ephemerides/clocks with the NGA antenna corrections are employed as the truth references. Both old and new NTE thresholds [19, 96] are used to detect anomalies.

Before interpreting the results, it should be noted that there are some limitations due to the data sources and the anomaly detection criteria. First, false anomalies may be claimed because there may be some errors in the precise ephemerides/clocks or the validated navigation messages. Second, some short-duration anomalies may not show up if they happened to fall into the 15-minute gaps of the precise ephemerides/clocks[6]. Third, some true anomalies may not be detected if the precise ephemerides/clocks are temporarily missing. The third limitation is especially significant for the results before 2004-01-03, because only the IGS precise ephemerides/clocks are available, which feature a high rate of bad/absent data[7]. Last but not least, users might not experience some anomalies because the satellites

[6]This situation has been alleviated since 2012-02-28, when NGA started providing 5-minute precise ephemerides/clocks (Table 3.1). Interpolating precise ephemerides and clocks can completely solve this problem (Section 7.3.1).

[7]For instance, the IGS precise clocks for PRN 23 was absent on 2004-01-01. The PRN 23 clock anomaly

were not trackable [19,21] at that time. Therefore, all the SIS anomalies identified in Phase I are potential and under further investigation in Phase II.

3.6.1 GPS SIS integrity performance evolution

A total of 1256 potential SIS anomalies are identified per SPS PS 2008 (or 377 potential SIS anomalies per SPS PS 2001). Figure 3.5 shows all these anomalies in a Year-SVN plot. In the figure, the horizontal lines depict the periods when the satellites were operational

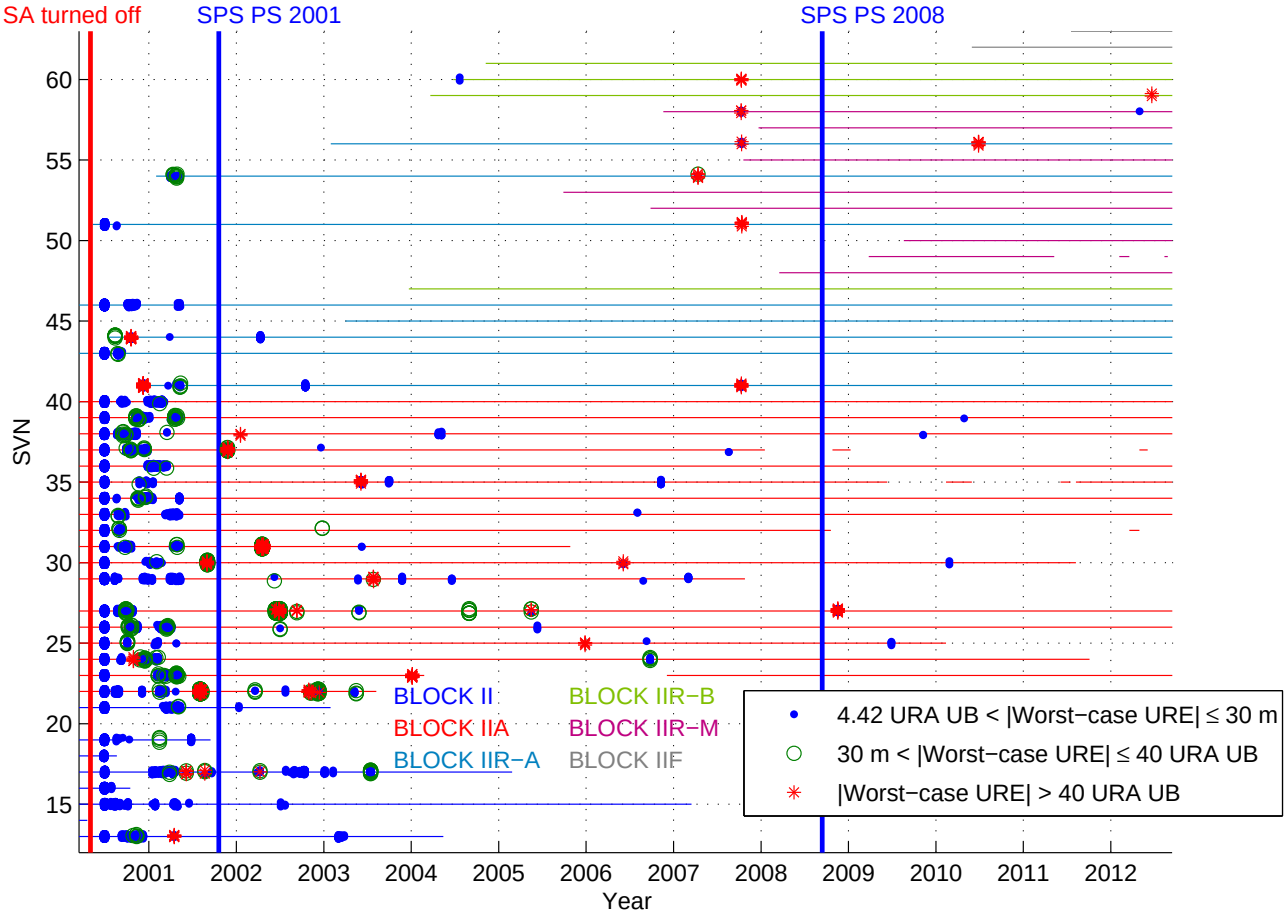

Figure 3.5: Identified GPS SIS anomalies between 2000-06-01 and 2012-07-16. The horizontal lines depict the periods when the satellites were operational (not necessarily healthy). The color of the lines indicates the satellite's block type.

occurred on that day [41,114] would have been missed if a third precise clock product was not tried (Table 3.5).

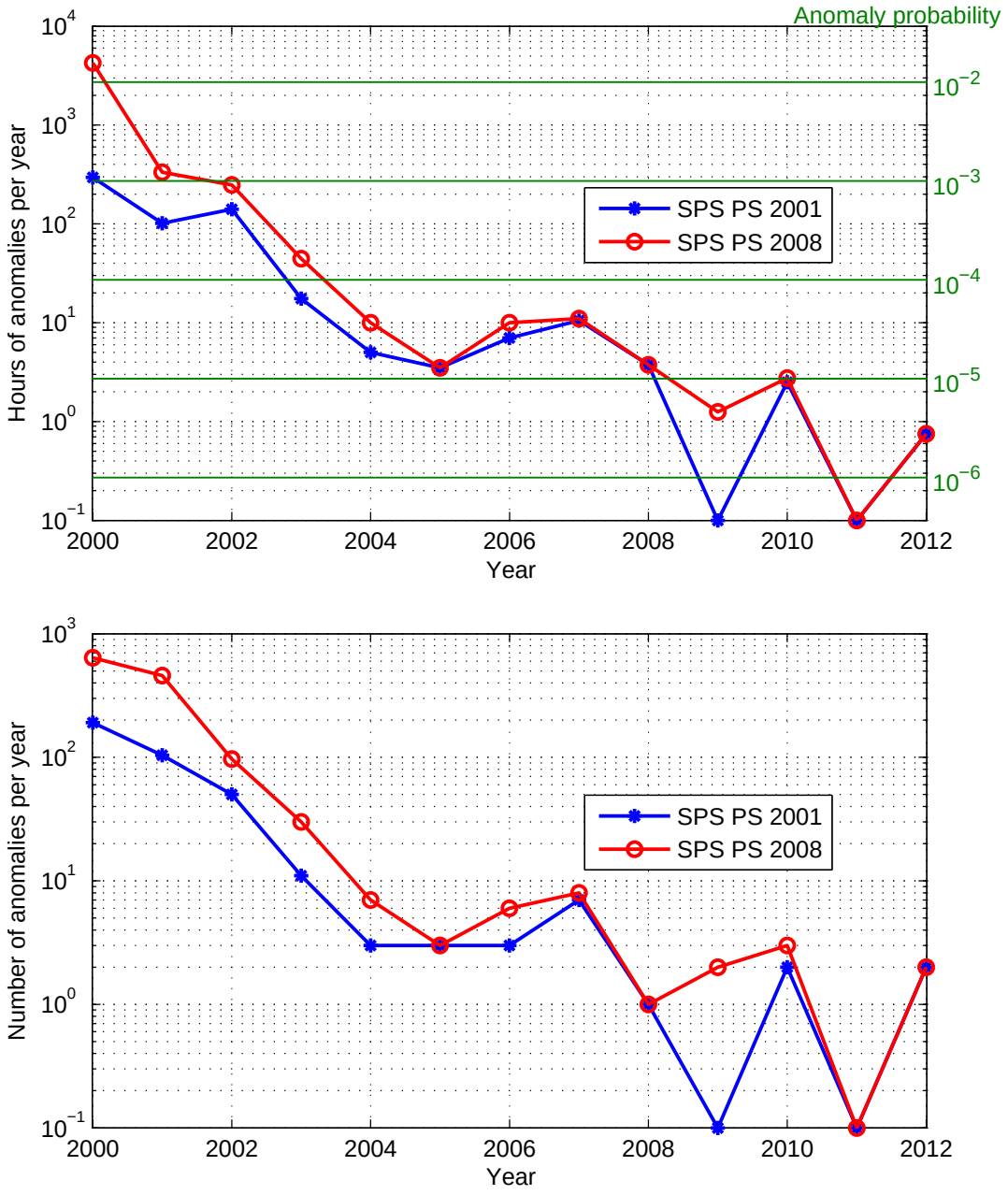

Figure 3.6: Total hours/number of identified GPS SIS anomalies per year. Zeros are represented by 0.1 in both figures. The anomaly probability is based on a full constellation (31 active satellites) with zero outage. The values for 2000 or 2012 are not based on a whole year of data.

(not necessarily healthy). Additionally, the color of the lines indicates the satellite's block type. Markers of blue dots represent the small anomalies with WC UREs less than 30 meters; although all of them exceed the NTE threshold defined in SPS PS 2008 [19], they are not regarded as anomalies per SPS PS 2001 [96]. Markers of green circles and red stars represent the medium and large anomalies, which are anomalies even according to the SPS PS 2001 [96]. It can be seen that during the first year after SA was turned off, SIS anomalies occurred frequently for the whole constellation. The cause of some of these anomalies have been discussed in [64].

Moreover, 2004 is apparently a watershed: before 2004 anomalies occurred for all GPS satellites (except two satellites lunched in 2003, SVN 45/PRN 21 and SVN 56/PRN 16); after 2004 anomalies occurred much less frequently and more than 10 satellites have never been anomalous. Figures 3.6 further confirms the improving GPS SIS integrity performance in the last decade, regardless of the NTE threshold.

Table 3.5 lists all the 32 potential SIS anomalies since January 2004. Many of the anomalies in the table have been confirmed by other literature, as shown by the citations in the last column. Table 3.5 reveals two important and exciting pieces of information:

- Probability of anomaly[8] has been lower than 10^{-5} since 2009, an excellent performance surpassing the performance standard [19];
- Never have two SIS anomalies or more occurred simultaneously since 2004.

3.6.2 Excellence of validated navigation messages

For the purpose of evaluation and verification, we compare the anomalies found using our validated navigation messages with those found using the IGS daily global combined broadcast navigation messages, `brdc`*`ddd`*`0.`*`yy`*`n` and `auto`*`ddd`*`0.`*`yy`*`n`. In this comparison, the NGA APC precise ephemerides/clocks are employed as the truth reference. The SPS PS 2008 NTE threshold [19] is used to detect anomalies. The other criteria for anomaly detection are the same as in Section 3.5.

All the potential SIS anomalies between 2006 and 2009 are found using the three different kinds of navigation messages. Table 3.6 shows a comparison of the total hours of anomalies per year. It can be seen that `brdc`*`ddd`*`0.`*`yy`*`n` and `auto`*`ddd`*`0.`*`yy`*`n` result in approximately 11 times more false anomalies than true ones. Moreover, all potential anomalies derived from

[8] For a constellation of 31 satellites, a 10^{-5} anomaly probability is approximately equivalent to 3-satellite-hour anomalies per year.

Start date/time	SVN	PRN	Duration	Anomaly†	URA UB (m)	References	Confirmed by
2004-01-01 18:45	23	23	2.75 hr	clock 28.4 km	2.40	CODE‡	[41, 114]
2004-04-22 13:15	38	08	1.5 hr	clock 29.0 m	4.85	NGA	
2004-05-03 11:15	38	08	15 min	clock −30.2 m	3.40	NGA, IGS	
2004-05-05 08:30	38	08	1 hr	clock −29.5 m	2.40	NGA	
2004-06-17 11:15	29	29	1.75 hr	ephemeris 13.0 m	2.40	NGA, IGS	
2004-07-20 07:15	60	23	45 min	ephemeris 13.0 m	2.40	NGA, IGS	
2004-08-29 00:45	27	27	2 hr	clock 70.4 m	3.40	NGA, IGS	[114, 115]
2005-05-14 20:15	27	27	1.5 hr	clock 116 m	2.40	NGA, IGS	
2005-06-09 03:45	26	26	1 hr	clock −37.9 m	3.40	NGA, IGS	[50]
2005-12-25 21:15	25	25	1 hr	clock 2.05 km	2.40	NGA, IGS	
2006-06-02 20:30	30	30	30 min	clock −1045 m	2.40	NGA	[50]
2006-06-27 04:45	36	06	30 min	clock −10.8 m	2.40	NGA, IGS	
2006-07-31 22:15	33	03	1 hr	clock −12.7 m	2.40	NGA, IGS	[50]
2006-08-25 12:30	29	29	1.5 hr	clock −11.6 m	2.40	NGA, IGS	[50]
2006-09-22 19:45	24	24	2.75 hr	ephemeris 41.2 m	2.40	NGA, IGS	[50]
2006-11-07 01:45	35	05	3.75 hr	clock −30.7 m	2.40	NGA, IGS	[50]
2007-03-01 14:45	29	29	2.5 hr	clock −42.3 m	2.40	NGA, IGS	[50, 51]
2007-04-10 16:00	54	18	1.75 hr	ephemeris 688 m	2.40	NGA, IGS	[50, 51, 114, 116]
2007-08-17 07:30	37	07	30 min	clock −14.3 m	2.40	NGA, IGS	[50, 97]
2007-10-08 09:45	58	12	2.25 hr	clock −86 km	2.40	NGA	[40]
2007-10-08 23:00	41	14	1.5 hr	clock −112 km	2.40	NGA	[40]
2007-10-09 09:45	60	23	1 hr	clock 27 km	6.85	NGA	[40]
2007-10-09 13:15	56	16	15 min	clock −18 km	4.85	NGA, IGS	[40]
2007-10-10 08:45	51	20	1.25 hr	clock 48 km	2.40	NGA, IGS	[40]
2008-11-14 05:45	27	27	3.75 hr	clock −70 km	2.40	NGA	
2009-06-26 09:30	25	25	45 min	clock −22.3 m	2.40	NGA	[114]
2009-11-05 18:45	38	08	30 min	clock −18.5 m	2.40	IGS	[114]
2010-02-22 21:00	30	30	30 min	clock −42.9 m	3.40	NGA	
2010-04-25 19:45	39	09	15 min	ephemeris 11 m	2.40	NGA, IGS	
2010-06-24 18:30	56	16	2 hr	clock 374 m	2.40	NGA	
2012-04-27 03:05	58	12	20 min	ephemeris −119 m	2.40	NGA	
2012-06-17 00:15	59	19	25 min	ephemeris 452 m	2.40	NGA	

† "ephemeris" or "clock" means the anomaly is mainly due to ephemeris or clock inaccuracy, respectively.

‡ The IGS precise clocks for PRN 23 on 2004-01-01 were absent. The values such as start time, duration, and WC URE are obtained from a comparison with the precise ephemerides and clocks provided by the Center for Orbit Determination in Europe (CODE) [117].

Table 3.5: List of 32 identified GPS SIS anomalies between 2004-01-04 and 2012-07-16.

Year	With our data cleansing	Without our data cleansing	
	sugl*	auto*	brdc*
2006	10.00	22.25	17.00
2007	11.00	225.00	131.25
2008	3.75	23.25	40.50
2009	0.75	52.00	125.75
Sum	25.50	322.50	314.50

Table 3.6: Total hours of anomalies per year computed from our validated navigation messages and two kinds of IGS daily global combined broadcast navigation messages.

sugl*ddd*m.*yy*n are confirmed by brdc*ddd*0.*yy*n and auto*ddd*0.*yy*n, which indicates that our sugl*ddd*m.*yy*n does not introduce any more false anomalies than brdc*ddd*0.*yy*n and auto*ddd*0.*yy*n.

3.7 Summary

This chapter describes Phase I of GPS SIS anomaly monitoring: anomaly identification using the space approach. In this approach, the anomalies are identified by a comparison between the broadcast ephemerides/clocks and the precise values. The most important contribution is our voting-based data cleansing algorithm that can recover the original broadcast navigation messages from imperfect broadcast navigation data files collected by the IGS global tracking network. In comparison to the brdc*ddd*0.*yy*n or auto*ddd*0.*yy*n files from IGS, our validated navigation messages exclude most receiver-caused errors, making the assessment of the GPS SIS integrity performance possible.

After processing 454,335,307 navigation messages collected by on average 400 IGS stations between 2000-06-01 and 2012-07-16, 1256 GPS SIS anomalies have been identified. Approximately two thirds of the anomalies between 2004 and 2012 are confirmed by other literature. The total number of SIS anomalies per year demonstrates the improving SIS integrity performance in the last decade. The results also show that the probability of anomaly has been lower than 10^{-5} since 2009, and never have two anomalies or more occurred simultaneously since 2004.

Chapter 4

Automated Verification of Identified GPS Anomalies

This chapter describes Phase II of GPS SIS anomaly monitoring—automated verification of identified anomalies using the ground approach. In Chapter 3, potential GPS SIS anomalies have been identified by the space approach—a comparison between broadcast and precise ephemerides and clocks. Unfortunately, the Phase I results may have the following issues:

- False anomalies due to uncorrected data-logging errors in our validated navigation messages;
- False anomalies due to rare errors in precise ephemerides and clocks;
- False anomalies due to untrackable SIS;
- Inaccurate start time and duration due to untrackable SIS and/or low sampling rate of precise ephemerides and clocks.

In addition, one thirds of the anomalies listed in Table 3.5 are discovered for the first time and have not yet been confirmed by other publicly-available literature. Therefore, it is necessary to use the ground observation data to verify the identified anomalies and gain more accurate information about each anomaly. Traditional implementations of the ground approach usually require too much manual intervention, such as handpicking data sources and verifying an anomaly with eyes [50, 97]. This chapter develops an automated anomaly verification process in order to speed up the processing and to avoid human error.

The rest of this chapter is organized as follows. Section 4.1 outlines the verification process. Sections 4.2 to 4.4 elaborate on the three major steps of anomaly verification.

Section 4.5 shows the verification results and compares them with the Phase I results. Section 4.6 analyzes the two anomalies that occurred in 2012. Section 4.7 summarizes the major findings in this chapter.

4.1 Overview of Anomaly Verification

Figure 4.1 shows the whole verification process. For each potential anomaly identified in Phase I, the following information is already known.

- The start time and the duration of the anomaly at the resolution of 15 minutes (or 5 minutes after 2012-02-28);
- The broadcast and precise satellite orbits and clocks at 15-minute intervals (or 5-minute intervals after 2012-02-28);
- The broadcast URA.

The first step in the verification process is to determine preferred IGS stations based on the above information and the coordinates of all IGS stations. Then, the GPS navigation and observation data collected by these preferred IGS stations are downloaded from the IGS archive site CDDIS [102]. The second step is to compute the I UREs of the anomalous satellite using (3.2). In the last step, the I UREs experienced by each preferred IGS station generate a decision among "anomalous," "nominal," and "untracked;" these independent decisions are combined to determine if the potential anomaly is true, false, untracked, or paradoxical. The whole process is fully automated, as a manual intervention is only needed

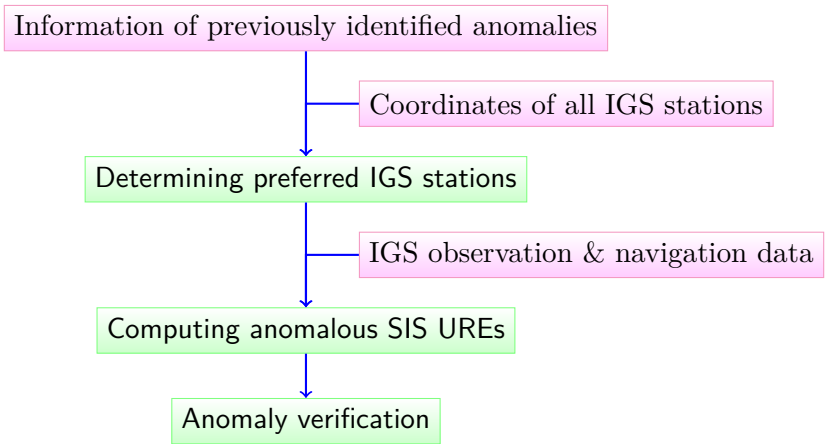

Figure 4.1: Whole process of GPS SIS anomaly verification.

when a decision is "paradoxical."

4.2 Determination of Preferred Stations

As shown by the left map in Table 3.2, the IGS tracking network is made up of more than 350 volunteer stations all over the world. A GPS satellite can usually be tracked by tens or even hundreds of stations simultaneously. In order to reduce the computational cost, for each identified anomaly our process computes the I UREs based on the data from 10–32 preferred stations[1]. These stations are selected according to the following requirements:

- The station must be active when the anomaly occurred;
- The station must be visible to the anomalous satellite through the whole anomaly event, or as long as possible;
- The station should experience as large anomalous UREs as possible.

Among the three requirements, it is easy to meet the first one by simply checking the filenames in the CDDIS server. To coordinate the last two requirements, we propose a simple criterion that a station is more preferred if the sum of the absolute values of the anomalous UREs observed by this station is larger. For example, supposing there was a 30-minute anomaly, and Station A experienced 15-meter and 20-meter UREs for the first 15 minutes and the last 15 minutes respectively, while Station B experienced 30-meter URE for the first 15 minutes but was out of the coverage of the satellite for the last 15 minutes. Then, Station A is preferred because $15 + 20 > 30$. However, if Station B had experienced 40-meter URE for the first 15 minutes only, it would have been preferred because $15 + 20 < 40$. Although this criterion seems to be arbitrary, it is very efficient and effective in processing the actual data.

The criterion can be implemented as follows. Assuming that we want to verify an anomaly of PRN p occurring at $\{t_1, \ldots, t_n\}$ (epochs at 15-minute intervals) on Day d of the Year y, a list of preferred stations can be generated by the following algorithm.

[1]The default setting of the process is to use the data from 16 stations to verify an anomaly. For some old anomalies, the process may find 10 or a little more stations that experienced anomalous UREs because the current map of the IGS tracking network does not include some old stations. For some ephemeris anomalies, the process may find 10 stations or fewer that experienced anomalous UREs because the large I UREs were observable in a small area. For some "untracked" anomalies (see Section 4.4 for more details), the process uses the data from up to 32 stations in order to make sure that the satellite was not tracked.

1: **for all** IGS station s such that s has the GPS navigation and observation data on Day d of the Year y **do**
2: Assign an initial priority value of this station $w_s \leftarrow 0$
3: **for all** $t \in \{t_1, \ldots, t_n\}$ **do**
4: **if** station s in the coverage of PRN p at t **then**
5: Compute I URE e of PRN p observed by s at t {using the station latitude, longitude and elevation provided by IGS [118] and the broadcast and precise satellite orbits and clocks obtained in Phase I}
6: **if** $|e| < 4.42 \cdot$ URA UB **then**
7: $e \leftarrow 0$
8: **end if**
9: Update the priority value $w_s \leftarrow w_s + |e|$
10: **end if**
11: **end for**
12: **end for**
13: Sort the IGS stations in descending order for the priority values w_s

For each identified GPS SIS anomaly, the above algorithm gives a list of the IGS stations whose navigation and observation data can be used to verify the anomaly. In addition, these IGS stations are sorted from the most preferred to the least preferred. Therefore, our process sequentially downloads the RINEX navigation and observation data from the first 10–32 station in the list, and computes I UREs for each station.

4.3 Computation of I UREs

4.3.1 Range error model

For a dual-frequency GPS receiver, the ionospheric delay can be removed by the following combination [72]

$$\rho = \frac{f_{\mathrm{L1}}^2}{f_{\mathrm{L1}}^2 - f_{\mathrm{L2}}^2}\rho_{\mathrm{L1}} - \frac{f_{\mathrm{L2}}^2}{f_{\mathrm{L1}}^2 - f_{\mathrm{L2}}^2}\rho_{\mathrm{L2}} = 2.546\rho_{\mathrm{L1}} - 1.546\rho_{\mathrm{L2}}, \tag{4.1}$$

where $f_{\mathrm{L1}} = 1575.42$ MHz and $f_{\mathrm{L2}} = 1227.6$ MHz. The ionosphere-free pseudorange measurement ρ can be modeled as

$$\rho = r + c(b_u - b^s) + T + \epsilon, \tag{4.2}$$

where r is the true range, c is the speed of light, b_u is the receiver clock bias, b^s is the true satellite clock bias, T is the tropospheric delay, and ϵ is a composition of all unmodeled effects, modeling errors, and measurement noises except the SIS URE.

The receiver derives real-time satellite orbits and clocks from broadcast navigation messages. The true range can be written as

$$r = \hat{r} - \epsilon_e, \tag{4.3}$$

where $\hat{r}$ is the "true range" based on the broadcast ephemeris, and ϵ_e is the broadcast ephemeris error projected onto the ray from the receiver to the satellite. Similarly, the true satellite clock bias can be written as

$$b^s = \hat{b}^s - \epsilon_c, \tag{4.4}$$

where $\hat{b}^s$ is the broadcast satellite clock bias, and ϵ_c is the broadcast clock error.

Plugging (4.3) and (4.4) into (4.2), we can obtain

$$\text{I URE} = \epsilon_e - c\epsilon_c = \hat{r} + c(b_u - \hat{b}^s) + T + \epsilon - \rho. \tag{4.5}$$

The values on the right side of (4.5) can be computed or estimated as follows.

- ρ is ionosphere-free pseudorange derived from L1 and L2 pseudoranges measured by the receiver;
- $\hat{r}$ is the distance between the broadcast satellite position (computed from the broadcast ephemeris) and the receiver position (estimated or known);
- b_u is the estimated receiver clock bias;
- $\hat{b}^s$ is the broadcast satellite clock bias computed from the clock correction terms in the navigation message;
- T is the tropospheric delay estimated using the Saastamoinen model [72, 119];
- ϵ is not modeled or estimated in this study.

According to [72], the total estimation error for the right side of (4.5) is around 3 meters, mainly attributable to the multipath boosted by the ionosphere-free combination[2]. This accuracy is acceptable for the purpose of this study because anomalous UREs are always larger than $4.42 \cdot 2.4 = 10.6$ meters.

[2]Assuming that the multipath and noise at L1 and L2 are uncorrelated and have the same variance, the noise in the ionosphere-free pseudorange is $\sqrt{2.546^2 + 1.546^2} = 2.98$ times larger than that in ρ_{L1} and ρ_{L2}. Additionally, the semicodeless pseudorange measurement at L2 is very noisy, making the noise in the ionosphere-free pseudorange even larger.

4.3.2 Estimation of receiver position and clock biases

The above analysis of range error model shows that we need only the accurate receiver position and clock bias in order to estimate the I URE. Usually, a RINEX observation file provides the receiver position in its header. Unfortunately, not all IGS stations report a survey-grade receiver position in their RINEX files. We use the following strategy to cope with this problem.

1. Estimate the receiver position from the observation data;
2. If the estimated receiver position is within 5 meters of the receiver position given by the header of the RINEX file, then use the given receiver position, otherwise use the estimated receiver position.

Since the receivers in the IGS network are usually static, a receiver position can be accurately estimated by averaging many position estimates. In this chapter, we estimate a receiver position using three days of data around the day when the anomaly occurred. To avoid any interference due to outliers, not only is the anomalous satellite excluded in the computation, but a 10% trimmed mean [113] is also used.

With a known or estimated receiver position $\boldsymbol{x}$, the pseudoranges obtained after accounting for satellite clock bias and tropospheric delay can be modeled as [72]

$$\tilde{\rho}^{(k)} = ||\boldsymbol{x}^{(k)} - \boldsymbol{x}|| + b_u + \epsilon^{(k)}, \tag{4.6}$$

where $k = 1, \ldots, K$ is the index of the K available satellites at this epoch (excluding the anomalous satellite), and $\boldsymbol{x}^{(k)}$ is the satellite position. A minimum-mean-square-error estimator of b_u is given by the weighted mean

$$b_u = \frac{1}{\sum_{k=1}^{K} w_k} \sum_{k=1}^{K} w_k (\tilde{\rho}^{(k)} - ||\boldsymbol{x}^{(k)} - \boldsymbol{x}||), \tag{4.7}$$

where the weights $w_k = 1/\operatorname{var}(\epsilon^{(k)})$ can be derived from the signal-to-noise (SNR) ratio, satellite elevations, etc. using the algorithms described in [13, 120].

Finally, with $\boldsymbol{x}$ and b_u, we are ready to use (4.5) to compute the I UREs observed the receiver.

4.4 Verification of Anomalies

Like Chapter 3, this chapter employs the following criteria to detect an "anomalous" GPS SIS behavior:

- The I URE exceeds the NTE threshold (see Section 2.4 for details);
- The broadcast navigation message is healthy, i.e.,
  - The RINEX field `SV health` [99] is 0, and
  - The URA UB $\leq$ 48 meters [19];
- The broadcast navigation message is in its fit interval, i.e., $\Delta t = t - \text{TTOM} \leq 4$ hours;
- The L1 C/A signal was tracked with an acceptable SNR, i.e.,
  - The RINEX SNR flag[3] value ≥ 4.

In addition, a "nominal" GPS SIS behavior is decided when the last condition is fulfilled but any of the first three conditions is not. When the L1 C/A signal was not tracked with an acceptable SNR, the decision is "untracked" because (1) the SIS might be nominal as the satellite could indicate an unhealthy state through ceasing transmission or using nonstandard code or data [19,21], or (2) the SIS might be anomalous as the satellite could be excluded by a built-in integrity monitor of the receiver. In short, for each identified GPS SIS anomaly, the observation and navigation data sets from one IGS station give one of the three decisions: anomalous, nominal, and untracked.

As mentioned in Section 4.2, each identified GPS SIS anomaly is verified using the observation and navigation data from 10–32 preferred IGS stations. The data from each of these stations give an independent decision, and the final verification decision is made by combining these 10+ independent decisions. Table 4.1 shows the decision table that our process uses to combine these independent decisions.

According to Table 4.1, an identified GPS SIS anomaly is proven to be "true" if the observation data from at least one of the 10+ preferred IGS stations show anomalous UREs while the rest could not track the satellite during the anomaly event. Similarly, an identified anomaly is proven to be "false" if the observation data from at least one of the 10+ stations show nominal UREs while the rest could not track the satellite. An "untracked" decision is made when all IGS stations visible to the anomalous satellite could not track it; the anomaly

[3]The RINEX format [99] requires signal strength projected into the interval 1–9: 1 is the minimum possible signal strength, 5 is the threshold for a good SNR, and 9 is the maximum possible signal strength.

	Number of IGS stations that decide		
Final decision	Anomalous	Nominal	Untracked
True	≥ 1	$= 0$	≥ 0
False	$= 0$	≥ 1	≥ 0
Untracked	$= 0$	$= 0$	≥ 10
Paradoxical	≥ 1	≥ 1	≥ 0

Table 4.1: Decision table for combining independent decisions into the final verification decision.

is, although *not proven* to be false, *most likely* to be false. A "paradoxical" decision is made when some IGS stations show anomalous UREs but some show nominal. The automated verification process can issue a warning when a "paradoxical" decision is made. This is the only case that requires a manual intervention. Fortunately, we have not encountered any "paradoxical" anomalies in this study.

4.5 Verification Results

We apply the automated verification process to the 32 GPS SIS anomalies between 2004-01-01 and 2012-07-16 identified in Phase I (Section 3.6). Table 4.2 shows a side-by-side comparison of the verification results with the Phase I results found by the space approach. It can be seen that

- 28 identified anomalies have been verified to be true;
- 0 identified anomalies have been verified to be false[4];
- 4 identified anomalies are most likely to be false because they were not tracked through the whole anomaly event.

The verification result confirms that the space approach, although with some shortcomings, is an efficient and effective method for finding anomalies. The result also shows that our data cleansing algorithm is very capable based on no false anomalies due to data-logging errors.

[4]Our previous work [67] found a false anomaly of PRN 19 on 2007-05-20. This false anomaly was due to unresolved TTOM ambiguity during the GPS week cutover on that day (Section 3.4.4).

Potential anomalies found in Phase I (space approach)								Verification result in Phase II (ground approach)						
SVN	PRN	Date	Start Time	Duration (minutes)	Anomaly Type	WC URE (meters)	URA UB (meters)	Start Time	Duration (minutes)	WC URE (meters)	Reference	Number of stations that decide		
												Anomalous	Nominal	Untracked
23	23	2004-01-01	18:45	165	clock	284000	2.40	18:31	169	298600	bhr1	5	0	5
38	8	2004-04-22	13:15	90	clock	29	4.85	13:07	32	29.5	qui1	2	0	11
38	8	2004-05-03	11:15	15	clock	-30.2	3.40	10:58	19	-32.86	bue1	3	0	10
38	8	2004-05-05	08:30	60	clock	-29.5	2.40	08:23	34	-35.18	eil1	3	0	10
29	29	2004-06-17	11:15	105	ephemeris	13	2.40	11:09	48	13.26	wel2	2	0	8
60	23	2004-07-20	07:15	45	ephemeris	13	2.40	06:31	73	17.35	suth	13	0	3
27	27	2004-08-29	00:45	120	clock	70.4	3.40	00:42	160	71.5	brmu	11	0	5
27	27	2005-05-14	20:15	90	clock	116	2.40	20:01	18	31.63	gmsd	12	0	4
26	26	2005-06-09	03:45	60	clock	-37.9	3.40	03:38	17	-35.24	irkj	14	0	2
25	25	2005-12-25	21:15	60	clock	2050	2.40	21:05	25	-173.7	osn2	14	0	2
30	30	2006-06-02	20:30	30	clock	1045	2.40	20:04	11	160.2	mas1	15	0	0
36	6	2006-06-27	04:45	30	clock	-10.8	2.40	04:42	29	-11.39	mcm4	16	0	0
33	3	2006-07-31	22:15	60	clock	-12.7	2.40	22:13	51	-13.14	hrm1	16	0	0
29	29	2006-08-25	12:30	90	clock	-11.6	2.40	12:24	95	-11.85	sey1	16	0	0
24	24	2006-09-22	19:45	165	ephemeris	41.2	2.40	19:54	22	12.78	mcm4	7	0	9
35	5	2006-11-07	01:45	225	clock	-30.7	2.40	01:44	31	-17.93	tah2	15	0	1
29	29	2007-03-01	14:45	150	clock	-42.3	2.40	14:38	8	-13.01	faa1	8	0	8
54	18	2007-04-10	16:00	105	ephemeris	688	2.40	16:04	61	398.2	tah2	13	0	3
37	7	2007-08-17	07:30	30	clock	-14.3	2.40	07:22	38	-16.24	jplm	16	0	0
58	12	2007-10-08	09:45	135	clock	-86000	2.40	satellite was not tracked				0	0	23
41	14	2007-10-08	23:00	90	clock	-112000	2.40	satellite was not tracked				0	0	32
60	23	2007-10-09	09:45	60	clock	27000	6.85	09:53	46	26650	tid2	5	0	11
56	16	2007-10-09	13:15	15	clock	-18000	4.85	12:55	37	-18450	nrl1	6	0	9
51	20	2007-10-10	08:45	75	clock	48000	2.40	09:06	47	47690	osn1	6	0	10
27	27	2008-11-14	05:45	225	clock	-69800	2.40	satellite was not tracked				0	0	32
25	25	2009-06-26	09:30	45	clock	-22.3	2.40	09:05	40	-22.42	guao	15	0	0
38	8	2009-11-05	18:45	30	clock	-18.5	2.40	18:40	22	-18.32	bue1	15	0	1
30	30	2010-02-22	21:00	30	clock	-42.9	3.40	20:46	5	-15.3	areq	14	0	2
39	9	2010-04-25	19:45	15	ephemeris	11	2.40	19:31	29	11.65	xian	9	0	1
56	16	2010-06-24	18:30	120	clock	374	2.40	satellite was not tracked				0	0	29
58	12	2012-04-27	03:05	20	ephemeris	-119	2.40	03:02	24	-144.8	darw	13	0	3
59	19	2012-06-17	00:15	25	ephemeris	452	2.40	00:11	26	161.9	sfer	11	0	5

Table 4.2: Verification results compared with previous identification results

It should be noted that for a certain SIS anomaly, different stations may observe different anomalous URE behaviors. For each of the 28 true anomalies, the values of start time, duration, and WC URE[5] in the verification results of Table 4.2 are based on the RINEX data from the station listed in the "Reference" column.

Comparing the verification results of the 28 true anomalies with our prior results, we can see that the anomaly start time or duration derived from the ground approach sometimes disagrees with that from the space approach. One of the reasons for this is that the IGS daily observation data are recorded at sampling intervals of 30 seconds, while the precise

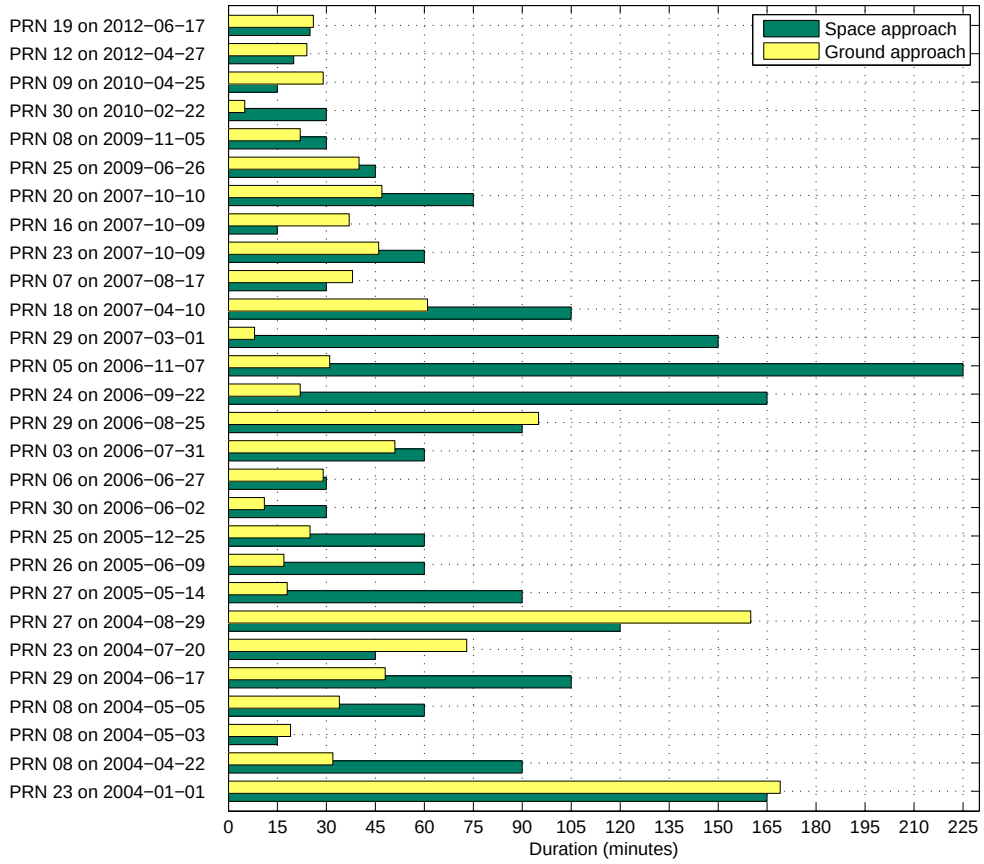

Figure 4.2: Duration of GPS SIS anomalies. For nearly half of the anomalies, the duration given by the ground approach is significantly shorter than that of the space approach.

[5]Because the ionosphere-free pseudorange measurement is often very noisy, a 10-minute low-pass filter is used and then the WC URE is calculated.

ephemerides and clocks used in the space approach are usually given at 15-minute intervals. The different sampling frequencies naturally cause the start time given by the ground approach to be earlier than that of the space approach, and the duration given by the ground approach to be longer than that of the space approach.

Nevertheless, Figure 4.2 shows that, for nearly half of the true anomalies, the duration given by the ground approach is significantly shorter than that of the space approach. The reason is that, when an SIS anomaly is detected by the satellite or the ground control, a GPS satellite may alert the users by ceasing to transmit the L1 signal or using nonstandard code or data [19, 21] before updating the navigation messages. In fact, half of the true anomalies ended with the receivers losing track of the anomalous satellites. In the space approach, due to the lack of the information about the signal trackablity, the end of an anomaly is usually the instant at which the anomalous navigation message expired or a new navigation message was issued. Therefore, the anomaly duration given by the space approach may be longer than the actual duration.

The last apparent disagreement between the ground approach and the space approach is the WC URE. One reason for this disagreement is that, as just mentioned, an anomaly might end earlier than the space approach thought, and the UREs did not actually grow to as large a value as the space approach found. Besides, the UREs computed by the ground approach depend on the receiver's location, and sometimes there is no station near the spot that experienced the WC URE. Lastly, the maximum URE in the ground approach is affected by meter-level estimation errors.

4.6 Case Studies

This section presents in-depth case studies of the two anomalies that occurred recently: the SVN 58/PRN 12 anomaly on 2012-04-27 and the SVN 59/PRN 19 anomaly on 2012-06-17. Some other interesting anomalies, such as the SVN 33/PRN 03 anomaly on 2006-07-31 and the SVN 29/PRN 29 anomaly on 2007-03-01 have been studied in [67].

4.6.1 SVN 58/PRN 12 anomaly on 2012-04-27

Figure 4.3 shows the I UREs of PRN 12 observed by two IGS stations, `darw` and `stk2`. In the figure, the I UREs obtained from the ground approach (blue dots) are based on the navigation and observation data from the receiver. The I UREs obtained from the space

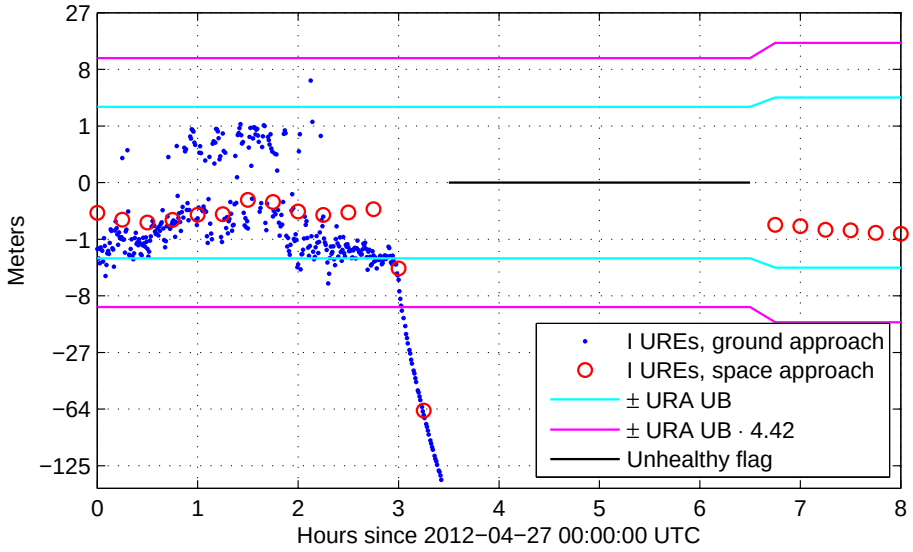

(a) IGS station `darw` at Darwin, Northern Territory, Australia

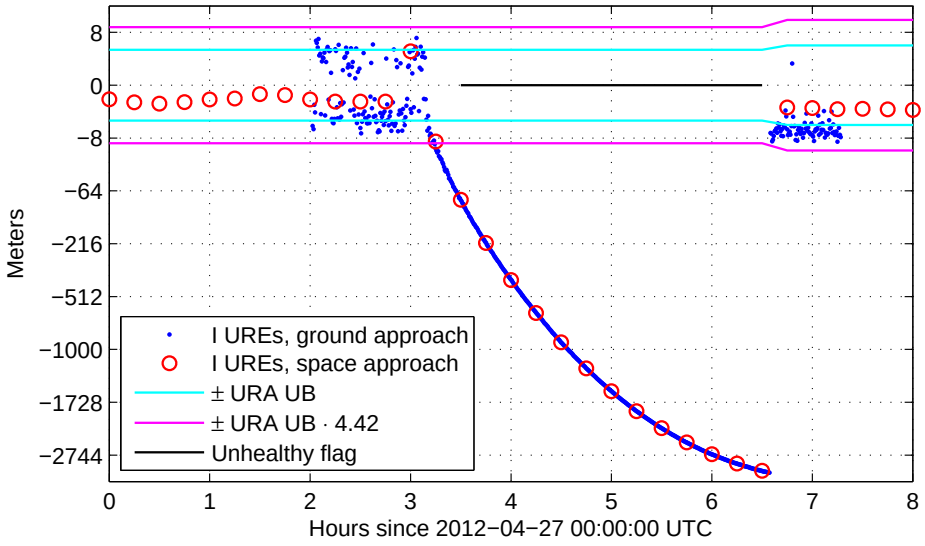

(b) IGS station `stk2` at Shintotsukawa, Hokkaido, Japan

Figure 4.3: I UREs of SVN 58/PRN 12 anomaly on 2012-04-27. The y-axis is in a cubic root scale. The receiver `darw` functioned nominally, while the receiver `stk2` ignored the healthy bits in the broadcast navigation message.

approach (red circles) as well as the URA information and the unhealthy flag are computed with respect to the location of the receiver using our validated navigation messages and the NGA precise ephemeris and clock data.

The anomaly experienced by `darw` started at 03:02 and ended at 03:26, when a new navigation message flagged unhealthy was broadcast. Accordingly, the maximum I URE that `darw` experienced was −144.8 meters.

In contrast, `stk2` experienced a very different story because this receiver has never paid attention to the healthy bits in the broadcast navigation message. In fact, all navigation messages it has reported to IGS are marked healthy. Therefore, this receiver experienced huge I UREs for approximately 3 hours, and the errors grew to more than 3000 meters until a navigation message with correct parameters was issued.

4.6.2 SVN 59/PRN 19 anomaly on 2012-06-17

Figure 4.4 shows the I UREs of PRN 19 observed by two IGS stations, `sfer` and `dgar`. The anomaly experienced by `sfer` started at 00:11 and ended at 00:37, when a new navigation message with correct parameters was broadcast. Accordingly, the maximum I URE that `sfer` experienced was 161.9 meters.

Unlike `sfer`, `dgar` missed three correct navigation messages broadcast between 00:37 and 04:00 for some inexplicable reason, although it nominally tracked the satellite without any problem. As a result, `dgar` experienced huge I UREs for nearly 4 hours.

The station `dgar` is not the only one having this problem. We discover that at least 14 other IGS stations, `abpo`, `artu`, `chpi`, `iisc`, `kit3`, `mad2`, `mal2`, `mas1`, `pol2`, `sey1`, `sola`, `sthl`, `vaes`, and `yibl`, missed at least one of the correct navigation messages broadcast between 00:37 and 04:00 on that day. These stations all experienced huge I UREs for more than 1 hour.

Both cases studied in this section indicate that some GPS receivers are not always designed or operated to the specification of GPS SIS [21, 86], even though most of them are geodetic grade. This also explains why there are many data-logging errors in the RINEX navigation message data files. Since ignoring the healthy bits or missing navigation messages can cause unexpectedly large UREs, it is probably a more timely and reliable way to alert users by means of making the anomalous satellite untrackable than updating the navigation message.

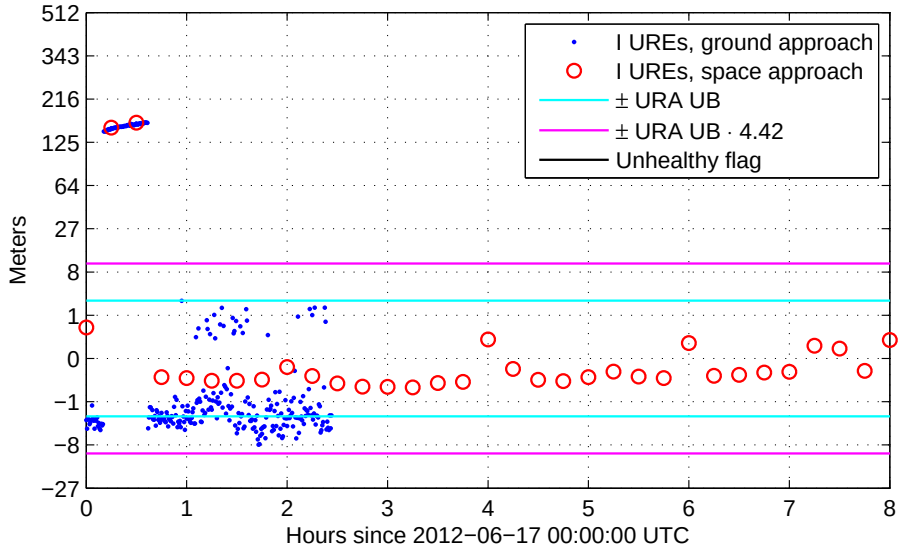

(a) IGS station `sfer` at San Fernando, Cadiz, Spain

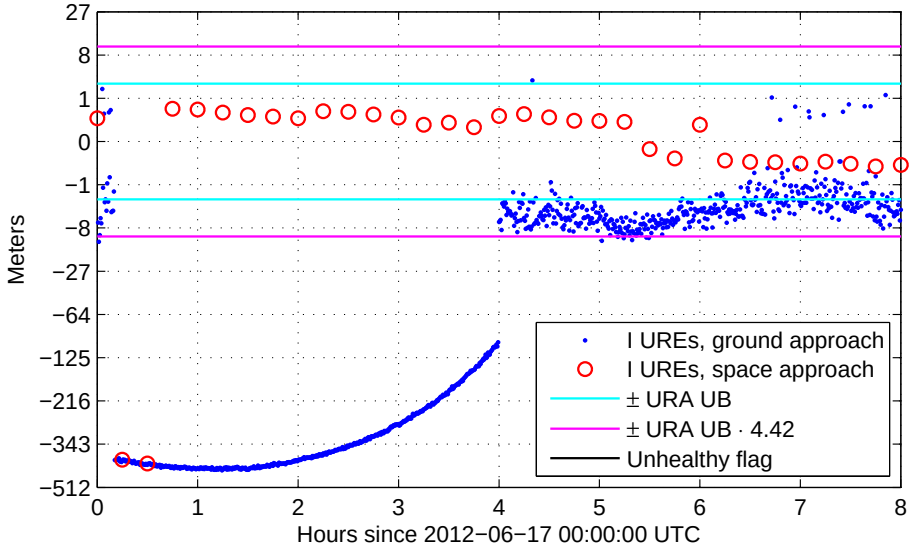

(b) IGS station `dgar` at Diego Garcia, British Indian Ocean Territory

Figure 4.4: I UREs of SVN 59/PRN 19 anomaly on 2012-06-17. The y-axis is in a cubic root scale. The receiver `sfer` functioned nominally, while the receiver `dgar` missed three correct navigation messages broadcast between 00:37 and 04:00. The anomalous UREs that the two stations experienced are opposite in sign because the anomaly was mainly attributable to huge crosstrack ephemeris errors.

4.7 Summary

In this chapter, we developed an automated process to verify the GPS SIS anomalies identified in Chapter 3 using the IGS ground observation data. Given necessary information about each potential anomaly, our process can automatically select 10–32 preferred IGS stations, retrieve their observation and navigation data, compute I UREs, and decide if the potential anomaly is true, false, untracked, or paradoxical. The highlights in this process include:

- Using the results obtained from the space approach to focus the ground approach to questionable times and locations, which greatly decreases the computational cost;
- Automating data source selection and anomaly verification to speed up the processing and to avoid human error;
- Combining independent decisions made by each station into the final decision to address the issue of unreliable ground observation data.

We applied this process to the 32 potential GPS SIS anomalies found from 2004-01-01 to 2012-07-16. The results show that 28 anomalies are true, and 4 are most likely to be false due to untracked SIS. The result proves that our data cleansing algorithm developed in Chapter 3 is very capable because there is no false anomaly due to data-logging errors.

A comparison between the verification results and our prior results shows that the UREs computed from observation data provide more accurate information and deeper insights of the anomalous SIS behaviors, especially when an anomaly ends with untrackable SIS. We have also studied the SVN 58/PRN 12 anomaly on 2012-04-27 and the SVN 59/PRN 19 anomaly on 2012-06-17. Our case studies show that unexpected anomalous behavior can appear when a receiver ignores integrity information in the navigation message or mistakenly misses some navigation messages.

Chapter 5

GLONASS Anomaly Monitoring

This chapter extends SIS anomaly monitoring to GLONASS. As described in Chapter 2, although GLONASS and GPS employ the same concept of multilateration, GLONASS is different from GPS in many ways. Notable differences include the ephemeris format, navigation message update frequency, reference frame, and reference time. These differences just pose some minor problems; the major challenges, however, come from the fact that GLONASS is less mature and less widely used than GPS, as shown by the following long-standing issues:

1. No generally accepted precise clock solutions for GLONASS;
2. No official GLONASS integrity performance standard;
3. No URA information in the RINEX navigation data for GLONASS.

In addition to the above list, another long-standing issue is that broadcast GLONASS navigation message data obtained from a global tracking network also contain data-logging errors.

This chapter describes our techniques to realize global monitoring of GLONASS anomalies, with emphasis on our innovative methods for addressing the above four issues. For the remainder of this chapter, we start with a description of the data sources in Section 5.1. Then, we elaborate on our key methods in Section 5.2. Next, Section 5.3 presents identified anomalies, and Section 5.4 provides an in-depth analysis of these anomalies in terms of anomaly probability, simultaneous multiple anomalies, and geographic dependency. Finally, a summary appears in Section 5.5.

5.1 Data Sources

5.1.1 Broadcast navigation message data

GLONASS broadcast navigation message data are publicly available at IGS [44]. Archived in the RINEX n-type format [108], these data include the immediate information of the GLONASS broadcast navigation message [78] such as reference time, clock corrections, satellite position, satellite velocity, lunisolar acceleration, URA, and healthy flag.

Unfortunately, the RINEX n-type format for GLONASS, unlike its counterpart for GPS, does not include any information about URA. When the RINEX format was defined in the 1990s, the first generation GLONASS satellites did not broadcast URA. The second generation GLONASS-M satellites with the ability to broadcast URA [78] have joined the constellation since 2003, but the RINEX format has not yet been updated to capture the URA values.

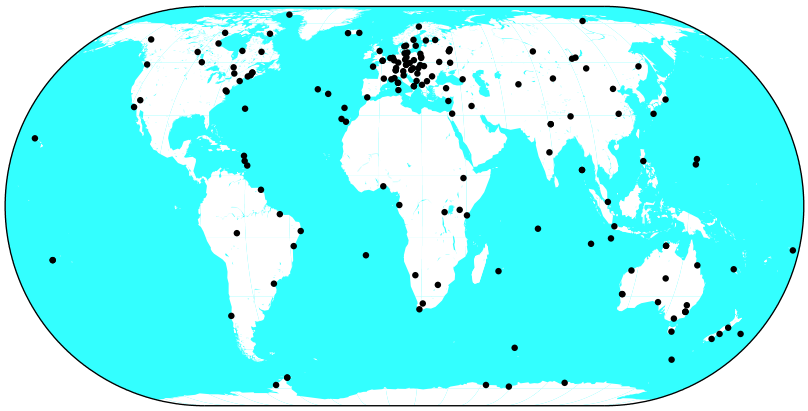

Figure 5.1: IGS GPS/GLONASS stations as of 2012-01-29 (adapted from `http://igscb.jpl.nasa.gov`).

As shown in Figure 5.1, the IGS tracking network contains more than 100 GPS/GLONASS stations all over the world. Like the situation of GPS, no single station can collect all navigation messages because they are updated every 30 minutes. Therefore, an IGS archive site, CDDIS, routinely generates daily global combined broadcast navigation message data files `brdc`*`ddd`*`0.`*`yy`*`g` (or `igex`*`ddd`*`0.`*`yy`*`g` before December 2004) [121]. Unfortunately, these files occasionally contain errors made by ground receivers or processing software. For example, the reference time t_b in the navigation is a multiple of 15 minutes [78], but we observed the following lines in `brdc0020.09g`:

```
                                                    ⋮
 4 09  1  2  0 15  0.0 0.119622796774E-03-0.636646291241E-11 0.000000000000E+00
                                                    ⋮
 4 09  1  2  0 15  1.0 0.119622796774E-03-0.636646291241E-11 0.000000000000E+00
                                                    ⋮
```

The first line indicates a navigation message with t_b = 2009-01-02 00:15:00, whereas the second line indicates a navigation message with the same parameters as the first one but an incorrect t_b = 2009-01-02 00:15:01.

Therefore, we develop a data cleansing algorithm similar to the one used for GPS (Section 3.4). It generates validated GLONASS navigation messages, `sugl`*`ddd`*`0.`*`yy`*`g`, from all available raw navigation message data files collected by all the IGS GPS/GLONASS stations. This data cleansing algorithm is detailed in Section 5.2.1.

5.1.2 Precise ephemeris data

In addition to the broadcast navigation message data, IGS has been providing precise GLONASS ephemerides `igl`*`wwwwd`*`.sp3` (or `igx`*`wwwwd`*`.sp3` before December 2004) since the IGEX-98 experiment (Section 1.3.2). The IGS precise GLONASS ephemeris is a weighted-mean combination of the precise ephemeris solutions independently produced by a number of IGS Analysis Centers (ACs). Each AC routinely post-processes the observation data collected by some IGS GPS/GLONASS stations using its own processing strategy. The `igl`*`wwwwd`*`.sp3` data have an accuracy of 5 centimeters [106] and thus are regarded as the ground truth in this study. To compare the broadcast ephemerides with the precise values, we need to pay attention to the following three issues.

First, the precise ephemeris is available at 15-minute intervals synchronized to GPS Time, whereas the reference time in the navigation message is synchronized to GLONASS Time. In addition to the fixed three-hour difference between GLONASS Time and UTC [78], the difference between GPS time and GLONASS time includes the leap seconds (between UTC and GPS) and a sub-second bias τ_{GPS} [78]. τ_{GPS} varies slowly and can be derived from the GLONASS almanacs[1]. Considering the fact that τ_{GPS} is usually within 1 microsecond and the resulting ephemeris and clock error is less than 4 millimeters, in this study we only take the leap second into account.

[1]The IGS weekly summary report (`igl`*`wwwwd`*`.sum` files) also provides sub-second GPS/GLONASS time offsets, but these values do not agree with the τ_{GPS} in the GLONASS almanacs.

The second issue is that the precise ephemeris is based on ITRF, but the broadcast ephemeris has been based on PZ-90.02 since September 2007. According to the discussion in Section 2.2, a reference system transformation is not considered necessary in this study.

Last but not least, the IGS precise ephemeris refers to satellite center of mass (CoM). Since the broadcast ephemeris is based on antenna phase center (APC), the CoM precise ephemeris must be converted into APC before being used. In this study, the IGS antenna corrections [110, 122, 123] are adopted.

5.1.3 Precise clock data

Although IGS does not provide precise GLONASS clocks [106], the precise products from some ACs include precise clocks. The list below shows the GLONASS products from the IGS ACs.

bkg[2] GPS + GLONASS, without precise clocks, data available until 2011-05-21

cod[3] GPS + GLONASS, without precise clocks

emx[4] GPS + GLONASS, with precise clocks, data available since 2011-09-11

esa[5] GPS + GLONASS, with precise clocks, data available since 2008-10-18

gfz[6] GPS + GLONASS, with precise clocks, data available since 2010-04-11

grg[7] GPS + GLONASS, without precise clocks, data available since 2011-01-09

iac[8] GLONASS only, with precise clocks, data available since 2005 or earlier

mcc[9] GLONASS only, without precise clocks, for only a few satellites

In this study, we use the four products with precise clocks: `emx`, `esa`, `gfz`, and `iac`.

Figure 5.2 shows the clock errors of GLONASS-M 721 (PRN[10] 13) computed from the four precise clocks. They do not exactly agree with each other. This may be one of the reasons why the `igl`*wwwwd*`.sp3` files do not to include precise GLONASS clocks.

However, as shown in Figure 5.3, a zoomed-in portion of Figure 5.2 reveals that these

[2] Produced by Bundesamt fuer Kartographie und Geodaesie, Germany.
[3] Produced by Center for Orbit Determination in Europe (CODE), AIUB, Switzerland.
[4] Producer unspecified.
[5] Produced by European Space Operations Center, ESA, Germany.
[6] Produced by GeoForschungsZentrum, Germany.
[7] Produced by French Space Agency.
[8] Produced by Information-Analytical Center, Russia.
[9] Produced by Mission Control Center, Russia.
[10] The GLONASS satellites uses FDMA and all satellites broadcast the same PRN code. In the context of GLONASS, "PRN" refers to the orbit slot number.

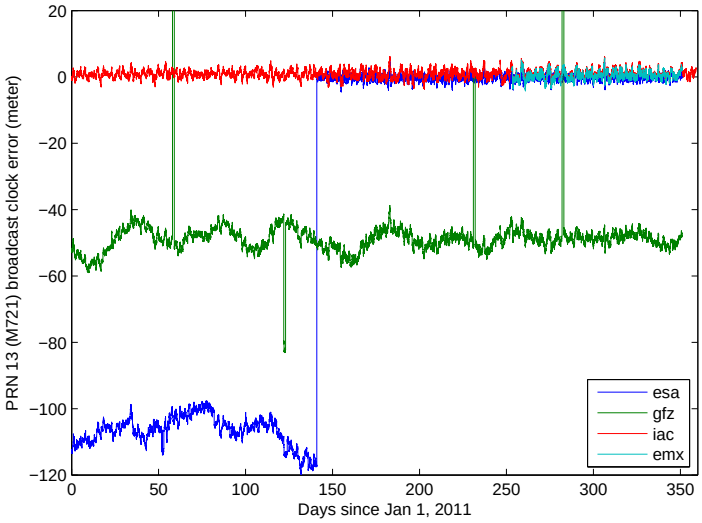

Figure 5.2: GLONASS-M 721 (PRN 13) clock errors in 2011, computed from `esa`, `gfz`, `iac`, and `emx` precise clocks. These precise clocks do not agree with each other.

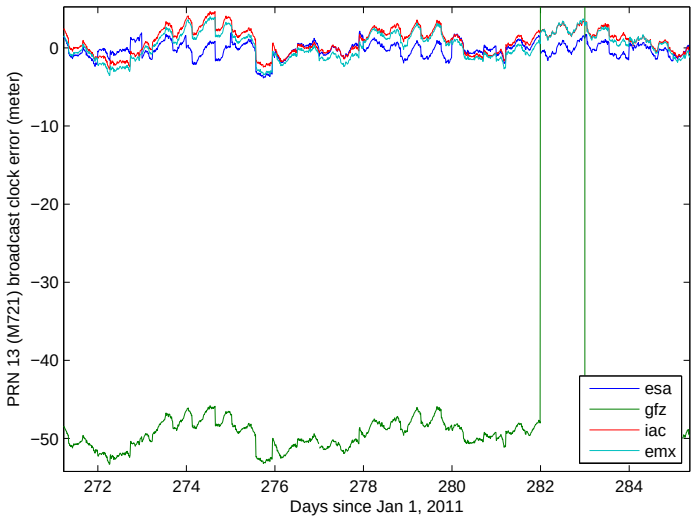

Figure 5.3: GLONASS-M 721 (PRN 13) clock errors from Day 272 to 285 of 2011, computed from `esa`, `gfz`, `iac`, and `emx` precise clocks. These precise clocks differ by a set of time-variant biases.

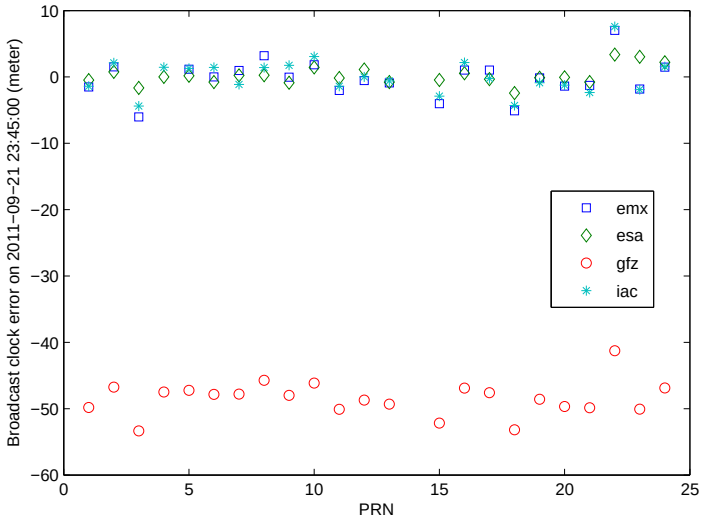

Figure 5.4: Clock errors of all GLONASS satellites at 23:45:00 on 2011-09-21, computed from `emx`, `esa`, `gfz`, and `iac` precise clocks. Common clock bias exists in `esa` and `gfz` precise clocks.

precise clocks could agree with each other if the time-variant biases were removed.

Figures 5.2 to 5.4 further shows that, at any instant, the satellite clock errors computed from `esa` or `gfz` precise clocks are offset by a common bias, while the clock errors computed from `emx` and `iac` precise clocks do not show obvious biases. This feature helps build a clock alignment algorithm to remove the time-variant common biases. The clock alignment algorithm is detailed in Section 5.2.3.

5.2 Methods

Figure 5.5 illustrates the whole process of identifying GLONASS SIS anomalies. First, we vote the validated values from the raw broadcast navigation message data using the data cleansing algorithm, and then propagate them at 15-minute intervals synchronized to the precise ephemeris and clock. The precise ephemerides extracted from the `igx`*wwwwd*`.sp3` files are converted from CoM to APC; the difference between the propagated broadcast ephemerides and the precise ephemerides in APC are the raw ephemeris errors. The precise clocks extracted from the `emx`*wwwwd*`.sp3`, `esa`*wwwwd*`.sp3`, `gfz`*wwwwd*`.sp3`, and `iac`*wwwwd*`.sp3` files are compared with the propagated broadcast clocks, generating four versions of raw

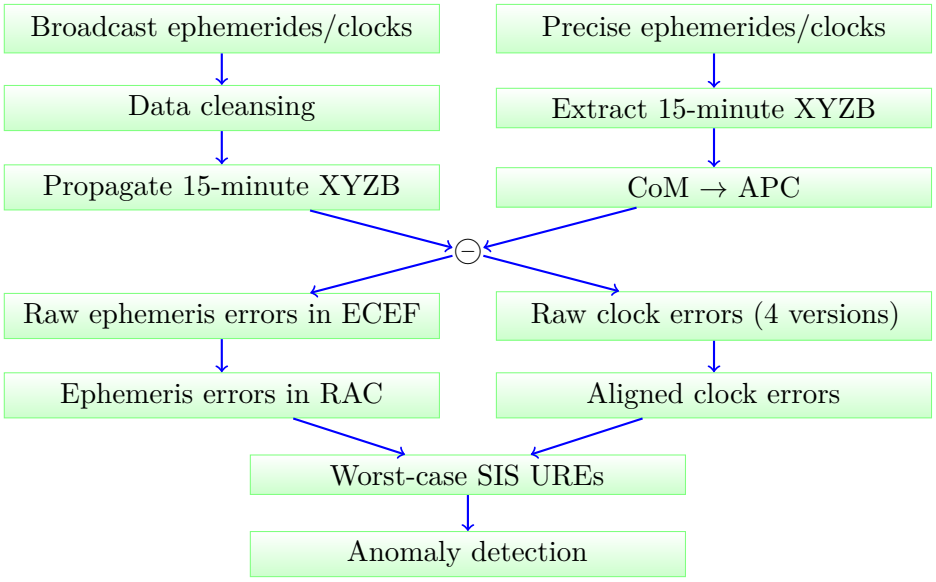

Figure 5.5: Whole process of GLONASS SIS anomaly identification. XYZB values refer to the coordinates of satellite position in ECEF and satellite clock bias. RAC refer to the radial, alongtrack, and crosstrack-based satellite centered coordinate system.

clock errors. After converting the ephemeris errors into the satellite centered coordinate system and aligning the four versions of raw clock errors, the WC UREs are computed by the geometric method described in Section 3.5, and then used for anomaly detection. The algorithms for data cleansing, clock alignment, WC UREs, and anomaly detection are discussed in the following subsections.

5.2.1 Data cleansing

As mentioned in Section 5.1.1, a small portion of the RINEX navigation message data files include data-logging errors. The data cleansing algorithm developed for GPS is adapted to process GLONASS navigation message data. Fortunately, the GLONASS data cleansing task is even easier thanks to the simplicity of the RINEX format for GLONASS navigation message data. The major differences from the GPS data cleansing are outlined as follows.

- The navigation reference time t_b is used as a uniqueness criterion in minority discard. t_b is never reused; hence, it is a better uniqueness criterion than IODC and t_{oc}, both of which are used in GPS data cleansing.

- The URA classification is no longer needed because the RINEX format for GLONASS does not capture URA values.
- The TTOM estimation is no longer needed because the first TTOM of a GLONASS navigation message is $t_b - 15$ minutes.

Except for the above differences, the whole GLONASS data cleansing process is the same as the GPS data cleansing process, i.e., composed of two steps: voter registration and majority voting. Both of the two steps have been thoroughly described in Section 3.4, and are not repeated here.

5.2.2 Broadcast ephemeris propagation

While GPS, Galileo, and Compass broadcast quasi-Keplerian ephemeris parameters, GLONASS broadcasts relatively raw Cartesian ephemeris parameters which consists of the instantaneous satellite position, satellite velocity, and lunisolar acceleration in ECEF at a reference time t_b. In this dissertation, we use the force model recommended by the GLONASS Interface Control Document (ICD)[11] to propagate the satellite position at any valid time t ($|t - t_b| \leq 15$ minutes):

$$\ddot{x} = \eta_1 x + \eta_2(1 - \eta_3)x + \omega^2 x + 2\omega\dot{y} + \ddot{x}_{LS}, \tag{5.1}$$

$$\ddot{y} = \eta_1 y + \eta_2(1 - \eta_3)y + \omega^2 y - 2\omega\dot{x} + \ddot{y}_{LS}, \tag{5.2}$$

$$\ddot{z} = \eta_1 z + \eta_2(3 - \eta_3)z + \ddot{z}_{LS}. \tag{5.3}$$

In the above equations, $\eta_1 = -GM/r^3$ accounts for the Earth's gravity; $\eta_2 = -1.5J_2GMa_e^2/r^5$ and $\eta_3 = 5z^2/r^2$ account for the perturbation due to the Earth's oblateness; ω is the Earth's rotation rate; $\ddot{x}_{LS}$, $\ddot{y}_{LS}$, and $\ddot{z}_{LS}$ are the lunisolar acceleration given by the broadcast ephemeris. A thorough description of these equations can be found in [78, 124].

Following the recommendation in [78, 125], we use the fourth-order Runge-Kutta method with 50-second step to propagate broadcast ephemerides at the 15-minute intervals that coincide with the precise ephemerides. The resulting numerical integration errors are generally less than 1 millimeter at $t_b \pm 20$ minutes [125].

5.2.3 Clock alignment

The analysis in the section "Data Sources" has indicated that

[11] The equations given by the ICD [78] have a few typos. Equations (5.1) to (5.3) are adapted from [124].

- No obvious common clock biases exist in the `emx` and `iac` precise clocks;
- Common clock biases exist in the `esa` and `gfz` precise clocks;
- Common clock biases vary with time.

Accordingly, we model the common clock biases as follows:

$$
\begin{aligned}
\mathrm{ClkErr}_{1,\mathrm{iac}} &= \mathrm{TrueClkErr}_1 + \epsilon_{1,\mathrm{iac}} \\
&\vdots \\
\mathrm{ClkErr}_{24,\mathrm{iac}} &= \mathrm{TrueClkErr}_{24} + \epsilon_{24,\mathrm{iac}} \\
\mathrm{ClkErr}_{1,\mathrm{esa}} &= \mathrm{TrueClkErr}_1 + \mathrm{CommonBias}_{\mathrm{esa}} + \epsilon_{1,\mathrm{esa}} \\
&\vdots \\
\mathrm{ClkErr}_{24,\mathrm{esa}} &= \mathrm{TrueClkErr}_{24} + \mathrm{CommonBias}_{\mathrm{esa}} + \epsilon_{24,\mathrm{esa}} \\
\mathrm{ClkErr}_{1,\mathrm{gfz}} &= \mathrm{TrueClkErr}_1 + \mathrm{CommonBias}_{\mathrm{gfz}} + \epsilon_{1,\mathrm{gfz}} \\
&\vdots \\
\mathrm{ClkErr}_{24,\mathrm{gfz}} &= \mathrm{TrueClkErr}_{24} + \mathrm{CommonBias}_{\mathrm{gfz}} + \epsilon_{24,\mathrm{gfz}} \\
\mathrm{ClkErr}_{1,\mathrm{emx}} &= \mathrm{TrueClkErr}_1 + \epsilon_{1,\mathrm{emx}} \\
&\vdots \\
\mathrm{ClkErr}_{24,\mathrm{emx}} &= \mathrm{TrueClkErr}_{24} + \epsilon_{24,\mathrm{emx}}
\end{aligned}
$$

In the above equations, $\mathrm{ClkErr}_{i,\mathrm{xxx}}$ is the clock error of PRN i computed from precise clocks `xxxwwwwd.sp3`, $\mathrm{TrueClkErr}_i$ is the true clock error of PRN i, $\mathrm{CommonBias}_{\mathrm{xxx}}$ is the common clock bias of the precise clocks `xxxwwwwd.sp3`, and $\epsilon_{i,\mathrm{xxx}}$ is the fitting error in $\mathrm{ClkErr}_{i,\mathrm{xxx}}$. The known values in the equations are marked in green, whereas the unknown variables we are interested in are marked in red.

Obviously, this is a typical system of linear equations with $n + 2$ unknown variables $\mathrm{TrueClockError}_i$, $\mathrm{CommonBias}_{\mathrm{esa}}$, and $\mathrm{CommonBias}_{\mathrm{gfz}}$, where n is the number of healthy satellites at the instant. Fortunately, this linear system is usually overdetermined because the number of equations, $4n$, exceeds the number of unknown variables, $n + 2$.

Since outliers may exist in $\mathrm{ClkErr}_{i,\mathrm{xxx}}$ due to either SIS anomalies or accidental errors in precise clocks, we use a robust multilinear regression to solve the overdetermined linear system. This robust multilinear regression uses iteratively reweighted least squares [126]

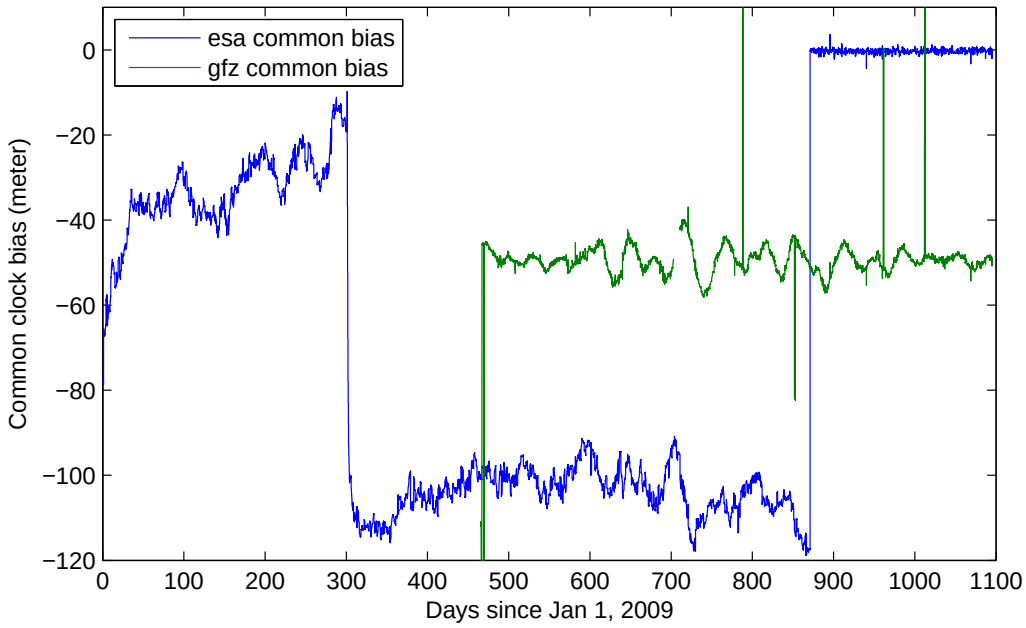

(a) Solutions of the common clock biases

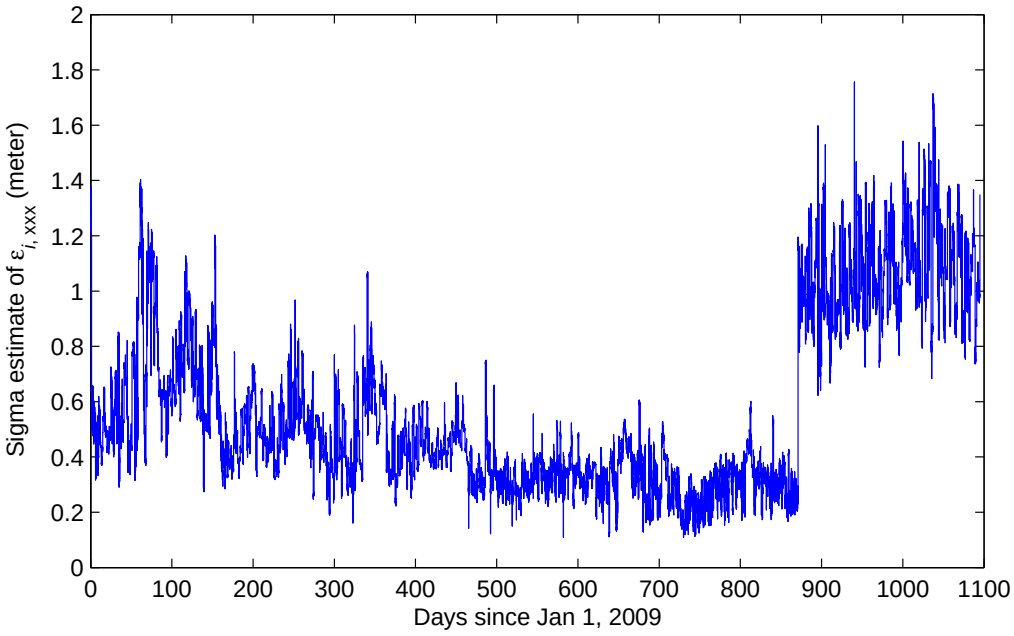

(b) Sigma estimate of fitting errors $\epsilon_{i,\mathrm{xxx}}$

Figure 5.6: Common clock biases and sigma estimates of fitting errors over the past three years.

with a bisquare weighting function [127].

Figures 5.6 (a) and (b) show the solutions of the common clock biases and the sigma estimate of the fitting errors $\epsilon_{i,\text{xxx}}$ during the past three years, respectively. One interesting phenomenon is that the `esa` precise clock changed its time reference twice, and the latter change resulted in almost zero common clock biases but larger fitting errors. Another interesting phenomenon is that `gfz` precise clocks had a few spikes in the common clock biases, which may imply some irregularities in their time reference.

5.2.4 Anomaly detection

As mentioned at the beginning of this chapter, no official GLONASS integrity standard has been issued yet, and there is even no URA information in the RINEX navigation data. To get around these problems, we define a 50-meter threshold for WC UREs for the following two reasons.

First, the statistics of nominal GLONASS SIS URE behavior (Section 6.4) show that the standard deviation of UREs are generally less than 4 meters and the excess kurtosis of UREs is around 2. Therefore, we use 4 meters as the URA, and this value also matches most URAs broadcast by GLONASS satellites. Probability theory [128] has shown that a Student's t-distribution with 7 DoF random variable X has an excess kurtosis of 2, and $\text{Prob}(|X| > 11.2148) = 10^{-5}$. Therefore, a 10^{-5} significance level leads to a threshold of $4 \times 11.2148 \approx 45$ meters for GLONASS UREs.

Second, the nominal GLONASS UREs in the past three years are roughly twice as large as the GPS UREs before 2008 (Figure 6.3). GPS defined a 30-meter threshold before 2008 [96]; a rule-of-thumb analogy leads to a 60-meter threshold for detecting GLONASS SIS anomalies.

Considering both of the reasons above, we finally choose a 50-meter threshold. A potential GLONASS SIS anomaly is claimed when all the following conditions are fulfilled.

- The WC URE exceeds 50 meters;
- The broadcast navigation message is flagged healthy, i.e., the RINEX field `SV health` [108] is 0;
- The time of transmission is within the fit interval, i.e., $|t - t_b| \leq 15$ minutes;
- The precise ephemeris and clock are available and healthy.

5.3 Identified GLONASS SIS Anomalies

We have identified 192 potential GLONASS SIS anomalies using the aforementioned methods to process a total of 80,814,366 broadcast navigation messages collected between 2009-01-01 and 2012-08-11. Figure 5.7 depicts these anomalies. For a deeper insight, we divide the anomalies into four groups: small/large ephemeris/clock anomalies. The "small" means 50 m $<$ |WC URE| $\leq$ 500 m, whereas the "large" means |WC URE| $>$ 500 m. The "ephemeris" or "clock" means the anomalous URE is mainly attributable to broadcast ephemeris or clock inaccuracy, respectively.

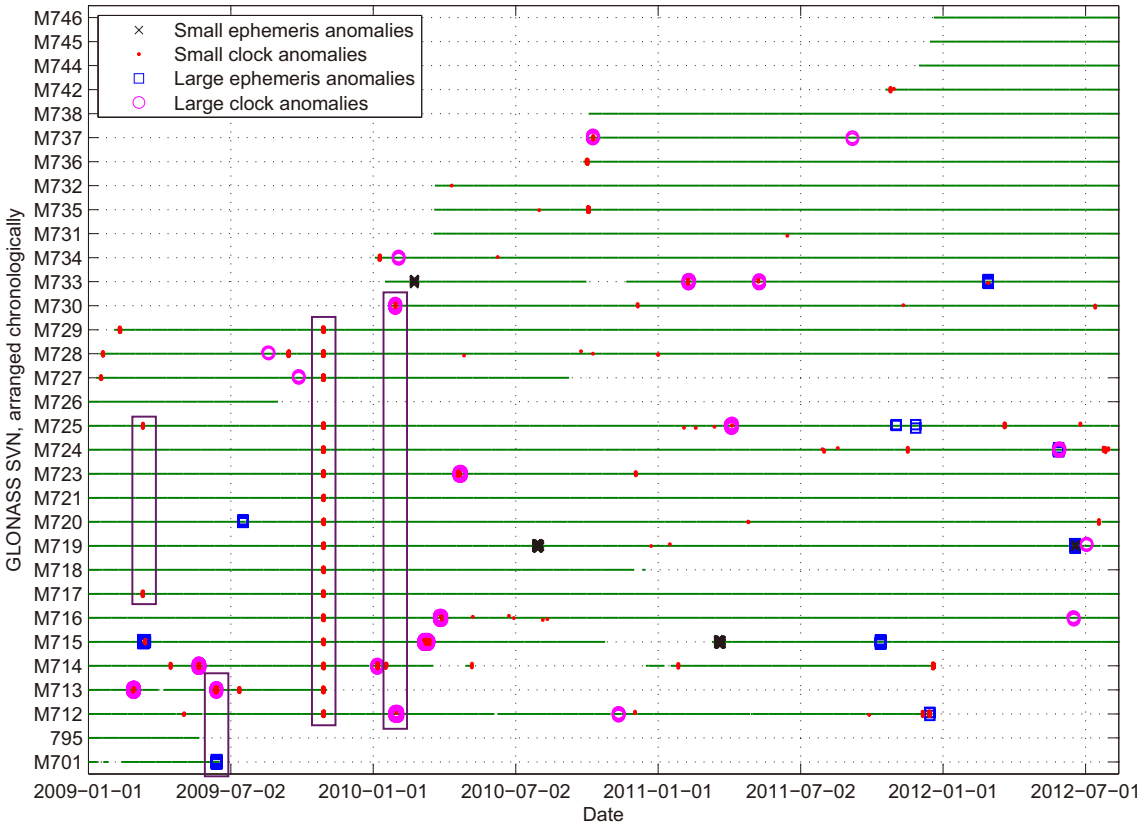

Figure 5.7: Identified GLONASS SIS anomalies between 2009-01-01 and 2012-08-11. The horizontal green lines depict the periods when the satellites were operational (not necessarily healthy). The purple rectangles indicate simultaneous multiple anomalies, including a constellation-wide event on 2009-10-28.

It can be seen from Figure 5.7 that most anomalies resulted from clock inaccuracies. A simple count shows that approximately 92% of the anomalies are clock anomalies. Additionally, the younger satellites launched after February 2010 had fewer anomalies than the older satellites did. The following section will further analyze the identified anomalies in terms of anomaly probability, simultaneous multiple anomalies, and geographic dependency.

5.4 Analysis of Identified Anomalies

5.4.1 Anomaly probability

The empirical probability of anomaly is not only a figure of merit to assess the GLONASS integrity performance, but also an essential parameter in ARAIM, as has been discussed in Section 1.2. Figure 5.8 shows the total hours and number of anomalies per year[12]. The total hours of anomalies per year, indicated by the blue solid polyline, can be compared to the

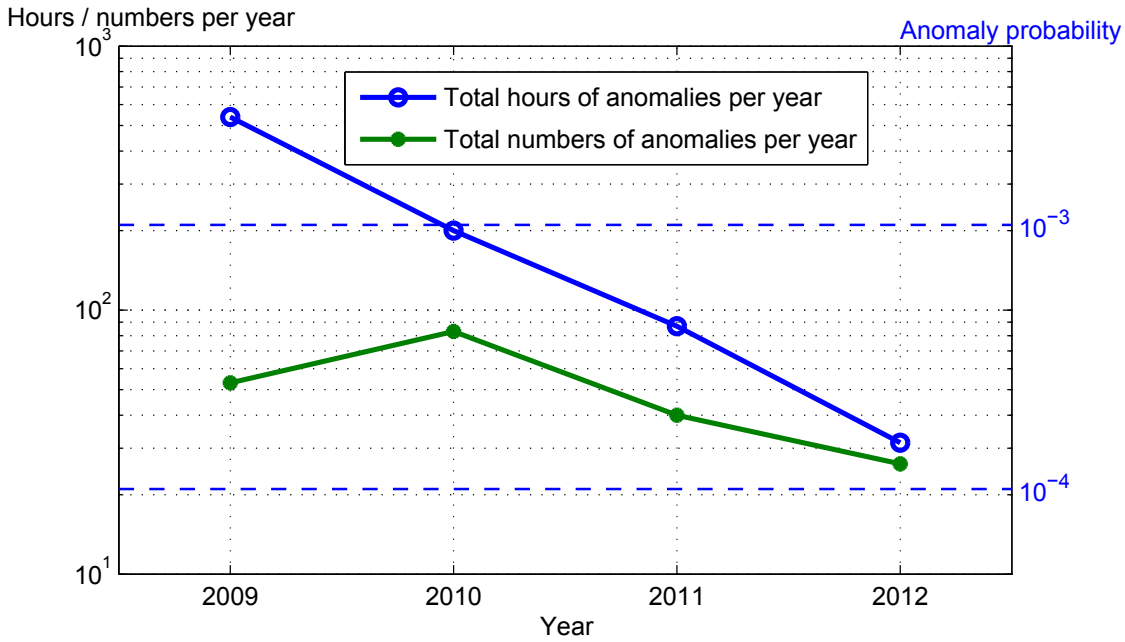

Figure 5.8: Total hours/number of identified GLONASS anomalies per year. The anomaly probability is based on a full constellation (24 active satellites) with zero outage.

[12]The total hours/number of anomalies in 2012 is extrapolated from the total hours/number of anomalies between 2012-01-01 and 2012-08-11.

two horizontal blue dashed lines, which indicate anomaly probability of 10^{-3} and 10^{-4} under the assumption of a full constellation (24 active satellites) and zero outage. Clearly, the anomaly probability has improved from 10^{-3} level to 10^{-4} level during the past three years. Dividing the total hours of anomalies by the total hours of anomalies, one can see that the average duration of an anomaly has also improved, from roughly 10 hours per anomaly in 2009 to 1 hour per anomaly in 2012.

5.4.2 Simultaneous multiple anomalies

Two other key assumptions in ARAIM are the number of simultaneous satellite faults and the probability of constellation failure (Section 1.2). GPS has not had simultaneous multiple anomalies since 2004 (Section 3.6). For GLONASS, as shown by the purple rectangles in Figure 5.7, simultaneous multiple anomalies have occurred four times: three in 2009, and one in early 2010. This discovery can help ARAIM systems make correct assumptions for the use of GLONASS. In addition, the fact that no simultaneous multiple anomalies have

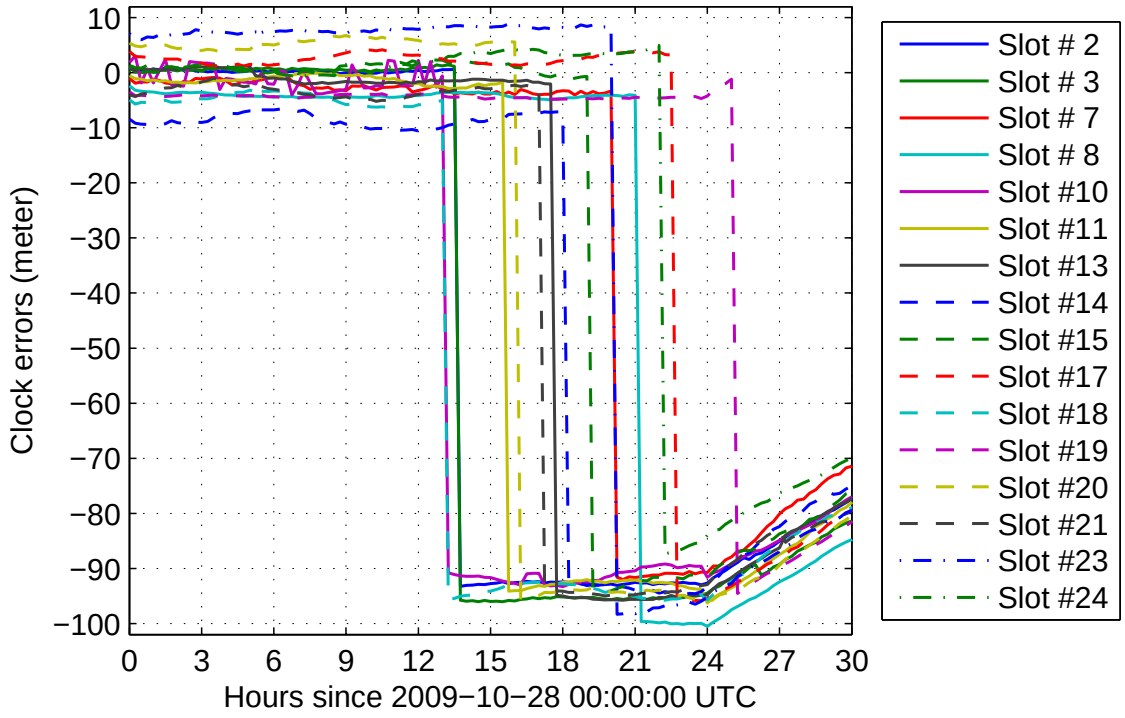

Figure 5.9: Broadcast clock errors of all 16 GLONASS satellites on 2009-10-28.

occurred since February 2010 implies an improving GLONASS SIS integrity performance over the past three years.

The simultaneous multiple anomalies on 2009-10-28 are definitely an eye-catcher because all 16 satellites in the constellation were anomalous. As shown in Figure 5.9, the constellation-wide anomalies were due to an abrupt change of broadcast clocks by approximately −90 meters (−300 nanoseconds)[13]. Unfortunately, the satellites made the change one by one, rather than at the same time. Therefore, from 13:30 UTC to midnight, the constellation consisted of satellites with changed clocks and satellites with original clocks, resulting in unusually large positioning errors in many parts on Earth. Figure 5.10 shows the worst period, from 16:30 to 17:45 UTC, when half of the constellation was anomalous, and a GLONASS user at any place on Earth could see both nominal and anomalous satellites.

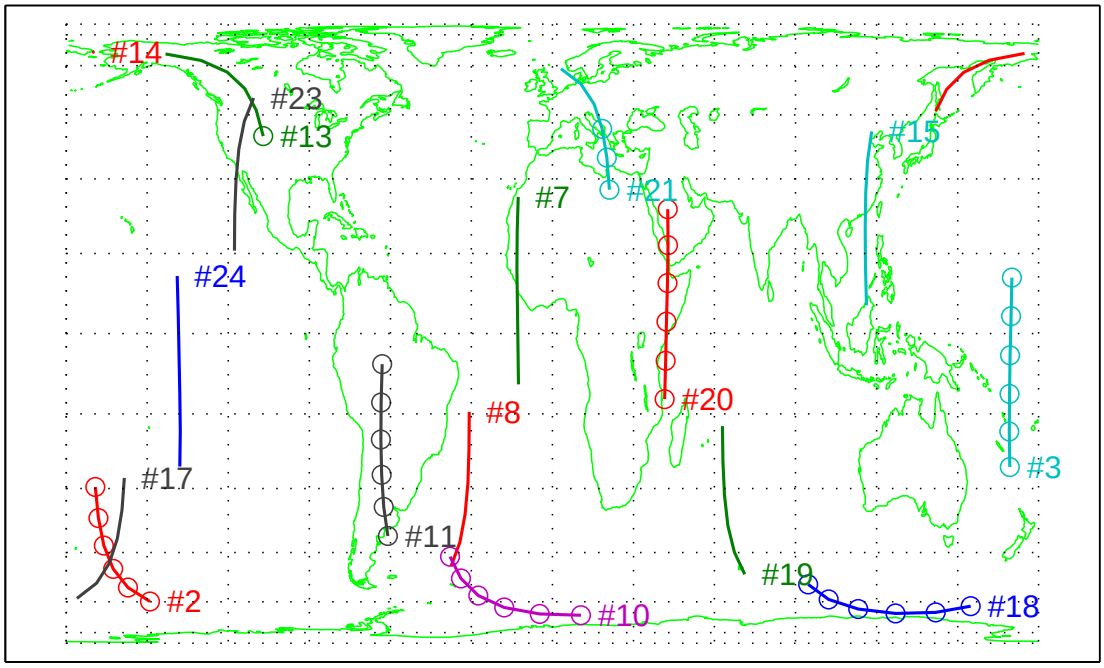

Figure 5.10: Ground tracks of all 16 GLONASS satellites from 16:30 to 17:45 UTC on 2009-10-28, when 8 satellites were anomalous. Circles indicate anomalous status.

[13]The precise clocks show that none of the onboard atomic clocks had a noticeable change during this event. The clock correction terms in broadcast navigation messages suddenly changed because of a jump of GLONASS Time on that day [129].

5.4.3 Geographic dependency

Section 2.1 has shown that all GLONASS monitor stations are within the Russian territory. When a satellite is not monitored, it may be more likely to become anomalous. Even worse, when such an anomaly occurs, it may last for hours until the ground control regains tracking of the satellite and fixes the problem. Therefore, a reasonable hypothesis is that the occurrence of GLONASS anomalies has geographic dependency. To verify this hypothesis, the ground tracks of anomalous GLONASS satellites since January 2010 are plotted in Figure 5.11, as shown by the red dots. Obviously, there are more red dots in the unshaded

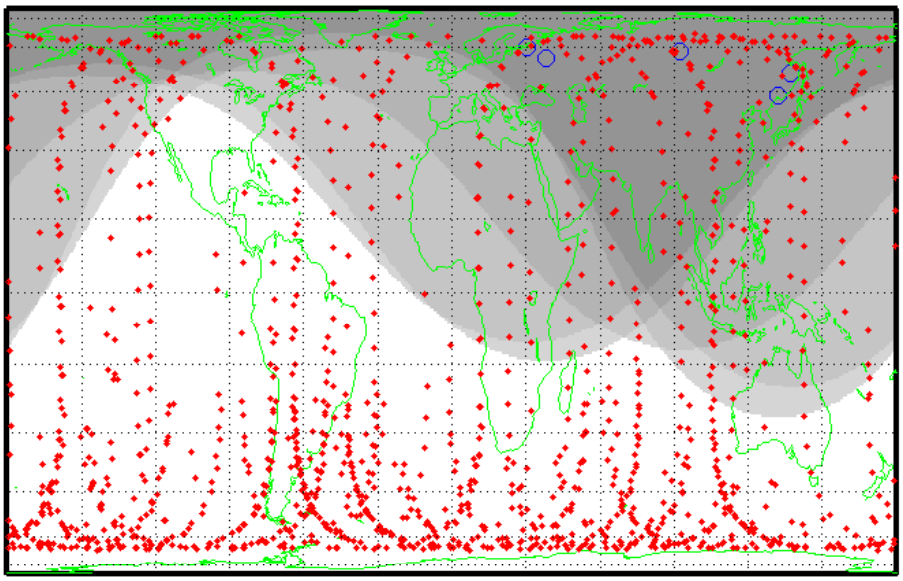

Figure 5.11: Ground tracks (denoted by red dots) of anomalous GLONASS satellites since January 2010. The blue circles represent the existing GLONASS monitor stations (Figure 2.4). The shaded areas indicate the tracking coverage of these monitor stations (Figure 2.5).

Condition	Total anomaly time	Anomaly probability
Unmonitored	212 satellite-hour	8.7×10^{-4}
Monitored	94 satellite-hour	3.9×10^{-4}

Table 5.1: Geographic dependency of anomaly occurrence. The statistics are based on the identified anomalies from January 2010 to August 2012.

area than in the shaded area. The quantitative results in Table 5.1 further confirm that anomalies are approximately twice as likely to occur when satellites are not monitored.

5.5 Summary

In this chapter, we devised and implemented a systematic data mining of GLONASS SIS anomalies from 80,814,366 navigation messages corrupted by data-logging errors. After removing the data-logging errors, aligning multiple inconsistent precise clock products, and defining our own statistic-based anomaly criteria that does not rely on URA, we successfully identified 192 potential SIS anomalies between 2009-01-01 and 2012-08-11. The results show that 92% of anomalies are due to clock inaccuracy, and younger satellites have better performance. The analysis of total hours of anomalies per year shows that the anomaly probability has been improving, from 10^{-3} level in 2009 to 10^{-4} level in 2012. We also discovered four events of simultaneous multiple anomalies, including a constellation-wide clock change on 2009-10-28 that impacted all satellites. In addition, the analysis of geographic dependency shows that anomalies occur twice as frequently when satellites are not monitored by the GLONASS ground control.

Although the observed GLONASS performance does not match the current GPS performance (Section 3.6), the GLONASS SIS does show an improving trend, especially in terms of constellation strength, anomaly probability, and occurrence of simultaneous multiple anomalies. The improvement of GLONASS SIS integrity performance will be very beneficial to not only numerous GLONASS users but also many multi-constellation GNSS applications.

Chapter 6

Statistical Characterization of GPS and GLONASS SIS Errors

Although the primary goal of this dissertation is the global monitoring of GPS and GLONASS SIS anomalies, an in-depth characterization of nominal SIS errors is still necessary because a thorough understanding of nominal errors helps design anomaly monitors. One telling example is the GPS SIS integrity performance standard [19]—for any healthy SIS,

$$\text{Prob}(|\text{I URE}| > 4.42 \cdot \text{URA UB}) \leq 10^{-5}. \tag{6.1}$$

This standard indicates an underlying assumption that I UREs are zero-mean Gaussian and properly overbounded by URA UB. In addition, one of the key assumptions in RAIM is that large (not necessarily anomalous) UREs occur on several satellites simultaneously with very low probability [32]. Therefore, this chapter aims at a statistical characterization of nominal GPS and GLONASS SIS errors with emphasis on validating these assumptions.

The chapter is organized as follows. Section 6.1 introduces additional SIS error metrics and statistical methods for characterizing GPS and GLONASS SIS errors. Section 6.2 discusses long-term SIS accuracy performance and selects an appropriate range of data for statistics. Sections 6.3 and 6.4 present the statistics for GPS and GLONASS, respectively. These statistics are used to examine the above assumptions about the distribution of nominal UREs and the correlation among UREs of different satellites. Additionally, two particular issues with GLONASS, ephemeris error growth with propagation distance and geographic dependency, are discussed. Finally, Section 6.5 summarizes the nominal GPS and GLONASS error performance in terms of the similarities and differences.

6.1 Methods

6.1.1 SIS error metrics

In addition to the global average (GA) URE and worst-case (WC) URE discussed in Sections 2.3 and 3.5, this chapter considers two more SIS error metrics:

- Instantaneous UREs (I UREs): computed for 20 points spread evenly on Earth, as shown in Figure 6.1;
- Global average SIS URE without the clock error (GA URE_0): the root mean square (rms) URE across the portion of the globe in view of the satellite under the assumption of zero clock errors, generally a performance metric of broadcast ephemeris accuracy,

$$\text{GA URE}_0 \approx \begin{cases} \sqrt{(0.98R)^2 + (A^2 + C^2)/49} & \text{for GPS,} \\ \sqrt{(0.98R)^2 + (A^2 + C^2)/45} & \text{for GLONASS,} \end{cases} \tag{6.2}$$

  where R is the radial ephemeris error, A is the alongtrack ephemeris error, C is the crosstrack ephemeris error, and T is the clock error.

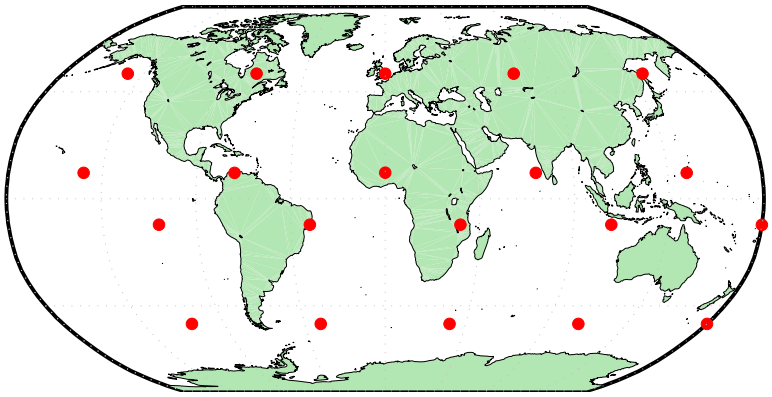

Figure 6.1: I UREs are computed for 20 points spread evenly on Earth. These points are derived from the vertices of a regular dodecahedron.

6.1.2 Robust statistics

Since this chapter focuses on the nominal core SIS error behavior, all GPS and GLONASS anomalies identified in Chapters 3 and 5 are precluded from taking part in the statistics.

In addition, several robust statistical methods are used to avoid excessive influence due to outliers or other small departures from statistical model assumptions.

Robust mean and standard deviation

Since SIS errors are not necessarily normally distributed and are not free from outliers, the traditional statistics such as sample mean and sample standard deviation may be affected by some extreme samples. Moreover, the sample mean is not necessarily the maximum likelihood (ML) estimator of expected value for non-Gaussian samples. For instance, sample median, rather than sample mean, is the ML estimator of expected value for the samples from a two-sided exponential distribution [130]. To cope with this problem, we use the trimmed mean (see definition in Section 3.3.2 and [113]) to measure the central tendency. Analogously, a trimmed standard deviation function is defined as

$$\mathrm{std}_\alpha(X) = \sqrt{\mathrm{mean}_\alpha((X - \mathrm{mean}_\alpha(X))^2)}. \tag{6.3}$$

In fact, the trimmed mean is a compromise between the sample mean and the sample median, and the trimmed standard deviation is a compromise between the sample standard deviation and the sample median absolute deviation. This study uses a small value $\alpha = 0.01$, i.e., 99% of the core data, to make the result close to the mean or the standard deviation.

Robust normality metric

A normality metric is used to assess how close the actual errors are to normally distributed. Well-known statistical hypothesis tests of normality, such as the Shapiro-Wilk test [131], Lilliefors test [132], and Jarque-Bera test [133], are so strict that they usually reject the null hypothesis that the SIS error samples comes from a distribution in the normal family. Even worse, common software implementations of these tests can seldom return a meaningful p-value [134] to indicate how far SIS error samples are from normally distributed. Therefore, we use sample kurtosis to quantify normality. Kurtosis (also known as excess kurtosis) is defined as

$$\gamma(X) = \frac{\mathbb{E}(X - \mathbb{E}X)^4}{\left(\mathbb{E}(X - \mathbb{E}X)^2\right)^2} - 3, \tag{6.4}$$

where $\mathbb{E}(\cdot)$ is the expectation function. As shown in Figure 6.2, a normal distribution has a kurtosis $\gamma = 0$; a sub-Gaussian distribution with light tails usually has a kurtosis $\gamma < 0$; a super-Gaussian distribution with heavy tails usually has a kurtosis $\gamma > 0$.

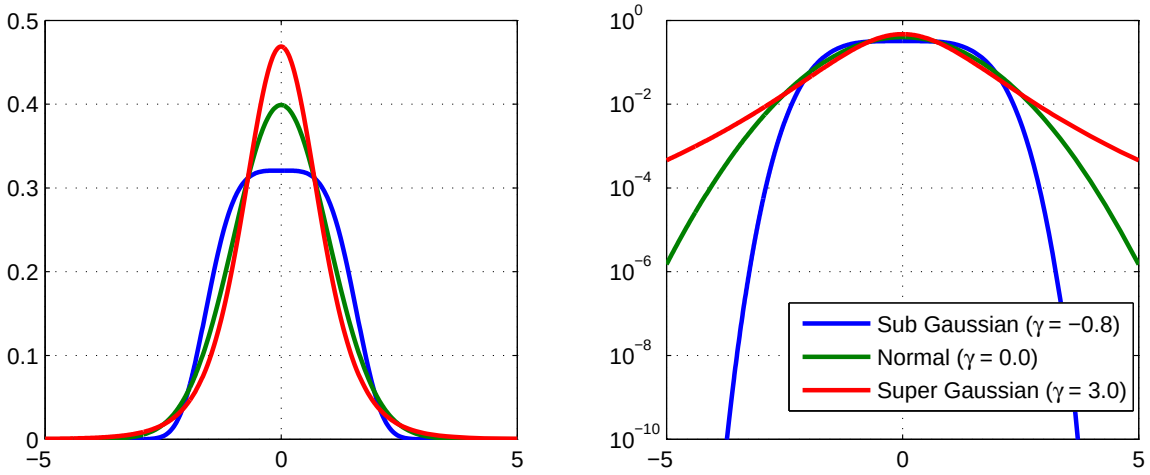

Figure 6.2: Examples of sub-Gaussian, normal, and super-Gaussian distributions. All three distributions have zero mean and unit variance. The probability density functions are shown in both linear and logarithm scales.

The sample kurtosis is not only a measure of normality, but also an indication of some mixture distributions. When a satellite does not have stationary performance, its SIS UREs may be modeled as a mixture of several zero-mean normal distributions. Let us consider the following simple case:

$$X \sim \begin{cases} N(0, \sigma_1^2) & \text{with probability } p, \\ N(0, \sigma_2^2) & \text{with probability } q, \end{cases} \tag{6.5}$$

where $p \geq 0$, $q \geq 0$, $p + q = 1$. Then the kurtosis is given by

$$\gamma(X) = \frac{\mathbb{E}X^4}{\left(\mathbb{E}X^2\right)^2} - 3 = \frac{p \cdot 3\sigma_1^4 + q \cdot 3\sigma_2^4}{(p \cdot \sigma_1^2 + q \cdot \sigma_2^2)^2} - 3 = 3\left(\frac{p\sigma_1^4 + q\sigma_2^4}{(p\sigma_1^2 + q\sigma_2^2)^2} - 1\right) \geq 0, \tag{6.6}$$

where the inequality holds because the function $f(x) = x^2$ is convex, and thus $pf(\sigma_1^2) + qf(\sigma_2^2) \geq f(p\sigma_1^2 + q\sigma_2^2)$.

Since kurtosis involves fourth-order statistics, it relies on extreme values but is vulnerable to statistical outliers. The "trimmed" method, discarding a certain percent of extreme samples, works well for estimating the mean and the standard deviation but may introduce a significant bias for kurtosis. Alternatively, we compute kurtosis after discarding the samples with the absolute value greater than six times interquartile range. For a normal distribution,

six times interquartile range is approximately equal to eight-sigma, equivalent to 1.2×10^{-15} tail probability. Since the sample size is on the order of 10^5 for each satellite, this tail probability ensures that only statistical outliers are discarded. This step is important to improve the robustness of kurtosis estimation.

6.2 Long-Term Performance and Data Selection

Ideally, any reliable statistical characterization should be based on a period of data set that is statistically stationary and ergodic, because stationarity and ergodicity indicate that the random process does not change its statistical properties with time and the statistical properties can be deduced from a sufficiently long sample of the process [135]. In practice, a very large number of samples are usually a guarantee of not only ergodicity but also high statistical confidence. Nevertheless, a too large number of samples may affect stationarity because the long-term SIS URE performance can hardly be completely stationary. The

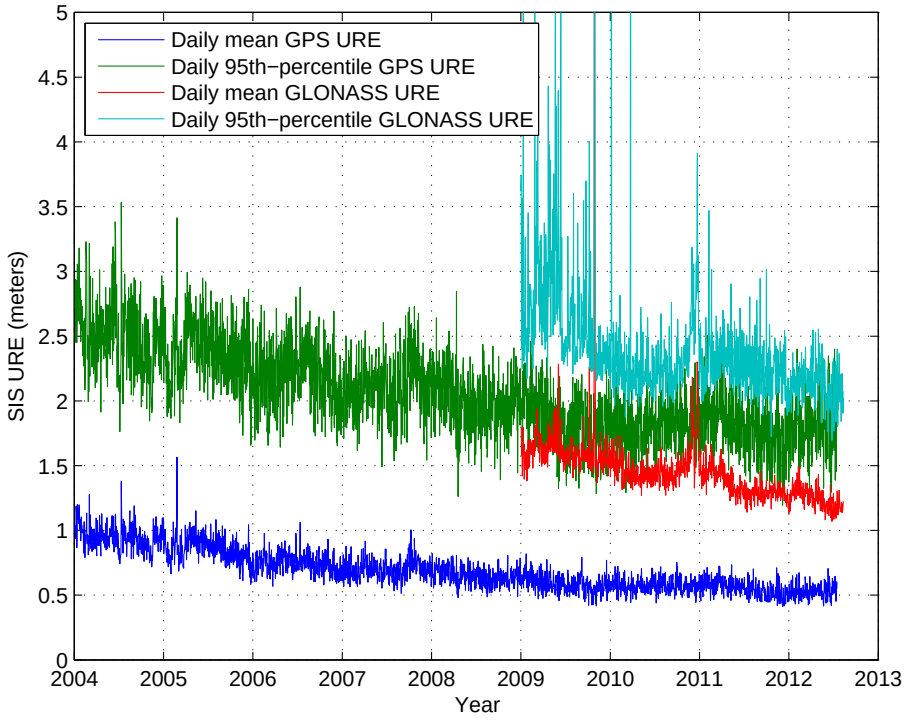

Figure 6.3: Long-term GPS and GLONASS SIS accuracy performance. The daily mean is obtained after trimming daily URE samples by 15%.

explanations for this include the facts that old satellites are wearing out, young satellites are being fine-tuned, and the ground control personnel are trying every way to improve SIS accuracy and integrity.

As shown by Figure 6.3, neither GPS nor GLONASS SIS URE performance over the past many years was completely stationary. Therefore, we use three years of data to form the statistics because the performance over three years is close to stationary, and $3 \times 365 \times 24 \times 4 \approx 10^5$ samples per satellite ensure ergodicity and high statistical confidence. Specifically, Section 6.3 uses the data between 2008-01-01 and 2010-12-31 to characterize nominal GPS SIS errors, and Section 6.4 uses the data between 2009-01-01 and 2011-12-31 to characterize nominal GLONASS SIS errors.

6.3 Statistics of Nominal GPS SIS Errors

6.3.1 Mean and standard deviation

Although ephemeris errors are generally assumed to have a zero mean distribution, the actualities may be different. Figure 6.4 plots the mean of ephemeris errors, clock errors, I UREs, and WC UREs with a comparison to their standard deviations. The satellites are arranged roughly chronologically according to their Block Type[1] and SVN along the y-axis.

Figure 6.4 tells many stories. First of all, almost all satellites have zero mean for their crosstrack errors, while about one third of the satellites have significant nonzero mean for their alongtrack errors. Fortunately, nonzero alongtrack or crosstrack errors do not result in nonzero mean of UREs. The mean of UREs are mainly correlated with the mean of clock errors and radial errors. The nonzero mean of UREs is not very critical because no satellite has a mean exceeding 20% of the standard deviation.

Secondly, in terms of standard deviation, the IIR and IIR-M satellites obviously have better performance than the IIA. Table 6.1 summarizes the standard deviation of various SIS errors grouped by Block Type. The better SIS performance of the younger satellites is mainly due to better onboard clocks and better radial estimation. Nevertheless, SIS error behavior is different from satellite to satellite even for those within the same Block Type and of similar age. A precise model of SIS errors should treat each satellite individually.

Lastly, both Figure 6.4 and Table 6.1 imply that clock performance dominates the

[1] In Figure 6.4, we follow the IGS convention to subdivide IIR satellites into two subgroups IIR-A and IIR-B because the last four IIR satellites were equipped with improved antennas [112].

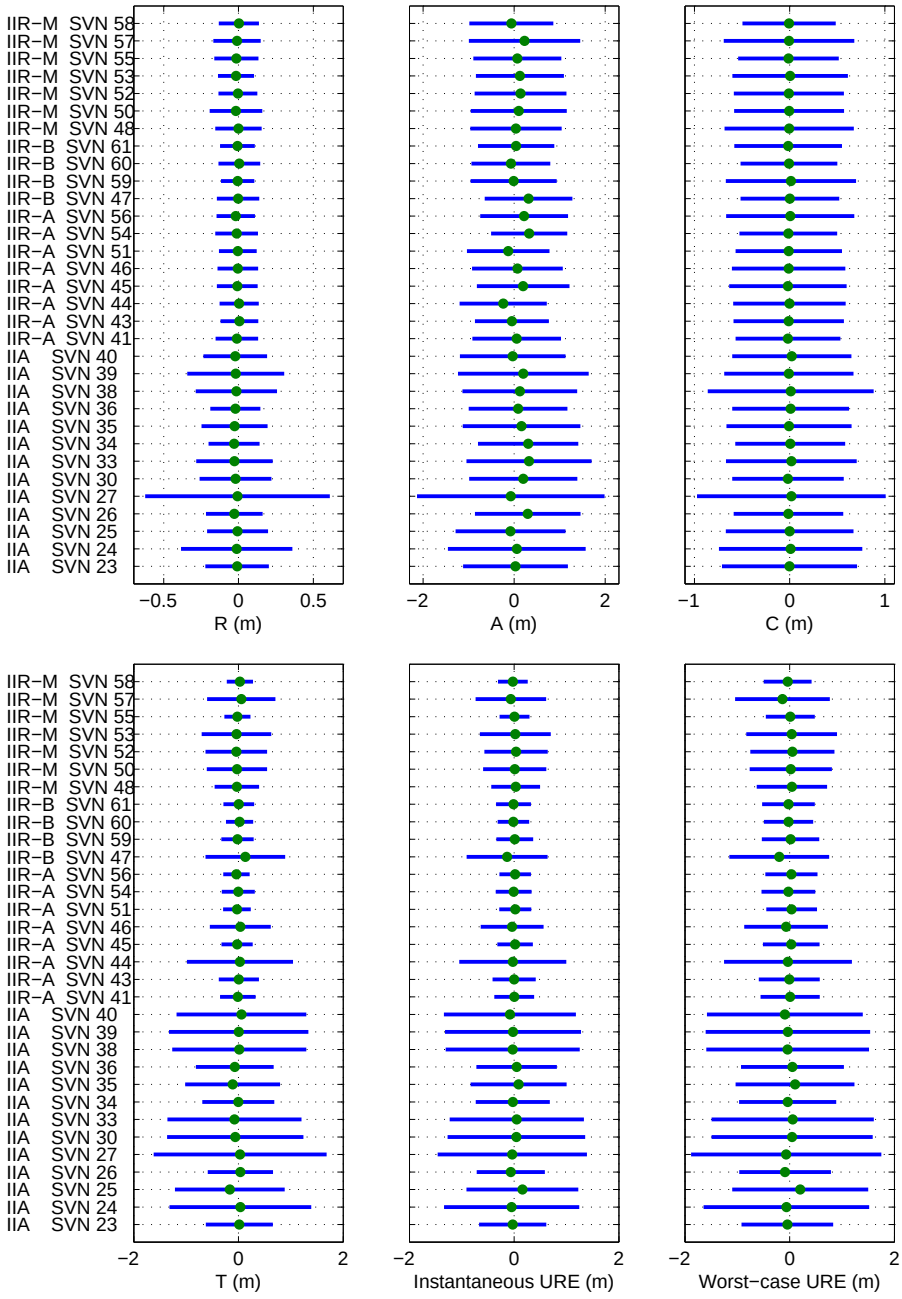

Figure 6.4: Mean of GPS SIS errors with a comparison to the standard deviation. The mean is denoted by the green dot, and the blue line with a length of twice the standard deviation is centered at the mean.

	IIA	IIR	IIR-M
Radial (meters)	0.243	0.130	0.145
Alongtrack (meters)	1.258	0.921	1.000
Crosstrack (meters)	0.675	0.575	0.594
Clock (meters)	1.074	0.384	0.498
I URE (meters)	1.076	0.418	0.527

Table 6.1: Standard deviation of GPS SIS errors grouped by Block Type.

performance of SIS UREs. This observation agrees with our analysis in Section 2.3.

6.3.2 Distribution

Figure 6.5 shows the sample kurtosis of ephemeris errors, clock errors, I UREs, and WC UREs. It can be seen that as for ephemeris errors, all satellites have a super-Gaussian distribution for alongtrack, and about half of the satellites have a super-Gaussian distribution for radial and crosstrack. Nevertheless, no ephemeris errors have a kurtosis greater than 3, which means that the tail is not very strong and a normal distribution with inflated sigma should be able to overbound ephemeris errors. In contrast, clock errors, especially those of some younger satellites, have a very large kurtosis. This observation is contrary to general expectations that the clock errors of younger satellites should be closer to normally distributed. One of the reasons for this unexpected behavior is that the onboard clocks of some younger satellites had been tuned during the first several months, and their clock errors show a certain degree of mixture distribution, which can result in a positive kurtosis, as proven by (6.6).

Another interesting phenomenon in Figure 6.5 is that WC UREs generally have a lower kurtosis than I UREs, which contradicts the common sense that "worst-case" should come with heavier tails. In fact, although WC UREs have heavier tails than I UREs, the distribution of WC UREs has two peaks (it is improbable for the worst-case values to reach zero) rather than one peak seen in the distribution of I UREs. The two peaks boost the variance more than the fourth central moment, and thus reduce the kurtosis[2].

In addition to kurtosis, we use a quantile-quantile (Q-Q) plot to compare the empirical

[2]To understand this, consider an extreme example, the Bernoulli distribution with $p = 1/2$, whose probability density function has two peaks, and the kurtosis is -2 [136].

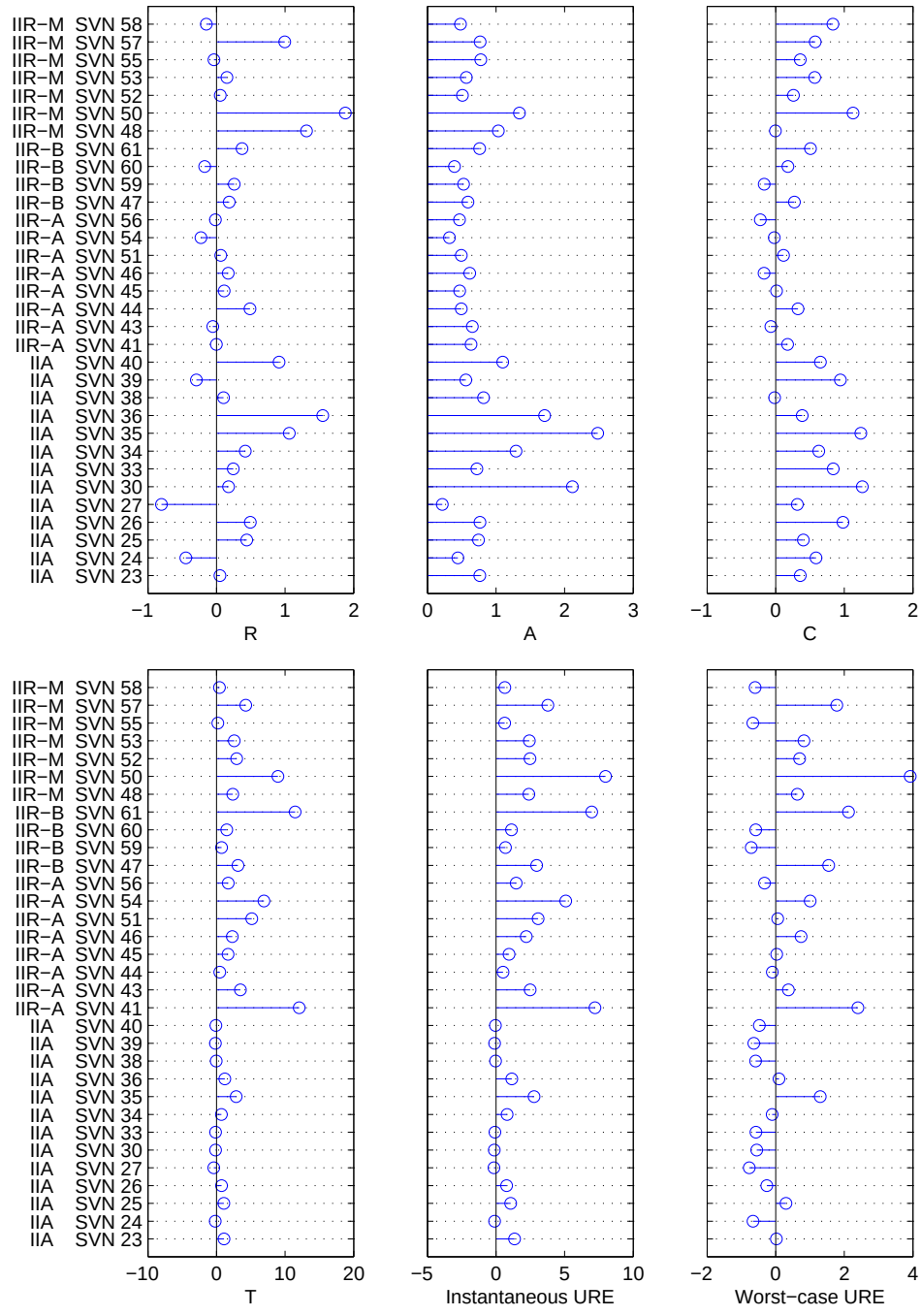

Figure 6.5: Sample kurtosis of GPS SIS errors.

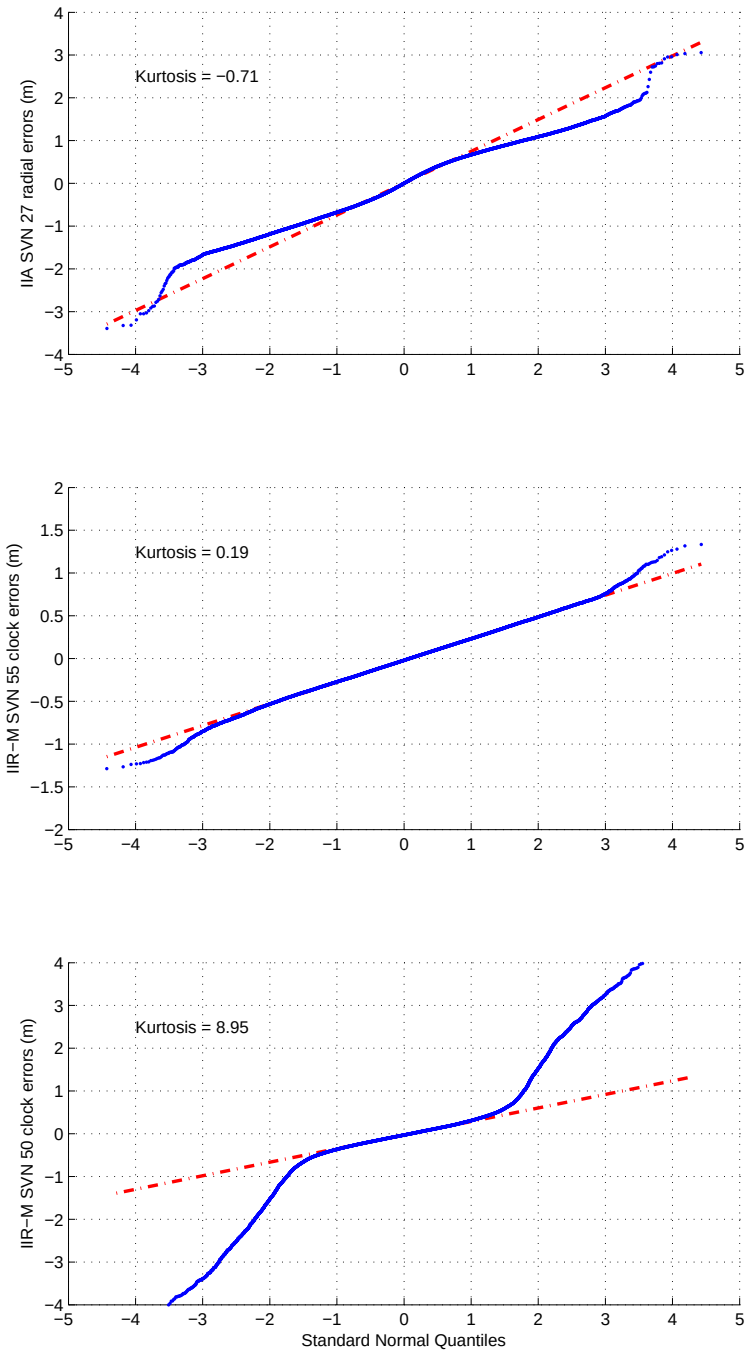

Figure 6.6: Q-Q plots of three typical distributions of GPS SIS errors: sub-Gaussian, almost-Gaussian, and super-Gaussian.

distribution of SIS errors with the standard normal distribution. Figure 6.6 shows three typical distributions: the sub-Gaussian distribution of IIA SVN 27 radial errors, the almost-Gaussian distribution of IIR-M SVN 55 clock errors, and the super-Gaussian distribution of IIR-M SVN 50 clock errors. It can be seen that even with a negative kurtosis, the IIA SVN 27 radial errors have slightly heavy tails[3]. When the kurtosis is positive, the tails are much heavier. Therefore, the Student's t-distribution, the mixture distribution given by (6.5), and the paired Gaussian distribution [137], may be good choices to model the UREs of most GPS satellites.

6.3.3 URA relationship to actual UREs

As mentioned in Section 2.4, broadcast URA is intended to be a conservative representation of the expected rms behavior of the corresponding I UREs. Since URA is used extensively

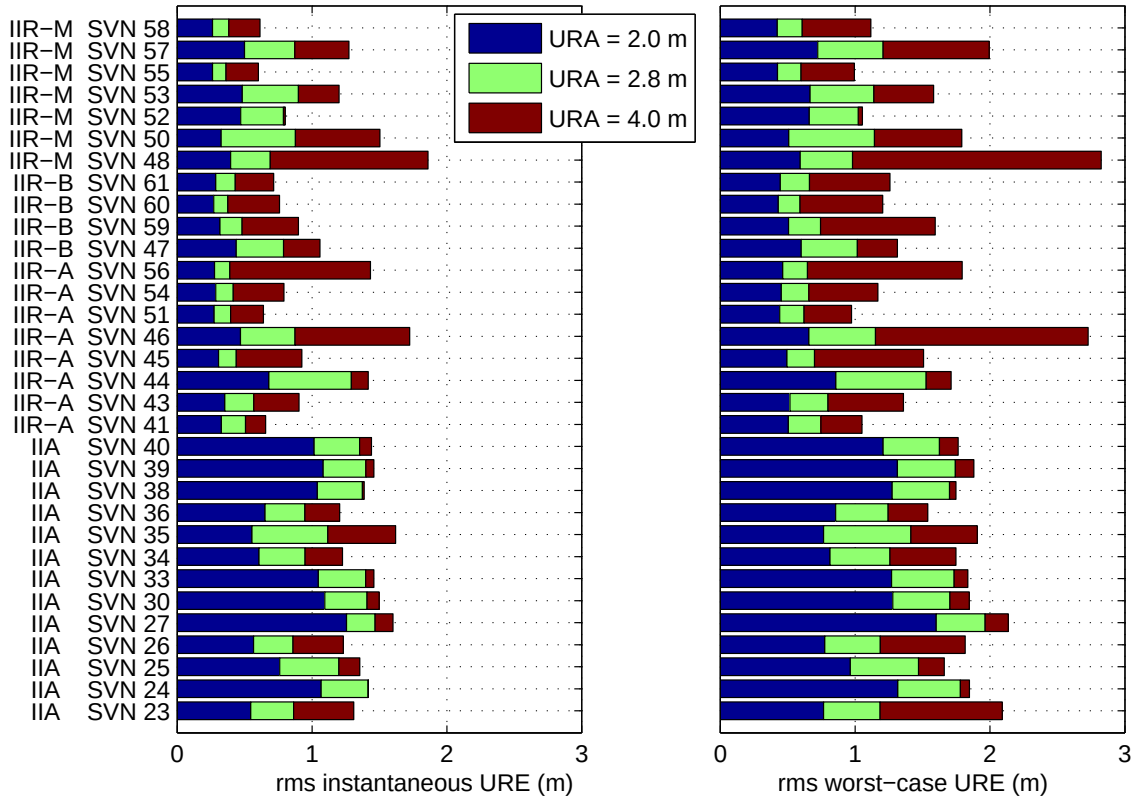

Figure 6.7: GPS rms I URE and rms WC URE grouped by different URA values.

[3]This apparent contradiction is because the kurtosis characterizes the normality of the majority of 10^5 samples, and the strong upper and lower tails are comprised of less than 50 samples.

in both position fixing and integrity monitoring, it is important to know how conservative URA is. Figure 6.7 plots the rms I URE and rms WC URE grouped by different URA. As can be seen in the left subfigure, URA is truly conservative: for some IIA satellites, URA is two times the expected rms URE; for most IIR and IIR-M satellites, URA is four times the expected rms URE. Furthermore, the rms WC URE in the right subfigure implies that even for the most unlucky, unrealistic user who always experiences the WC URE, he can still expect the rms URE to be much lower than URA. Besides, it can be seen that different satellites interpret URA very differently. For example, the rms I URE for IIA SVN 27 is around 1.3 meters despite the URA, whereas for IIR-M SVN 50 different URA does indicate different levels of rms I URE.

6.3.4 Correlation among UREs of different satellites

As mentioned in the beginning of this chapter, it is necessary to verify whether or not large UREs occur on several satellites simultaneously with very low probability. In other words, for an arbitrary user on Earth, the correlation among the UREs of the satellites in view is expected to be close to zero. Under this assumption, if UREs are close to normal, the sum of their squares should be close to chi-square distributed. Therefore, multiple satellite monitoring in ARAIM requires the following chi-square test [32]

$$S = \sum_{i=1}^{k} \Big(\frac{\text{I URE}^i - \overline{\text{I URE}}}{\text{URA}^i} \Big)^2 \leq K^2_{\text{prob}} = 50.2, \tag{6.7}$$

where K is the number of the satellites in view. Here we consider only one case $K = 12$, which happened most often for the three-year period of data. Because the removal of the common clock error in (6.7) causes loss of one degree of freedom (DoF), Figure 6.8 plots S against the chi-square distribution with 11 DoF.

The red dots in Figure 6.8 are computed using the broadcast URA as the URA^i in (6.7). Clearly, the RAIM/ARAIM requirement was met as the maximum value is less than 15. Nevertheless, the red dots are far below the blue dash-dot line because the broadcast URA is so conservative that the broadcast URA values are usually much greater than the standard deviation of UREs, as shown in Section 6.3.3.

Furthermore, we replace the URA^i in (6.7) by the actual standard deviation of UREs obtained in Section 6.3.1, and get the chi-square statistics shown by the blue plus signs. It seems that the UREs of different satellites are highly correlated because the blue plus

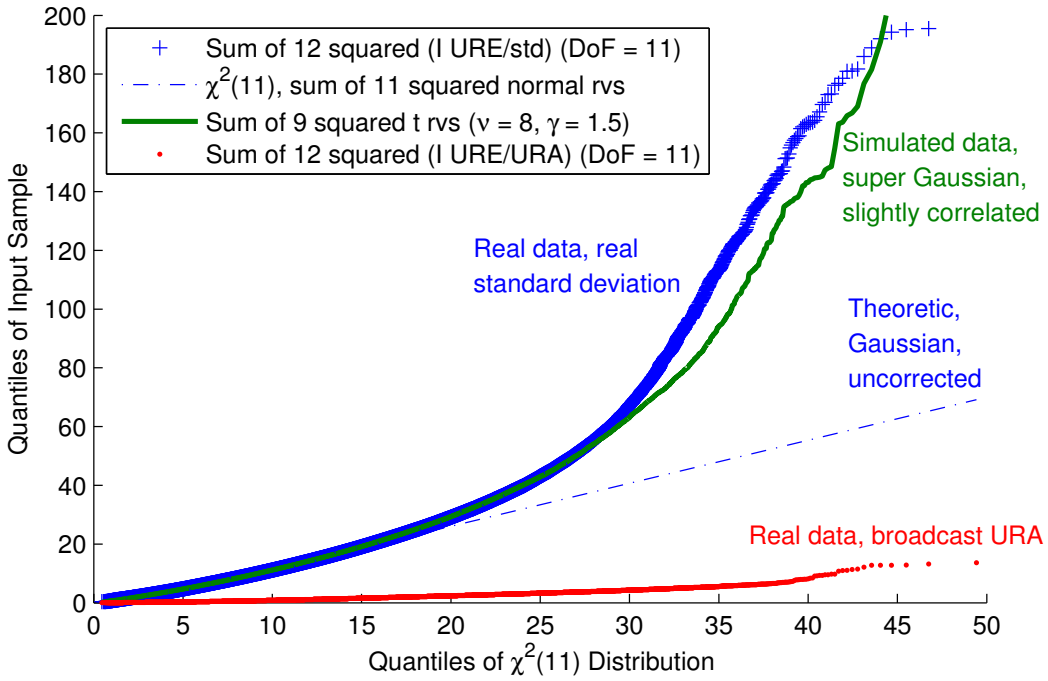

Figure 6.8: Chi-square statistics of actual GPS UREs (red dots and blue plus signs) in comparison to uncorrelated Gaussian (blue dashed line) and slightly correlated super Gausian (green dots).

signs are high above the blue dash-dot line. However, the actual UREs are not normally distributed, and on average they have a kurtosis of 1.5. Accordingly, we plot the green curve using the sum of several squared Student's t-random variables with $\nu = 8$ DoF. A Student's t-distribution with $\nu = 8$ has a kurtosis of 1.5, which can be seen as an approximation of the distribution of UREs. We tried the sum of 6, 7, ..., and 13 squared t-distributed random variables, and the sum of 9 fits the majority of the blue plus signs best, as shown in Figure 6.8. Therefore, a possible quantification of the slight correlation among UREs of different satellites is that the correlation causes loss of two DoF.

6.4 Statistics of Nominal GLONASS SIS Errors

6.4.1 Mean and standard deviation

Figure 6.9 plots the mean of GLONASS ephemeris errors, clock errors, I UREs, and WC

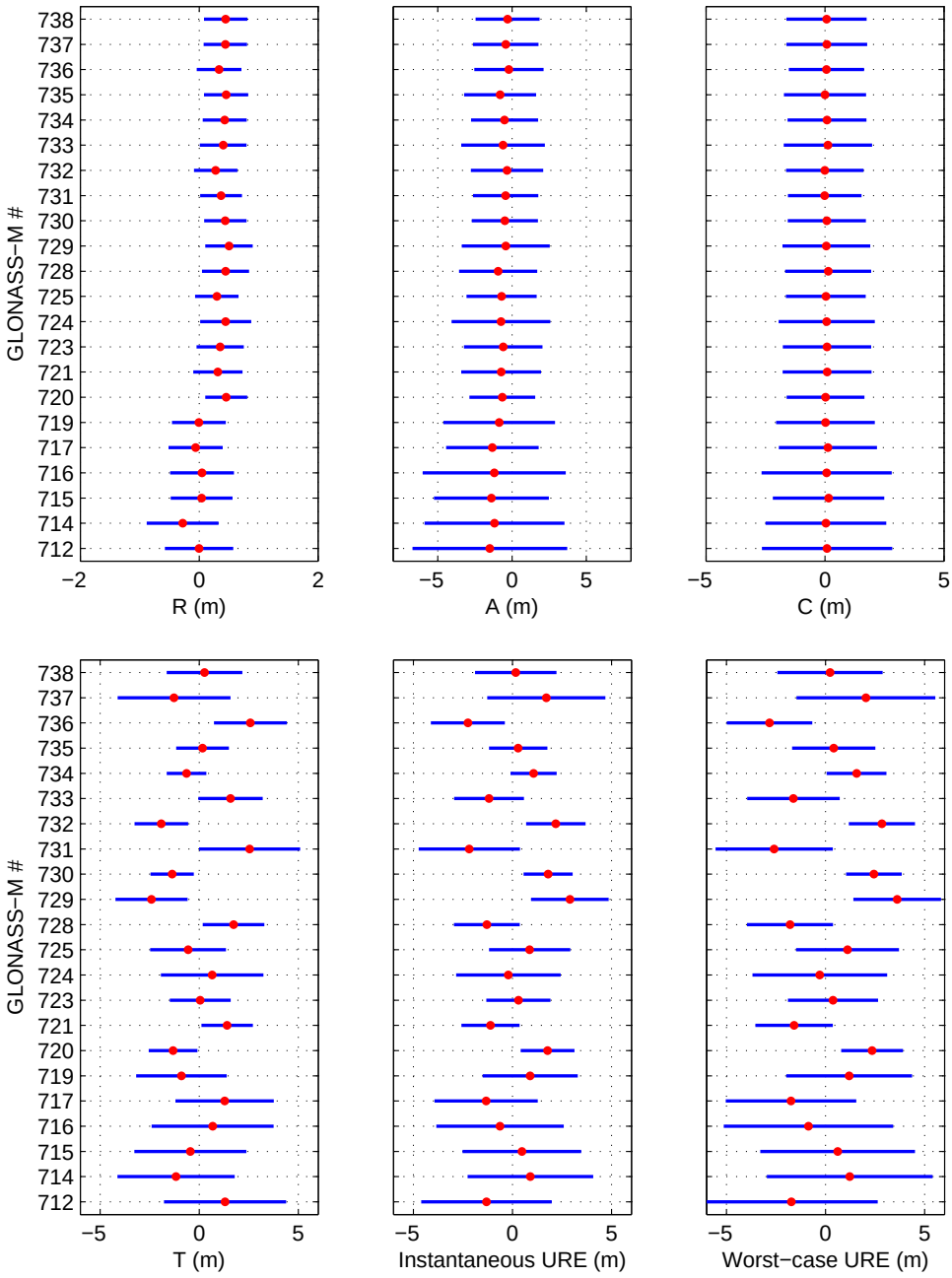

Figure 6.9: Mean of GLONASS SIS errors with a comparison to the standard deviation. The mean is denoted by the red dot, and the blue line with a length of twice the standard deviation is centered at the mean.

UREs with a comparison to their standard deviations. It can be seen that most satellites have a significant nonzero mean for radial ephemeris errors and clock errors. For nearly half of the satellites, the clock errors are so strongly biased that the mean is as large as the standard deviation. The biases in clock errors directly lead to significantly biased I UREs and WC UREs. This performance, though not quite matching the recent GPS SIS performance (Section 6.3.1), is much better than five years ago [59].

Figure 6.9 also reveals a close similarity among clock errors, I UREs, and WC UREs. This is another example to demonstrate that the clock performance dominates SIS URE performance.

6.4.2 Distribution

Figure 6.10 shows the sample kurtosis of ephemeris errors, clock errors, I UREs, and WC UREs. Clearly, super-Gaussian distribution is extremely common. In terms of I UREs, about 80% of the satellites have a kurtosis greater than 1, and the average kurtosis is approximately equal to 2. Moreover, as in GPS, in GLONASS the UREs of younger satellites do not necessarily have a smaller kurtosis than those of older satellites.

For a more intuitive understanding of the distribution of UREs, Figure 6.11 shows the Q-Q plots of the I UREs of two satellites, GLONASS-M 731 and GLONASS-M 732. Both of them were launched at the same time and in the same orbital plane. Nevertheless, the former represents an atypical almost-Gaussian distribution, whereas the latter represents a typical super-Gaussian distribution. We have observed that the UREs of most satellites have very heavy tails, and sometimes the tails can be very asymmetric.

6.4.3 Correlation among UREs of different satellites

The same method used in Section 6.3.4 is used here to characterize the correlation among the UREs of different satellites. We consider only one case, $K = 8$ satellites in view, which happened most often for the three-year period of data. Since the RINEX format for GLONASS does not include URA, we replace the URA in (6.7) by the sample standard deviations computed in Section 6.4.1.

Figure 6.12 plots the chi-square statistic S against the chi-square distribution with seven DoF, because the removal of the common clock error in (6.7) causes loss of 1 DoF. The blue plus signs are S computed from actual UREs. They are high above the blue dash-dot

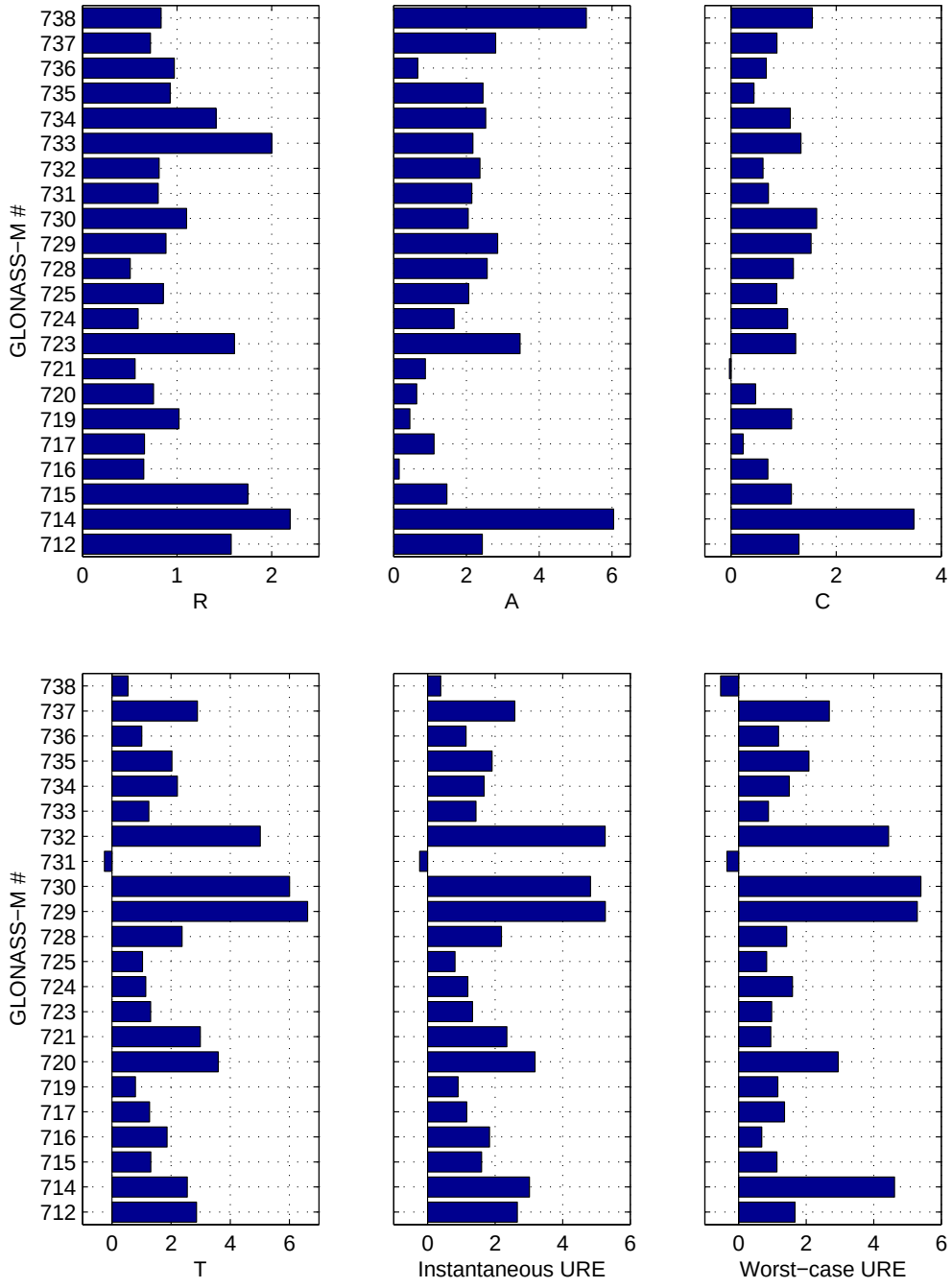

Figure 6.10: Sample kurtosis of GLONASS SIS errors.

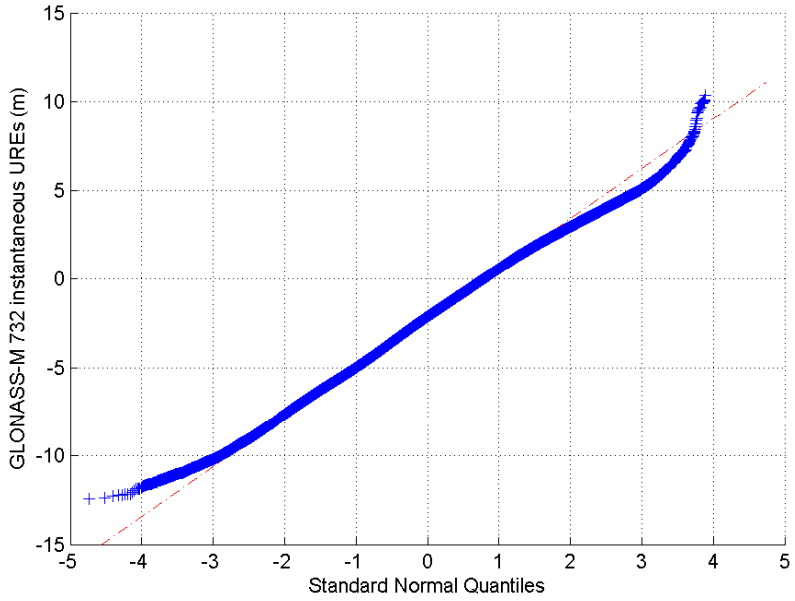

(a) GLONASS-M 731 instantaneous UREs
(kurtosis = −0.23, almost-Gaussian, atypical)

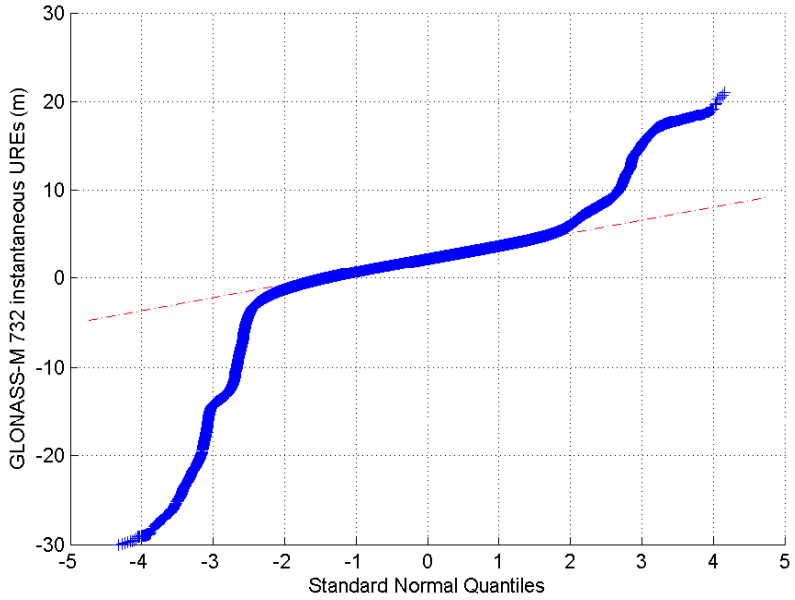

(b) GLONASS-M 732 instantaneous UREs
(kurtosis = 5.26, super-Gaussian, typical)

Figure 6.11: Q-Q plots of the I UREs of GLONASS-M 731 and 732. Both satellites were launched at the same time, are in the same orbital plane, and have been being active for more than 600 days.

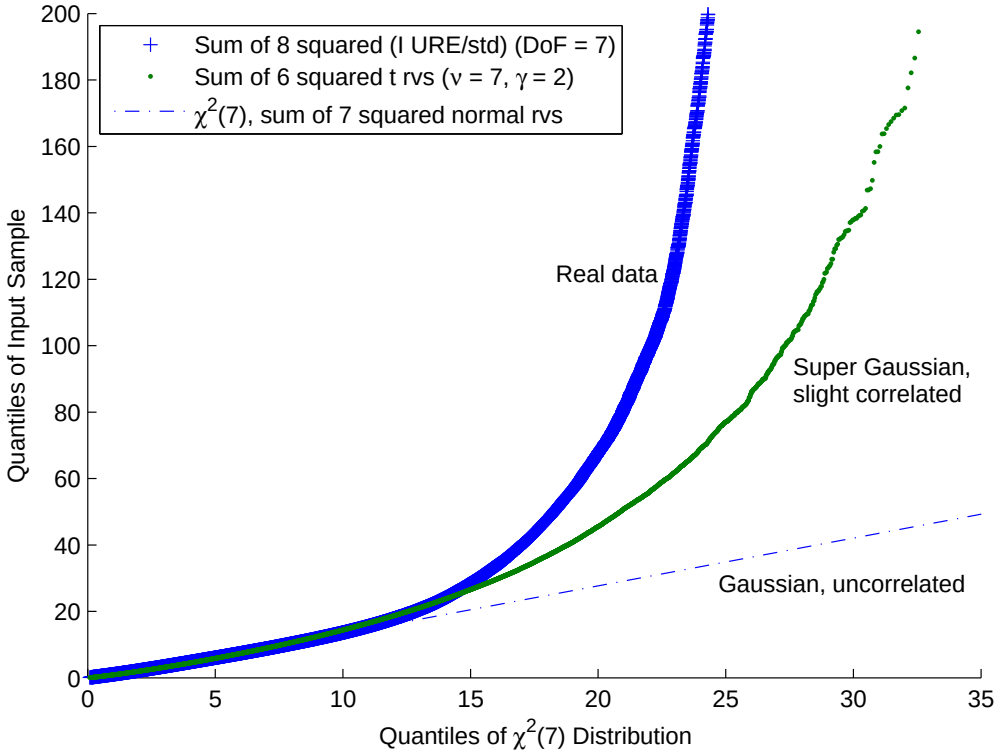

Figure 6.12: Chi-square statistics of actual GLONASS UREs (blue plus signs) in comparison to uncorrelated Gaussian (blue dashed line) and slightly correlated super Gausian (green dots).

line, mainly because the actual UREs are not normally distributed. Since the analysis in Section 6.4.2 shows that the UREs have an average kurtosis of 2, we plot the green dots using the sum of several squared Student's t-distributed random variables with parameter $\nu = 7$. A Student's t-distribution with $\nu = 7$ has a kurtosis of 2, which can be seen as an approximation of the distribution of UREs. We tried the sum of 3, 4, ..., and 9 squared t-distributed random variables; the sum of 6 fits the majority of the blue plus signs best, as shown in Figure 6.12. Therefore, a possible quantification of the slight correlation among UREs of different satellites is that the correlation causes loss of one DoF.

As can be seen in Figure 6.12, although the green dots can match the blue plus signs in terms of the core behavior, the tail of blue plus signs are much greater than the green dots. This is a strange phenomenon in comparison to GPS, for which we could make the tail of blue plus signs match the green dots, as shown in Figure 6.8. One possible explanation for

this is that the UREs are biased, as shown in Section 6.4.1; these biases cause large UREs sometimes occurring on several satellites simultaneously.

6.4.4 Ephemeris error growth with propagation distance

Figure 6.13 compares the global average URE without the clock error (GA URE_0) at different propagation distances. As expected, the 0-minute propagation (actually 15 seconds due to the leap seconds) exhibits a smaller error. The 15-minute propagation results in on average 0.13-meter degradation. This is a particular problem with the GLONASS Cartesian ephemeris format and the recommended force model [78]; we have not observed any similar problem with the GPS quasi-Keplerian ephemeris format.

Although a 0.13-meter degradation looks negligible at present, it will probably become problematic if GLONASS achieves better ephemeris accuracy in the future.

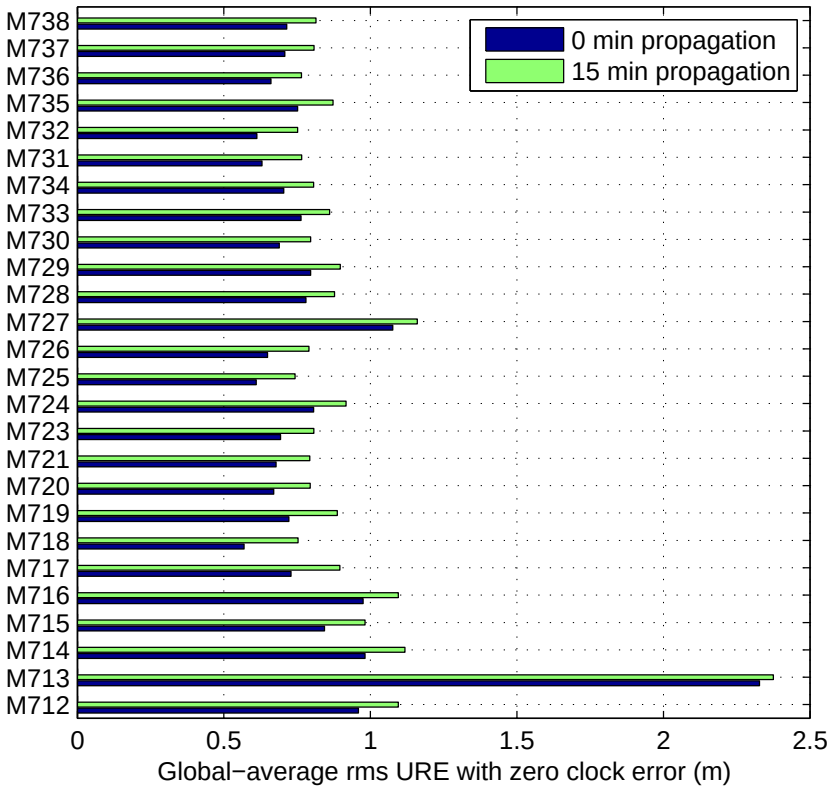

Figure 6.13: GA URE_0 for 0- and 15-minute propagation.

6.4.5 Geographic dependency

Section 2.1 mentioned that all GLONASS monitor stations are within the Russian territory. Section 5.4.3 has further shown that anomalies are approximately twice as likely to occur when satellites are not monitored. In light of this, it is worth examining if the nominal GLONASS SIS errors exhibit obvious geographic dependency.

As shown by the left plot in Figure 6.14, the orbit-error-only SIS UREs show consistent geographic dependency: the UREs when the satellites were monitored are about 0.1-meter less than those when the satellites were unmonitored. However, as shown by the right plot in Figure 6.14, with clock errors, the geographic dependency is no longer consistent. For some satellites, such as GLONASS-M 731 and 737, the UREs when the satellites were monitored are about 1.5-meter less than those when the satellites were unmonitored. For some satellites, such as GLONASS-M 719 and 733, the UREs when the satellites were monitored are about 0.4-meter greater than those when the satellites were unmonitored! This paradox implies some unexpected behavior of GLONASS onboard clocks.

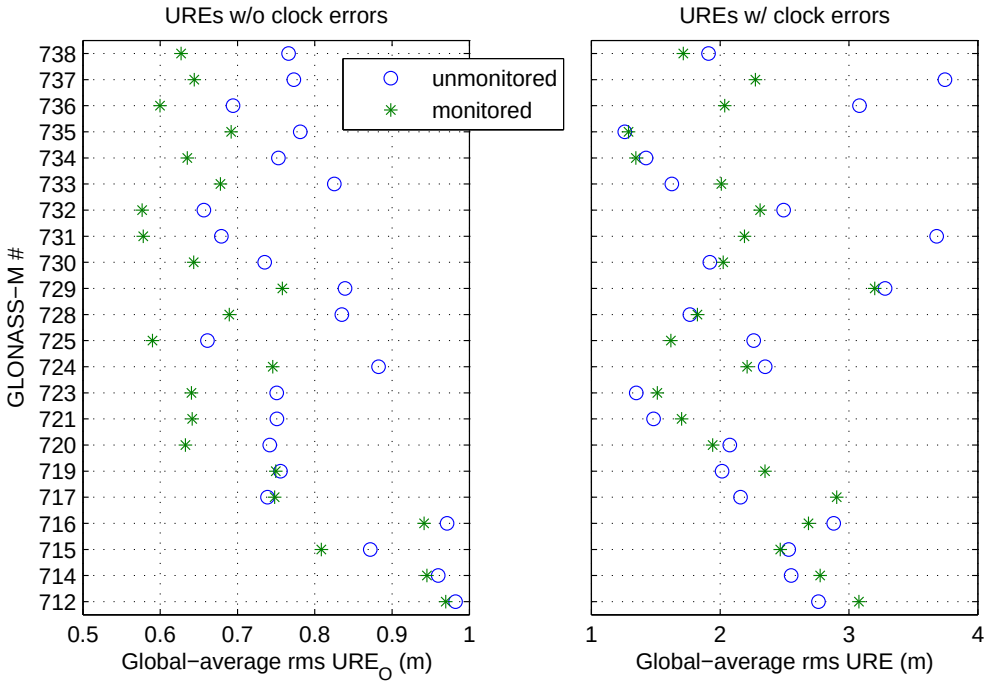

Figure 6.14: Geographic dependency of GLONASS SIS UREs.

6.5 Summary

This chapter characterizes nominal GPS and GLONASS SIS errors using three years of data. The anomalies detected in Chapters 3 to 5 are precluded. Robust statistical techniques are employed to analyze the biases, distributions, and correlations. The results show the following similarities between GPS and GLONASS:

- Younger satellites usually outperform older satellites in terms of SIS accuracy, but not necessarily in terms of the bias (normalized by the corresponding standard deviation) or normality of SIS errors.
- The error statistics of two satellites may differ significantly even though they belong to the same block type and are similar in age; a precise model of SIS errors should treat each satellite individually.

In addition to the similarities, the statistics of nominal UREs show many differences between GPS and GLONASS, as summarized in Table 6.2. These results exhibit a certain degree of deviation from traditional idealized assumptions. Some of the statistics help define correct criteria for anomaly monitoring.

Statistical properties	GPS SIS URE	GLONASS SIS URE
Bias	within $\pm 0.2\sigma$	within $\pm 1\sigma$
Super-Gaussian	half of satellites	almost all satellites
URA bounds rms URE	Yes, very conservative	Not studied†
Correlation among satellites	2 DoF loss, mild tail, meet ARAIM requirement	1 DoF loss, strong tail, ARAIM requirement not checked†
Ephemeris error growth with propagation distance	No	Yes, 0.13-meter degradation at $\pm$15-min propagation
Geographic dependency	No	Yes for ephemeris errors

† Due to lack of URA information in the RINEX format for GLONASS.

Table 6.2: Comparison between the statistics of nominal GPS and GLONASS SIS errors.

Chapter 7

Conclusions

7.1 Methods

> *Can we build a very reliable system from unreliable parts?*
>
> In the early 1950s, Hsue-Shen Tsien, one of the founders of the Jet Propulsion Laboratory, afterward the leader of the Chinese rocket program, proposed a principle that it is both feasible and practical to build a very reliable system from unreliable parts [138]. This principle, although sounding paradoxical, has been proven to be true in many fields of engineering [139, 140]. The methods developed in this dissertation may serve as another proof of this principle.

This dissertation documents the effort to enable comprehensive, systematic, efficient, low-cost global monitoring of GNSS SIS anomalies for the sake of safe navigation with multiple constellations. The main purpose of this section is to remind the reader of the following highlights of our methods.

Deep cleansing algorithms for messy navigation data: In comparison to the GPS and GLONASS SIS, the data from ground receivers are usually much less reliable, especially when they are free. Few people would believe that reliable SIS anomaly monitoring can be based on unreliable data. Nevertheless, our data cleansing algorithms trade redundancy for reliability, and finally make it possible. The validated navigation messages generated by the data cleansing algorithms are the foundation of all the studies presented in this dissertation.

Win-win combination of the space and ground approaches: The space approach is efficient for massive data but suffers from some missing information such as satellite trackability,

whereas the ground approach is the opposite. Rather than use either, we use both in an optimized order—first use the space approach to identify potential anomalies regardless of satellite trackability, then employ the ground approach to verify whether the anomalies actually existed. This combination is key to achieve efficient and reliable anomaly monitoring.

Innovative algorithm to align multiple inconsistent precise GLONASS clock estimates: It has been a long-standing issue that the precise GLONASS clock estimates from different IGS ACs are inconsistent. Our observation shows that this is due to time-variant common clock biases specific to each AC, and that the biases can be modeled using a linear system. The aligned precise clocks generated from our linear model enable all GLONASS-related studies in this dissertation.

Robust statistical techniques to characterize nominal GPS and GLONASS SIS errors: The standard statistical methods are mostly optimized for normally distributed samples, and thus not very suitable for characterizing SIS errors. We carefully select some robust estimators to analyze the biases, distributions, and correlations of nominal GPS and GLONASS SIS errors. The statistics help define correct criteria for monitoring anomalies.

Although the above methods are developed for GPS and GLONASS, they are not specific to the two constellations, and will be a legacy for other constellations. Since these methods do not require high-quality data, they are especially useful for constructing a low-cost global integrity monitoring system for all GNSS in the future.

7.2 Results

This dissertation presents the first comprehensive documentation of GPS and GLONASS SIS anomalies. Figure 7.1 charts one of our major findings—the evolution of the SIS integrity performance for the two constellations in the last decade. Comparing Figure 7.1 with the bathtub curve [141] in Figure 7.2, we can conclude that GPS has entered a maturity stage with an outstandingly low failure rate, while GLONASS is still in a burn-in stage with a promising decreasing failure rate. Interestingly, the GLONASS failure rate is decreasing as fast as the GPS failure rate did between 2000 and 2005.

In addition, this dissertation thoroughly characterizes GPS and GLONASS SIS anomalies and nominal errors. The detailed results have been presented in Chapters 3 to 6 and are not repeated here. Nevertheless, the major findings can be summarized by means of answering the five questions posed at the beginning of this dissertation.

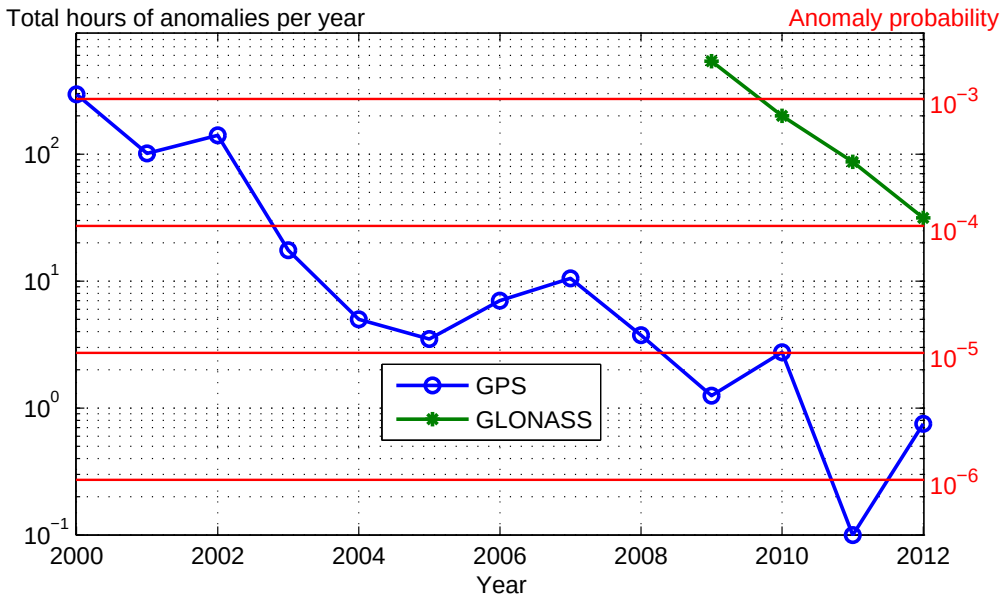

Figure 7.1: Evolution of GPS and GLONASS SIS integrity performance. The y-axis is in a logarithmic scale, and 0 is represented by 0.1. The anomaly probability is based on 31 active satellites with zero outage.

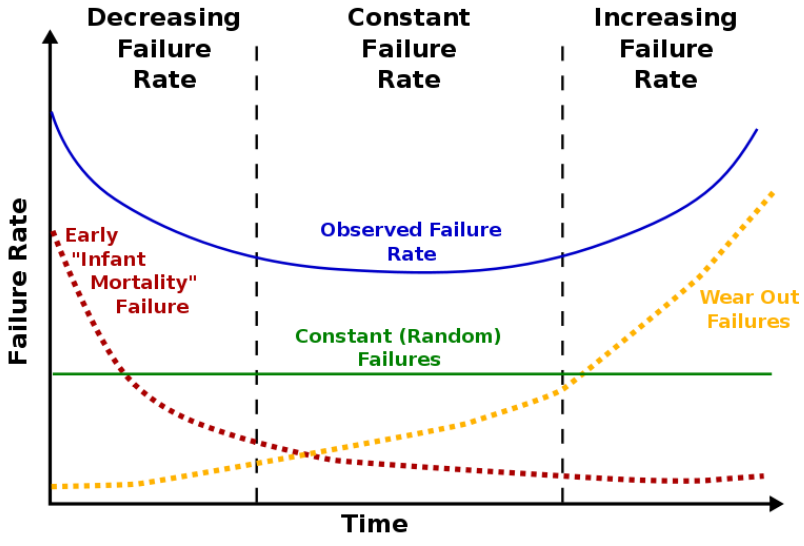

Figure 7.2: The bathtub curve (adapted from `http://en.wikipedia.org/wiki/Bathtub_curve`).

- How often does a satellite fault occur?
  GPS: less than 10^{-5} since 2009, surpassing the performance standard [19]
  GLONASS: from 10^{-3} level to 10^{-4} level in the past four years
- How often do n ($n \geq 2$) satellite faults occur simultaneously?
  GPS: 0 event since 2004
  GLONASS: 3 events of dual faults since 2009
- How often does a constellation fault occur?
  GPS: 0 event since 2004
  GLONASS: 1 event of constellation-wide faults in 2009
- How are UREs actually distributed for a certain URA?
  GPS: super-Gaussian for half of the satellites, and URA is usually 2–4 times the rms URE
  GLONASS: super-Gaussian for almost all the satellites
- Are UREs of different satellites correlated?
  GPS: slightly (loss of 2 DoF out of 12), with a mild tail in the chi-square statistic
  GLONASS: slightly (loss of 1 DoF out of 7), with a strong tail in the chi-square statistic

The results provided in this dissertation are fundamental to multi-constellation integrity monitoring systems, such as ARAIM [31]. Meanwhile, the results can also help many multi-constellation applications, including [15–17].

7.3 Suggestions for Future Work

7.3.1 Interpolation of precise ephemerides and clocks

One of the disadvantages in the space approach is that the temporal resolution is limited by the sampling rate of the precise ephemeris and clock data. Usually, the precise data are available at sampling intervals of 15 minutes. This sampling rate is too low to detect some short-duration anomalies. Although NGA has made the precise data with 5-minute sampling publicly available since 2012-02-28, this sampling rate is still not high enough.

A solution to this issue is to interpolate precise ephemerides and clocks. The interpolation method for satellite ephemeris has been well established [142, 143]. The interpolation of precise clocks is also possible at the precision level of decimeters or even centimeters for the NGA precise clocks with 5-minute sampling and the IGS dedicated precise clocks

with 30-second sampling [110]. Therefore, with the high frequency interpolated precise ephemerides and clocks, our anomaly monitoring will not miss short-duration anomalies, and will determine the start time and end time of an anomaly with very high accuracy.

7.3.2 Automated verification of GLONASS anomalies

In this dissertation, we verified the identified GPS anomalies using the ground approach (Chapter 4) because of the possibility of false anomalies due to untrackable SIS or uncorrected errors in validated navigation messages. However, we do not hurry to develop the automated anomaly verification algorithm for GLONASS for the following reasons.

- The GLONASS ICD [78] does not mention that the GLONASS satellites can alert users by means of untrackable SIS. Therefore, the probability of false anomaly due to untrackable SIS is minimal.
- The GLONASS navigation message is updated every 30 minutes. If a receiver reported a navigation message, it is very likely that the satellite transmitted trackable SIS during the 30 minutes. Therefore, again, the probability of false anomaly due to untrackable SIS is minimal.
- The RINEX format for GLONASS navigation messages is simpler than that for GPS, and does not include vulnerable parameters such as PRN, URA, and TTOM. Therefore, the probability of false anomaly due to uncorrected data-logging errors is minimal.
- There are a little more than 100 GLONASS receivers in the IGS tracking network, and the density of receivers is quite low for some regions such as the Pacific Ocean, North Africa, and Middle America, as can be seen in Figure 5.1. This situation makes the anomaly verification very difficult for some small ephemeris anomalies, which require that the receiver data are collected at a certain spot.

Nevertheless, with more GLONASS receivers joining the tracking network in the future, it will be practical to verify the identified GLONASS anomalies using the ground approach. The algorithms presented in Chapter 4 are a legacy for developing the automated verification process for GLONASS anomalies. In addition, care must be taken in computing GLONASS I UREs because the different processing strategies used by different receivers can cause meter-level differences in the pseudorange measurement [144].

7.3.3 Intelligent data cleansing

One of the key challenges in anomaly monitoring is the corrupted receiver data. Although the data cleansing algorithms developed in this dissertation have met this challenge, the design of the algorithms greatly relies on human observation and classification of data-logging error patterns. As new constellations are on the way to being fully operational and new receivers are joining the global tracking network, new error patterns are emerging. Meanwhile, the data cleansing algorithms need to be updated accordingly. In light of this situation, it would be very useful to make the data cleansing algorithms more intelligent, i.e., with the capability to discover new patterns of data-logging errors and automatically correct these errors. Some unsupervised techniques developed in data mining and statistical learning [145, 146] can be borrowed to develop the intelligent data cleansing algorithms.

Appendix A

List of Acronyms and Definitions

A	alongtrack ephemeris error
AC	Analysis Center
APC	antenna phase center
ARNS	Aeronautical Radio Navigation Services
C	crosstrack ephemeris error
c	the speed of light in vacuum
C/A code	coarse/acquisition code
CDDIS	Crustal Dynamics Data Information System
CDMA	code division multiple access
CODE	Center for Orbit Determination in Europe
CoM	center of mass
DGPS	differential GPS
DLR	Deutsches Zentrum für Luft- und Raumfahrt (German Aerospace Center)
DoD	Department of Defense
DoF	degree of freedom
ECEF	Earth Centred Earth Fixed
ephemeris	an accurate model of satellite orbits (clocks not included)
FAA	Federal Aviation Administration
FDMA	frequency division multiple access

GLONASS	Global'naya Navigatsionnaya Sputnikovaya Sistema (Global Navigation Satellite System)
GNSS	global navigation satellite system(s)
GPS	Global Positioning System
HOW	handover word
IODC	issue of data, clock
IODE	issue of data, ephemeris
ICD	Interface Control Document
IGS	International GNSS Service (formerly International GPS Service)
IGSO	inclined geosynchronous orbit
ITRF	International Terrestrial Reference Frame
L1	GPS SIS centered at 1575.42 MHz frequency and GLONASS SIS centered at 1602.00 MHz frequency
L2	GPS SIS centered at 1227.60 MHz frequency and GLONASS SIS centered at 1246.00 MHz frequency
L2C	civil GPS SIS at L2 frequency
L5	GPS SIS and planned GLONASS SIS centered at 1176.45 MHz frequency
LAAS	Local Area Augmentation System
LSB	least significant bit
MCS	master control station
MEO	medium Earth orbit
ML	maximum likelihood
multilateration	a positioning technique using TOA measurements from three or more sites, also referred to as trilateration
NASA	National Aeronautics and Space Administration
NIMA	National Imagery and Mapping Agency (latterly NGA)
NGA	National Geospatial-Intelligence Agency (formerly NIMA)
nominal	usual, ordinary, expected, being a condition that does not cause any anomaly
normal	relating to, involving, or being a normal (Gaussian) distribution

NTE not to exceed

OCS Operational Control System

PPS Precise Positioning Service

PRN pseudorandom noise

PS Performance Standard

P(Y) code encrypted precise code

PZ Parametry Zemli (Parameters of the Earth)

Q-Q quantile-quantile

QZSS Quasi-Zenith Satellite System

R radial ephemeris error

RAIM receiver autonomous integrity monitoring

- ARAIM advanced receiver autonomous integrity monitoring

RFI radio frequency interference

RINEX Receiver Independent Exchange Format

rms root mean square

RNSS regional navigation satellite system(s)

SA selective availability

SBAS satellite-based augmentation system(s)

SIS signal in space

- SIS anomaly misleading SIS information (a condition during which a healthy, trackable SIS results in WC URE exceeding the NTE threshold)

SNR signal-to-noise ratio

SOPAC Scripps Orbit and Permanent Array Center

SP3 Extended Standard Product 3 Orbit Format

SPS Standard Positioning Service

SVN Space Vehicle Number

T broadcast clock error

TDOA time difference of arrival

TLM telemetry word

TOA time of arrival

t_b reference time of ephemeris/clock in the GLONASS navigation navigation, also referred to as t_e

t_e another notation of t_b

t_{oc} reference time of clock in the GPS navigation navigation

t_{oe} reference time of ephemeris in the GPS navigation navigation

trilateration the same as multilateration

TTOM (the earliest) transmission time of message

URA user range accuracy

- URA UB upper bound of URA

UEE user equipment error (pseudorange inaccuracy due to the receiver)

UERE user equivalent range error (total pseudorange inaccuracy)

URE user range error (pseudorange inaccuracy due to the SIS)

- GA URE global average URE (the rms value of the URE across the portion of the globe in view of the satellite)
- GA URE_0 global average URE under the assumption of zero clock errors
- I URE instantaneous URE (the URE experienced by the receiver at a certain location)
- SIS URE the same as URE
- WC URE worst case URE (the largest [in terms of absolute value] URE across the portion of the globe in view of the satellite)

UTC Coordinated Universal Time

WAAS Wide Area Augmentation System

WGS World Geodetic System

Appendix B

Computation of Global Average URE

As described in Section 2.3, for arbitrary ephemeris and clock errors, the instantaneous URE (I URE) is dependent on the location of receiver. The global average SIS URE (GA URE) is defined as the root mean square (rms) URE across the portion of the globe in view of the satellite. The GA URE is commonly used in assessing the SIS accuracy performance because it is spatially independent. There are two generally accepted methods for computing the GA URE for a satellite at a particular time.

One method is numerical. The I URE can be evaluated at a large number of spatial points spread evenly across the satellite's coverage, and the GA URE can then be computed as the rms of the I URE value at each of those spatial points [19]. This method is not preferred in this dissertation because of the high computational cost.

The other method is analytical, as shown by (2.2). This appendix is devoted to a rigorous derivation of (2.2).

Let us still use the notations used in Section 2.3. Assume Earth is a perfect sphere with a normalized radius 1. Without loss of generality, assume the actual satellite position is $\boldsymbol{r} = (0, 0, d)$ in ECEF, where d is the normalized distance between the satellite and the center of Earth. In addition, assume the satellite instantaneous velocity is parallel to the x-axis.

Then, according to (2.1), the I URE of the receiver at latitude θ, longitude ϕ, and height 0 is given by

$$\begin{aligned}
\text{I URE} &= (\boldsymbol{r}' - \boldsymbol{r}) \cdot \frac{\boldsymbol{r} - \boldsymbol{u}}{\|\boldsymbol{r} - \boldsymbol{u}\|} - c(b' - b) \\
&= [(A, C, d + R) - (0, 0, d)] \cdot \frac{(0, 0, d) - (\cos\theta\cos\phi, \cos\theta\sin\phi, \sin\theta)}{\|(0, 0, d) - (\cos\theta\cos\phi, \cos\theta\sin\phi, \sin\theta)\|} - T, \\
&= (A, C, R) \cdot \frac{(-\cos\theta\cos\phi, -\cos\theta\sin\phi, d - \sin\theta)}{\sqrt{1 + d^2 - 2d\sin\theta}} - T \\
&= \frac{-A\cos\theta\cos\phi - C\cos\theta\sin\phi + R(d - \sin\theta)}{\sqrt{1 + d^2 - 2d\sin\theta}} - T,
\end{aligned} \tag{B.1}$$

where R is the radial ephemeris error, A is the alongtrack ephemeris error, C is the crosstrack ephemeris error, and T is the clock error. Therefore, the GA URE can be calculated by

$$\text{GA URE}^2 = \frac{1}{S}\int_{\vartheta}^{\pi/2}\int_{-\pi}^{\pi} \|\text{I URE}\|^2 \cos\theta \,\mathrm{d}\theta\mathrm{d}\phi, \tag{B.2}$$

where ϑ is the latitude of the edge of the satellite coverage, and $S = 2\pi(1 - \sin\vartheta)$ is the area of the satellite coverage. Considering the ugly closed-form integral of (B.2), we only show the following numerical results obtained using Mathematica [147].

For the purpose of verification, let us first compute the formula for GPS. Using $r = 4.175$ and $\vartheta = 13.85^\circ$ (assuming a zero mask angle), the corresponding GA URE is given by

$$\begin{aligned}
&\text{GA URE}^2_{\text{GPS}} \\
&= 0.9593R^2 - 1.959RT + T^2 + 0.02034(A^2 + C^2) \\
&\approx (0.979R - T)^2 + \frac{A^2 + C^2}{49.2},
\end{aligned} \tag{B.3}$$

which agrees with Equation (A-1) in [19].

For GLONASS, we have $r = 3.998$ and $\vartheta = 14.48^\circ$, and the corresponding GA URE is given by

$$\begin{aligned}
&\text{GA URE}^2_{\text{GLONASS}} \\
&= 0.9555R^2 - 1.955RT + T^2 + 0.02224(A^2 + C^2) \\
&\approx (0.977R - T)^2 + \frac{A^2 + C^2}{45.0}.
\end{aligned} \tag{B.4}$$

For Galileo, we have $r = 4.645$ and $\vartheta = 12.43^\circ$, and the corresponding GA URE is given by

$$\begin{aligned}
&\text{GA URE}^2_{\text{Galileo}} \\
&= 0.9673^2 - 1.967RT + T^2 + 0.01632(A^2 + C^2) \\
&\approx (0.984R - T)^2 + \frac{A^2 + C^2}{61.2}.
\end{aligned} \tag{B.5}$$

For Compass, we have $r = 4.375$ and $\vartheta = 13.21°$, and the corresponding GA URE is given by

$$\begin{aligned} &\text{GA URE}^2_{\text{Compass}} \\ &= 0.9631^2 - 1.963RT + T^2 + 0.01847(A^2 + C^2) \\ &\approx (0.981R - T)^2 + \frac{A^2 + C^2}{54.1}. \end{aligned} \tag{B.6}$$

For circular-geosynchronous-orbit satellites, including the WAAS geostationary satellites and the Compass inclined-geosynchronous-orbit (IGSO) satellite (but not the Quasi-Zenith Satellite System (QZSS) IGSO satellites, whose orbits are elliptical), we have $r = 6.618$ and $\vartheta = 8.69°$, and the corresponding GA URE is given by

$$\begin{aligned} &\text{GA URE}^2_{\text{circular geosynchronous orbit}} \\ &= 0.9841^2 - 1.984RT + T^2 + 0.007908(A^2 + C^2) \\ &\approx (0.992R - T)^2 + \frac{A^2 + C^2}{126}. \end{aligned} \tag{B.7}$$

Bibliography

[1] "GPS IIF: Up at last!" *Inside GNSS News*, May 2010. [Online]. Available: http://www.insidegnss.com/node/2100

[2] A. J. Van Dierendonck and C. Hegarty, "Innovation: The new L5 civil GPS signal," *GPS World*, vol. 11, no. 9, pp. 64–71, 2000.

[3] "GLONASS finally becomes global," *NTV News*, October 2011. [Online]. Available: http://www.ntv.ru/novosti/241055

[4] "They are up! EU launches first Galileo IOV satellites," *Inside GNSS News*, October 2011. [Online]. Available: http://www.insidegnss.com/node/2796

[5] "China launches 10th Compass Beidou-2 navigation satellite into geosynchronous orbit," *Inside GNSS News*, December 2011. [Online]. Available: http://www.insidegnss.com/node/2869

[6] The State Council Information Office of the People's Republic of China, "News conference on BeiDou (Compass) providing test-run services," December 2011. [Online]. Available: http://www.beidou.gov.cn/fbhzt.html

[7] M. Crews, "Long-term future of GPS," in *Proceedings of the 2008 National Technical Meeting of The Institute of Navigation (NTM 2008)*, San Diego, CA, January 2008, pp. 1–26.

[8] European Union, *European GNSS (Galileo) Open Service Signal In Space Interface Control Document*, September 2010.

[9] China National Administration of GNSS and Applications, "COMPASS view on compatibility and interoperability," in *4th Meeting of the International Committee on*

Global Navigation Satellite Systems (ICG 2009), Saint-Petersburg, Russian, September 2009. [Online]. Available: http://www.unoosa.org/pdf/icg/2009/workgroupinterop/04.pdf

[10] G. Gibbons, "Russia approves CDMA signals for GLONASS, discussing common signal design," *Inside GNSS News*, April 2008. [Online]. Available: http://www.insidegnss.com/node/648

[11] J. Blanch, M. J. Choi, T. Walter, P. Enge, and K. Suzuki, "Prototyping advanced RAIM for vertical guidance," in *Proceedings of the 23rd International Technical Meeting of the Satellite Division of the Institute of Navigation (ION GNSS 2010)*, Portland, OR, September 2010, pp. 285–291.

[12] J. Blanch, T. Walter, and P. Enge, "Satellite navigation for aviation in 2025," *Proceedings of the IEEE*, vol. 100, Special Centennial Issue, pp. 1821–1830, 2012.

[13] M. Choi, J. Blanch, T. Walter, and P. Enge, "Evaluation of multi-constellation advanced RAIM for vertical guidance using GPS and GLONASS signals with multiple faults," in *Proceedings of the 25th International Technical Meeting of the Satellite Division of the Institute of Navigation (ION GNSS 2012)*, Nashville, TN, September 2012.

[14] F. N. Bauregger, "Novel anti-jam antennas for airborne GPS navigation," Ph.D. dissertation, Stanford University, 2003.

[15] S. Pullen and G. X. Gao, "GNSS jamming in the name of privacy: Potential threat to GPS aviation," *Inside GNSS*, March/April 2012.

[16] G. X. Gao, L. Heng, T. Walter, and P. Enge, "Breaking the ice: Navigating in the Arctic," in *Proceedings of the 24th International Technical Meeting of the Satellite Division of the Institute of Navigation (ION GNSS 2011)*, Portland, OR, September 2011, pp. 3767–3772.

[17] L. Wang, P. D. Groves, and M. K. Ziebart, "Multi-constellation GNSS performance evaluation for urban canyons using large virtual reality city models," *Journal of Navigation*, vol. 65, no. 3, pp. 459–476, July 2012.

[18] R. B. Langley, "Innovation: The integrity of GPS," *GPS World*, vol. 10, pp. 60–63, March 1999.

[19] US DoD, *Global Positioning System Standard Positioning Service Performance Standard*, 4th ed., September 2008.

[20] J. L. Christopher M. Shank, "GPS integrity: An MCS perspective," in *Proceedings of the 6th International Technical Meeting of the Satellite Division of the Institute of Navigation (ION GPS 1993)*, Salt Lake City, UT, September 1993, pp. 465–474.

[21] B. C. Barker and S. J. Huser, "Protect yourself! Navigation payload anomalies and the importance of adhering to ICD-GPS-200," in *Proceedings of the 11th International Technical Meeting of the Satellite Division of the Institute of Navigation (ION GPS 1998)*, Nashville, TN, September 1998, pp. 1843–1854.

[22] M. H. Rivers, "2 SOPS anomaly resolution on an aging constellation," in *Proceedings of the 13th International Technical Meeting of the Satellite Division of the Institute of Navigation (ION GPS 2000)*, Salt Lake City, UT, September 2000, pp. 2547–2550.

[23] A. K. Brown, "Civil aviation integrity requirements for the Global Positioning System," *NAVIGATION*, vol. 35, no. 1, pp. 23–40, Spring 1998.

[24] T. M. Corrigan, J. F. Hartranft, L. J. Levy, K. E. Parker *et al.*, "GPS risk assessment study: Final report," Applied Physics Laboratory, Johns Hopkins University, Tech. Rep. VS-99-007, January 1999.

[25] W. Ochieng, K. Sauer, D. Walsh, G. Brodin *et al.*, "GPS integrity and potential impact on aviation safety," *Journal of Navigation*, vol. 56, no. 1, pp. 51–65, January 2003.

[26] P. Enge and A. J. Van Dierendonck, "Wide area augmentation system," in *Global Positioning System: Theory and Applications*, B. Parkinson, J. Spilker, P. Axelrad, and P. Enge, Eds. Washington, DC: American Institute of Aeronautics and Astronautics, 1996, vol. II, pp. 117–142.

[27] P. Enge, "Local area augmentation of GPS for the precision approach of aircraft," *Proceedings of the IEEE*, vol. 87, no. 1, pp. 111–132, January 1999.

[28] C. Kee, B. W. Parkinson, and P. Axelrad, "Wide area differential GPS," *NAVIGATION*, vol. 38, no. 2, pp. 123–146, Summer 1991.

[29] B. Parkinson and P. Enge, "Differential GPS," in *Global Positioning System: Theory and Applications*, B. Parkinson, J. Spilker, P. Axelrad, and P. Enge, Eds. Washington, DC: American Institute of Aeronautics and Astronautics, 1996, vol. II, pp. 3–50.

[30] RTCA Special Committee 159, *Minimum Operational Performance Standards for Global Positioning System/Wide Area Augmentation System Airborne Equipment*. RTCA DO-229D, December 2006.

[31] J. Blanch, T. Walter, and P. Enge, "RAIM with optimal integrity and continuity allocations under multiple failures," *IEEE Transactions on Aerospace and Electronic Systems*, vol. 46, no. 3, pp. 1235–1247, 2010.

[32] T. Walter, J. Blanch, and P. Enge, "Evaluation of signal in space error bounds to support aviation integrity," in *Proceedings of the 22nd International Technical Meeting of the Satellite Division of the Institute of Navigation (ION GNSS 2009)*, Savannah, GA, September 2009, pp. 1317–1329.

[33] L. Gratton, R. Pramanik, H. Tang, and B. Pervan, "Ephemeris failure rate analysis and its impact on Category I LAAS integrity," in *Proceedings of the 20th International Technical Meeting of the Satellite Division of the Institute of Navigation (ION GNSS 2007)*, Fort Worth, TX, September 2007, pp. 386–397.

[34] R. G. Brown and P. Y. C. Hwang, "GPS failure detection by autonomous means within the cockpit," *NAVIGATION*, vol. 33, no. 4, pp. 335–353, Winter 1986.

[35] S. Cobb, D. Lawrence, J. Christie, T. Walter *et al.*, "Observed GPS signal continuity interruptions," in *Proceedings of the 8th International Technical Meeting of the Satellite Division of the Institute of Navigation (ION GPS 1995)*, Palm Springs, CA, September 1995, pp. 793–795.

[36] A. Hansen, T. Walter, P. Enge, and D. Lawrence, "GPS satellite clock event on SVN 27 and its impact on augmented navigation," in *Proceedings of the 11th International Technical Meeting of the Satellite Division of the Institute of Navigation (ION GPS 1998)*, Nashville, TN, September 1998, pp. 1665–1673.

[37] J. W. Lavrakas and D. Knezha, "GPS receiver responses to satellite anomalies," in *Proceedings of the 1999 National Technical Meeting of The Institute of Navigation (ION NTM 1999)*, San Diego, CA, January 1999, pp. 621–626.

[38] B. B. Clyde Edgar, Frank Czopek, "A co-operative anomaly resolution on PRN-19," in *Proceedings of the 12th International Technical Meeting of the Satellite Division of the Institute of Navigation (ION GPS 1999)*, Nashville, TN, September 1999.

[39] N. Vary, "DR# 55: GPS satellite PRN18 anomaly affecting SPS performance," FAA William J. Hughes Technical Center, Pomona, New Jersey, Tech. Rep., April 2007.

[40] K. Kovach, J. Berg, and V. Lin, "Investigation of upload anomalies affecting IIR satellites in October 2007," in *Proceedings of the 21st International Technical Meeting of the Satellite Division of the Institute of Navigation (ION GNSS 2008)*, Savannah, GA, September 2008, pp. 1679–1687.

[41] D. Last, "GNSS: The present imperfect," *Inside GNSS*, vol. 5, no. 3, pp. 60–64, May 2010.

[42] M. J. Buonsanto, "Ionospheric storms—a review," *Space Science Reviews*, vol. 88, pp. 563–601, 1999.

[43] T. Walter, A. Hansen, J. Blanch, P. Enge *et al.*, "Robust detection of ionospheric irregularities," in *Proceedings of the 13th International Technical Meeting of the Satellite Division of the Institute of Navigation (ION GPS 2000)*, Salt Lake City, UT, September 2000, pp. 209–218.

[44] J. M. Dow, R. E. Neilan, and C. Rizos, "The International GNSS Service in a changing landscape of global navigation satellite systems," *Journal of Geodesy*, vol. 83, pp. 689–689, 2009.

[45] D. M. Warren and J. F. Raquet, "Broadcast vs. precise GPS ephemerides: A historical perspective," *GPS Solutions*, vol. 7, pp. 151–156, 2003.

[46] F. Van Diggelen, *A-GPS: Assisted GPS, GNSS, and SBAS*. Artech House, 2009.

[47] J. Zumberge and W. Bertiger, "Ephemeris and clock navigation message accuracy," in *Global Positioning System: Theory and Applications*, B. Parkinson, J. Spilker, P. Axelrad, and P. Enge, Eds. Washington, DC: American Institute of Aeronautics and Astronautics, 1996, vol. I, pp. 585–699.

[48] R. B. Langley, H. Jannasch, B. Peeters, and S. Bisnath, "The GPS broadcast orbits: an accuracy analysis," in *33rd COSPAR Scientific Assembly*, Warsaw, Poland, July 2000.

[49] D. C. Jefferson and Y. E. Bar-Sever, "Accuracy and consistency of broadcast GPS ephemeris data," in *Proceedings of the 13th International Technical Meeting of the Satellite Division of the Institute of Navigation (ION GPS 2000)*, Salt Lake City, UT, September 2000, pp. 391–395.

[50] C. Cohenour and F. Van Graas, "GPS orbit and clock error distributions," *NAVIGATION*, vol. 58, no. 1, pp. 17–28, Spring 2011.

[51] J. Lee, "Results on test of URA validation protocol using NGA data," in *GEAS Working Group*, May 2009.

[52] P. Misra, E. Bayliss, R. LaFrey, M. Pratt *et al.*, "GLONASS performance in 1992: A review," *GPS World*, vol. 4, no. 5, pp. 28–39, 1993.

[53] P. Misra, E. Bayliss, R. LaFrey, M. Pratt, and R. Muchnik, "Receiver autonomous integrity monitoring (RAIM) of GPS and GLONASS," *NAVIGATION*, vol. 40, no. 1, pp. 87–104, 1993.

[54] F. Van Graas and M. S. Braasch, "Selective availability," in *Global Positioning System: Theory and Applications*, B. Parkinson, J. Spilker, P. Axelrad, and P. Enge, Eds. Washington, DC: American Institute of Aeronautics and Astronautics, 1996, vol. I, pp. 601–621.

[55] C. Adrados, I. Girard, J.-P. Gendner, and G. Janeau, "Global Positioning System (GPS) location accuracy improvement due to selective availability removal," *Comptes Rendus Biologies*, vol. 325, no. 2, pp. 165–170, 2002.

[56] B. Burke, "GLONASS satellite clock bias anomaly," November 1998. [Online]. Available: http://igscb.jpl.nasa.gov/igscb/mail/igexmail/0080

[57] N. Jonkman and K. De Jong, "Integrity monitoring of IGEX-98 data—Part III: Broadcast navigation message validation," *GPS Solutions*, vol. 4, no. 2, pp. 45–53, 2000.

[58] R. Weber, J. A. Slater, E. Fragner, V. Glotov *et al.*, "Precise GLONASS orbit determination within the IGS/IGLOS pilot project," *Advances in Space Research*, vol. 36, no. 3, pp. 369–375, 2005.

[59] E. G. Oleynik, V. V. Mitrikas, S. G. Revnivykh, A. I. Serdukov *et al.*, "High-accurate GLONASS orbit and clock determination for the assessment of system performance," in *Proceedings of the 19th International Technical Meeting of the Satellite Division of the Institute of Navigation (ION GNSS 2006)*, Fort Worth, TX, September 2006, pp. 2065–2079.

[60] A. Hesselbarth and L. Wanninger, "Short-term stability of GNSS satellite clocks and its effects on precise point positioning," in *Proceedings of the 21st International Technical Meeting of the Satellite Division of the Institute of Navigation (ION GNSS 2008)*, Savannah, GA, September 2008, pp. 1855–1863.

[61] R. Píriz, D. Calle, A. Mozo, P. Navarro *et al.*, "Orbits and clocks for GLONASS precise-point-positioning," in *Proceedings of the 22nd International Technical Meeting of the Satellite Division of the Institute of Navigation (ION GNSS 2009)*, Savannah, GA, September 2009, pp. 2415–2424.

[62] H. Yamada, T. Takasu, N. Kubo, and A. Yasuda, "Effect of GLONASS orbit error on long baseline GPS/GLONASS RTK," in *Proceedings of the 22nd International Technical Meeting of the Satellite Division of the Institute of Navigation (ION GNSS 2009)*, Savannah, GA, September 2009, pp. 3290–3296.

[63] L. Heng, G. X. Gao, T. Walter, and P. Enge, "GPS ephemeris error screening and results for 2006–2009," in *Proceedings of the 2010 International Technical Meeting of the Institute of Navigation (ION ITM 2010)*, San Diego, CA, January 2010, pp. 1014–1022.

[64] ——, "GPS signal-in-space anomalies in the last decade: Data mining of 400,000,000 GPS navigation messages," in *Proceedings of the 23rd International Technical Meeting of the Satellite Division of the Institute of Navigation (ION GNSS 2010)*, Portland, OR, September 2010, pp. 3115–3122.

[65] ——, "Innovation: Digging into GPS integrity—charting the evolution of signal-in-space performance by data mining 400,000,000 navigation messages," *GPS World*, vol. 22, no. 11, pp. 44–49, November 2011.

[66] ——, "GPS signal-in-space integrity performance evolution in the last decade: Data mining 400,000,000 navigation messages from a global network of 400 receivers," *IEEE Transactions on Aerospace and Electronic Systems*, vol. 48, no. 4, pp. 2932–2946, October 2012.

[67] ——, "Automated verification of potential GPS signal-in-space anomalies using ground observation data," in *Proceedings of the 2012 IEEE/ION Position Location and Navigation Symposium (IEEE/ION PLANS 2012)*, Myrtle Beach, SC, April 2012, pp. 1111–1118.

[68] ——, "GLONASS signal-in-space anomalies since 2009," in *Proceedings of the 25th International Technical Meeting of the Satellite Division of the Institute of Navigation (ION GNSS 2012)*, Nashville, TN, September 2012.

[69] ——, "Statistical characterization of GPS signal-in-space errors," in *Proceedings of the 2011 International Technical Meeting of the Institute of Navigation (ION ITM 2011)*, San Diego, CA, January 2011, pp. 312–319.

[70] ——, "Statistical characterization of GLONASS broadcast ephemeris errors," in *Proceedings of the 24th International Technical Meeting of the Satellite Division of the Institute of Navigation (ION GNSS 2011)*, Portland, OR, September 2011, pp. 3109–3117.

[71] ——, "Statistical characterization of GLONASS broadcast clock errors and signal-in-space errors," in *Proceedings of the 2012 International Technical Meeting of the Institute of Navigation (ION ITM 2012)*, Newport Beach, CA, January 2012, pp. 1697–1707.

[72] P. Misra and P. Enge, *Global Positioning System: Signals, Measurements, and Performance*, 2nd ed. Lincoln, MA: Ganga-Jamuna Press, 2006.

[73] J. Spilker and B. Parkinson, "Overview of GPS operation and design," in *Global Positioning System: Theory and Applications*, B. Parkinson, J. Spilker, P. Axelrad, and

P. Enge, Eds. Washington, DC: American Institute of Aeronautics and Astronautics, 1996, vol. I, pp. 29–55.

[74] T. Creel, A. J. Dorsey, P. J. Mendicki, J. Little *et al.*, "Summary of accuracy improvements from the GPS legacy accuracy improvement initiative (L-AII)," in *Proceedings of the 20th International Technical Meeting of the Satellite Division of the Institute of Navigation (ION GNSS 2007)*, Fort Worth, TX, September 2007, pp. 2481–2498.

[75] National Geospatial-Intelligence Agency GPS Division, Accessed January 2012. [Online]. Available: http://earth-info.nga.mil/GandG/sathtml

[76] B. Wiley, D. Craig, D. Manning, J. Novak *et al.*, "NGA's role in GPS," in *Proceedings of the 19rd International Technical Meeting of the Satellite Division of the Institute of Navigation (ION GNSS 2006)*, Fort Worth, TX, September 2006, pp. 2111–2119.

[77] K. T. Woo, "Optimum semicodeless carrier-phase tracking of L2," *NAVIGATION*, vol. 47, no. 2, pp. 82–99, Summer 2000.

[78] Russian Institute of Space Device Engineering, *GLONASS Interface Control Document*, 2008.

[79] R. B. Langley, "GLONASS modernization: Maybe six planes, probably more satellites," *GPS World*, January 2012.

[80] A. T. Balaei and D. M. Akos, "Cross correlation impacts and observations in GNSS receivers," *NAVIGATION*, vol. 58, no. 4, pp. 323–333, Winter 2011.

[81] L. Wanninger, "Carrier-phase inter-frequency biases of GLONASS receivers," *Journal of Geodesy*, vol. 86, pp. 139–148, 2012.

[82] E. Oleynik and S. Revnivykh, "GLONASS status and modernization," in *51st Meeting of the Civil GPS Service Interface Committee at the Institute of Navigation GNSS 2011 Conference (CGSIC 51th Meeting)*, Portland, OR, September 2011.

[83] "Russia to lift GLONASS restrictions for accurate civilian use," November 2006. [Online]. Available: http://en.rian.ru/russia/20061113/55588641.html

[84] E. D. Kaplan and C. J. Hegarty, *Understanding GPS: Principles and Applications*, 2nd ed. Artech House, 2006.

[85] O. Montenbruck and E. Gill, *Satellite Orbits: Models, Methods and Applications*. Springer, 2005.

[86] GPS Wing, *Interface Specification IS-GPS-200E*, June 2010.

[87] S. Malys, J. A. Slater, R. W. Smith, L. E. Kunz, and S. C. Kenyon, "Refinements to the World Geodetic System 1984," in *Proceedings of the 10th International Technical Meeting of the Satellite Division of the Institute of Navigation (ION GPS 1997)*, Kansas City, MO, September 1997, pp. 841–850.

[88] M. J. Merrigan, E. R. Swift, R. F. Wong, and J. T. Saffel, "A refinement to the World Geodetic System 1984 reference frame," in *Proceedings of the 15th International Technical Meeting of the Satellite Division of the Institute of Navigation (ION GPS 2002)*, Portland, OR, September 2002, pp. 1519–1529.

[89] S. Revnivykh, "GLONASS ground contol segment: Orbit, clock, time scale and geodesy definition," in *GLONASS workshop of the 25th International Technical Meeting of the Satellite Division of the Institute of Navigation (ION GNSS 2012)*, Nashville, TN, September 2012.

[90] C. Boucher and Z. Altamimi, "ITRS, PZ-90 and WGS 84: current realizations and the related transformation parameters," *Journal of Geodesy*, vol. 75, pp. 613–619, 2001.

[91] "Absolute differences between GLONASS broadcast ephemeris and a posteriori orbits in ITRF system for several orbit slots of the first plane," Accessed January 2011. [Online]. Available: http://www.glonass-ianc.rsa.ru/docs/PZ-90-2-3-eng.pdf

[92] K. Kovach, "New user equivalent range error (UERE) budget for the modernized Navstar Global Positioning System (GPS)," in *Proceedings of the 2000 National Technical Meeting of The Institute of Navigation (NTM 2000)*, Anaheim, CA, January 2000, pp. 550–573.

[93] R. Schmid, M. Rothacher, D. Thaller, and P. Steigenberger, "Absolute phase center corrections of satellite and receiver antennas," *GPS Solutions*, vol. 9, pp. 283–293, 2005.

[94] R. E. Phelts, G. X. Gao, G. Wong, L. Heng *et al.*, "Aviation grade: New GPS signals—chips off the Block IIF," *Inside GNSS*, vol. 5, no. 5, pp. 36–45, July 2010.

[95] G. Wong, R. E. Phelts, T. Walter, and P. Enge, "Characterization of signal deformations for GPS and WAAS satellites," in *Proceedings of the 23rd International Technical Meeting of the Satellite Division of the Institute of Navigation (ION GNSS 2010)*, Portland, OR, September 2010, pp. 3143–3151.

[96] US DoD, *Global Positioning System Standard Positioning Service Performance Standard*, 3rd ed., October 2001.

[97] G. X. Gao, H. Tang, J. Blanch, J. Lee *et al.*, "Methodology and case studies of signal-in-space error calculation top-down meets bottom-up," in *Proceedings of the 22nd International Technical Meeting of the Satellite Division of the Institute of Navigation (ION GNSS 2009)*, Savannah, GA, September 2009, pp. 2824–2831.

[98] International GNSS Service, Accessed January 2012. [Online]. Available: http://igscb.jpl.nasa.gov

[99] W. Gurtner, *RINEX: The Receiver Independent Exchange Format Version 2.11*, Astronomical Institute, University of Berne. [Online]. Available: ftp://ftp.unibe.ch/aiub/rinex/rinex211.txt

[100] C. E. Noll, "The Crustal Dynamics Data Information System: A resource to support scientific analysis using space geodesy," *Advances in Space Research*, vol. 45, no. 12, pp. 1421–1440, 2010.

[101] SOPAC Description, Accessed September 2012. [Online]. Available: http://sopac.ucsd.edu/other/sopacDescription.html

[102] CDDIS, Accessed March 2012. [Online]. Available: http://igscb.jpl.nasa.gov/components/dcnav/cddis_data_daily_yyn.html

[103] SOPAC, Accessed September 2012. [Online]. Available: http://igscb.jpl.nasa.gov/components/dcnav/sopac_nav.html

[104] A. Roulston, N. Talbot, and K. Zhang, "An evaluation of various GPS satellite ephemerides," in *Proceedings of the 13th International Technical Meeting of the Satellite Division of the Institute of Navigation (ION GPS 2000)*, Salt Lake City, UT, September 2000, pp. 45–54.

[105] J. Griffiths and J. Ray, "On the precision and accuracy of IGS orbits," *Journal of Geodesy*, vol. 83, pp. 277–287, 2009.

[106] IGS Products, Accessed January 2012. [Online]. Available: http://igscb.jpl.nasa.gov/components/prods.html

[107] NGA/IGS GPS Orbit (Ephemeris) Comparison Page, Accessed June 2012. [Online]. Available: http://earth-info.nga.mil/GandG/sathtml/ngaigscompare.html

[108] IGS formats, Accessed January 2012. [Online]. Available: http://igscb.jpl.nasa.gov/components/formats.html

[109] K. Senior, P. Koppang, and J. Ray, "Developing an IGS time scale," *IEEE Transactions on Ultrasonics, Ferroelectrics and Frequency Control*, vol. 50, no. 6, pp. 585–593, June 2003.

[110] J. Kouba, *A Guide to Using IGS Products*, IGS, May 2009. [Online]. Available: http://igscb.jpl.nasa.gov/igscb/resource/pubs/UsingIGSProductsVer21.pdf

[111] *NGA GPS Ephemeris/Station/Antenna Offset Documentation*, Accessed September 2012. [Online]. Available: http://earth-info.nga.mil/GandG/sathtml/gpsdoc2010_09a.html

[112] R. Schmid, P. Steigenberger, G. Gendt, M. Ge, and M. Rothacher, "Generation of a consistent absolute phase-center correction model for GPS receiver and satellite antennas," *Journal of Geodesy*, vol. 81, pp. 781–798, 2007.

[113] J. W. Tukey and D. H. McLaughlin, "Less vulnerable confidence and significance procedures for location based on a single sample: Trimming/winsorization 1," *Sankhyā: The Indian Journal of Statistics, Series A (1961-2002)*, vol. 25, no. 3, pp. 331–352, 1963.

[114] J. W. Lavrakas, "GPS anomaly summary," unpublished.

[115] William J. Hughes Technical Center, *GPS SPS Performance Analysis Report #47*, October 2004.

[116] ——, *GPS SPS Performance Analysis Report #58*, July 2007.

[117] R. Dach, E. Brockmann, S. Schaer, G. Beutler *et al.*, "GNSS processing at CODE: Status report," *Journal of Geodesy*, vol. 83, pp. 353–365, 2009.

[118] IGS Tracking Network, Accessed March 2012. [Online]. Available: http://igscb.jpl.nasa.gov/network/netindex.html

[119] J. Saastamoinen, "Atmospheric correction for the troposphere and stratosphere in radio ranging satellites," *Geophysical Monograph Series*, vol. 15, pp. 247–251, 1972.

[120] M. Choi, J. Blanch, D. Akos, L. Heng *et al.*, "Demonstrations of multi-constellation Advanced RAIM for vertical guidance using GPS and GLONASS signals," in *Proceedings of the 24th International Technical Meeting of the Satellite Division of the Institute of Navigation (ION GNSS 2011)*, Portland, OR, September 2011, pp. 3227–3234.

[121] CDDIS, Accessed January 2012. [Online]. Available: http://igscb.jpl.nasa.gov/components/dcnav/cddis_data_daily_yyg.html

[122] F. Dilssner, T. Springer, C. Flohrer, and J. Dow, "Estimation of phase center corrections for GLONASS-M satellite antennas," *Journal of Geodesy*, vol. 84, pp. 467–480, 2010.

[123] R. Dach, R. Schmid, M. Schmitz, D. Thaller *et al.*, "Improved antenna phase center models for GLONASS," *GPS Solutions*, vol. 15, pp. 49–65, 2011.

[124] M. Stewart and M. Tsakiri, "GLONASS broadcast orbit computation," *GPS Solutions*, vol. 2, pp. 16–27, 1998.

[125] A. E. Zinoviev, "Using GLONASS in combined GNSS receivers: Current status," in *Proceedings of the 18th International Technical Meeting of the Satellite Division of the Institute of Navigation (ION GNSS 2005)*, Long Beach, CA, September 2009, pp. 1046–1057.

[126] P. W. Holland and R. E. Welsch, "Robust regression using iteratively reweighted least-squares," *Communications in Statistics: Theory and Methods*, vol. 6, no. 9, pp. 813–827, 1977.

[127] A. M. Gross, "Confidence intervals for bisquare regression estimates," *Journal of the American Statistical Association*, vol. 72, no. 358, pp. 341–354, June 1977.

[128] K. Krishnamoorthy, *Handbook of Statistical Distributions with Applications*. CRC Press, 2006.

[129] W. Lewandowski and L. Tisserand, "Relative characterization of GNSS receiver delays for GPS and GLONASS C/A codes in the L1 frequency band at the OP, SU, PTB and AOS," Bureau International des Poids et Mesures, Tech. Rep. 4, 2010. [Online]. Available: http://www.bipm.org/utils/common/pdf/rapportBIPM/2010/04.pdf

[130] S. Kotz, T. Kozubowski, and K. Podgorski, *The Laplace Distribution and Generalizations: A Revisit With Applications to Communications, Economics, Engineering, and Finance*. Birkhäuser, 2001.

[131] S. S. Shapiro and M. B. Wilk, "An analysis of variance test for normality (complete samples)," *Biometrika*, vol. 52, no. 3/4, pp. 591–611, 1965.

[132] H. W. Lilliefors, "On the Kolmogorov-Smirnov test for normality with mean and variance unknown," *Journal of the American Statistical Association*, vol. 62, no. 318, pp. 399–402, 1967.

[133] C. M. Jarque and A. K. Bera, "Efficient tests for normality, homoscedasticity and serial independence of regression residuals," *Economics Letters*, vol. 6, no. 3, pp. 255 – 259, 1980.

[134] J. W. Pratt, H. Raiffa, and R. Schlaifer, *Introduction to Statistical Decision Theory*. The MIT Press, 1995.

[135] P. Z. Peebles, *Probability, Random Variables and Random Signal Principles*. McGraw-Hill, 2001.

[136] B. S. Chissom, "Interpretation of the kurtosis statistic," *The American Statistician*, vol. 24, no. 4, pp. 19–22, 1970.

[137] J. Rife, S. Pullen, B. Pervan, and P. Enge, "Paired overbounding and application to GPS augmentation," in *Proceedings of 2004 IEEE/ION Position Location and Navigation Symposium (PLANS 2004)*, Monterey, CA, April 2004, pp. 439–446.

[138] H.-S. Tsien, *Engineering cybernetics*. McGraw-Hill, 1954.

[139] R. M. Murray, K. J. Astrom, S. P. Boyd, R. W. Brockett, and G. Stein, "Future directions in control in an information-rich world," *IEEE Control Systems*, vol. 23, no. 2, pp. 20–33, April 2003.

[140] S. Borkar, "Designing reliable systems from unreliable components: the challenges of transistor variability and degradation," *IEEE Micro*, vol. 25, no. 6, pp. 10–16, 2005.

[141] G. A. Klutke, P. C. Kiessler, and M. A. Wortman, "A critical look at the bathtub curve," *IEEE Transactions on Reliability*, vol. 52, no. 1, pp. 125–129, 2003.

[142] M. Horemuž and J. Andersson, "Polynomial interpolation of GPS satellite coordinates," *GPS Solutions*, vol. 10, pp. 67–72, 2006.

[143] H. Yousif and A. El-Rabbany, "Assessment of several interpolation methods for precise GPS orbit," *Journal of Navigation*, vol. 60, no. 3, pp. 443–455, 2007.

[144] S. Abbasian Nik and M. G. Petovello, "Implementation of a dual-frequency GLONASS and GPS L1 C/A software receiver," *Journal of Navigation*, vol. 63, no. 2, pp. 269–287, 2010.

[145] T.-M. Huang, V. Kecman, and I. Kopriva, *Kernel Based Algorithms for Mining Huge Data Sets: Supervised, Semi-supervised, and Unsupervised Learning*. Springer, 2006.

[146] T. Hastie, R. Tibshirani, and J. Friedman, *The Elements of Statistical Learning: Data Mining, Inference, and Prediction*, 2nd ed. Springer, 2009.

[147] S. Wolfram, *The MATHEMATICA Book*, 4th ed. Cambridge University Press, 1999.